



# LUND UNIVERSITY

## Acoustic manipulation of cells and microbeads in droplet microfluidics

Fornell, Anna

2018

*Document Version:*

Publisher's PDF, also known as Version of record

[Link to publication](#)

*Citation for published version (APA):*

Fornell, A. (2018). *Acoustic manipulation of cells and microbeads in droplet microfluidics*. Department of Biomedical Engineering, Lund university.

*Total number of authors:*

1

### General rights

Unless other specific re-use rights are stated the following general rights apply:

Copyright and moral rights for the publications made accessible in the public portal are retained by the authors and/or other copyright owners and it is a condition of accessing publications that users recognise and abide by the legal requirements associated with these rights.

- Users may download and print one copy of any publication from the public portal for the purpose of private study or research.
- You may not further distribute the material or use it for any profit-making activity or commercial gain
- You may freely distribute the URL identifying the publication in the public portal

Read more about Creative commons licenses: <https://creativecommons.org/licenses/>

### Take down policy

If you believe that this document breaches copyright please contact us providing details, and we will remove access to the work immediately and investigate your claim.

LUND UNIVERSITY

PO Box 117  
221 00 Lund  
+46 46-222 00 00

# Acoustic manipulation of cells and microbeads in droplet microfluidics

Anna Fornell



**LUND**  
UNIVERSITY

DOCTORAL DISSERTATION

by due permission of the Faculty of Engineering, LTH, Lund University, Sweden.

*Faculty opponent*

Professor Adrian Neild

**Public defence**

August 24, 2018, 09:15 in E:1406, E-huset, LTH, Lund University,  
Ole Römers väg 3, 223 63 Lund, Sweden

**Advisors**

Associate Professor Maria Tenje  
Department of Engineering Sciences, Uppsala University, Sweden

Associate Professor Johan Nilsson  
Department of Biomedical Engineering, Lund University, Sweden

Associate Professor Håkan Jönsson  
School of Biotechnology, KTH Royal Institute of Technology, Sweden

**Faculty opponent**

Professor Adrian Neild  
Department of Mechanical and Aerospace Engineering, Monash University,  
Australia

**Examination Committee**

Professor Thomas Franke  
School of Engineering, University of Glasgow, Scotland

Professor Marilyn Rayner  
Department of Food Technology, Lund University, Sweden

Professor Martin Viklund  
Department of Applied Physics, KTH Royal Institute of Technology, Sweden

Deputy member: Dr. Charlotta Nilsson  
Department of Physics, Lund University, Sweden

**Chairman**

Associate Professor Ingrid Svensson  
Department of Biomedical Engineering, Lund University, Sweden

ISBN: 978-91-7753-726-7 (print)

ISBN: 978-91-7753-727-4 (pdf)

Report nr: 4/18

Printed in 2018 by Tryckeriet i E-huset, Lund, Sweden

© Anna Fornell 2018

|  |                         |  |
|--|-------------------------|--|
| Organisation<br>LUND UNIVERSITY<br>Department of Biomedical Engineering<br>P.O. Box 118, SE-221 00, Lund, Sweden   |                         | Document name<br>DOCTORAL DISSERTATION   |
| Author: Anna Fornell   |                         | Date of issue: August 24, 2018<br>Sponsoring organisations: the Swedish Research Council, the Crafoord Foundation, the Royal Physiographic Society of Lund |
| Title: Acoustic manipulation of cells and microbeads in droplet microfluidics  |                         |  |
| <p>Abstract</p> <p>Droplet microfluidics has emerged as a promising platform for miniaturisation of biological assays on-chip. In droplet microfluidics small water droplets (nL-pL) surrounded by an immiscible carrier oil are generated at high throughput. In these droplets particles such as cells or microbeads can be encapsulated, and the idea is that each of these droplets can be used as small reaction chambers for biological analyses. However, one key bottleneck for the full implementation of droplet microfluidics in biology has been the lack of a method to position and enrich particles inside droplets. In this thesis I present for the first time a microfluidic system where cells and microbeads encapsulated inside droplets can be manipulated using acoustic standing waves (i.e. acoustophoresis).</p> <p>The developed microfluidic systems were fabricated in silicon and sealed with glass lids. In the experiments, water droplets containing particles were generated, and an acoustic standing wave-field was created between the channel walls by actuating a piezoelectric transducer attached to the chip. In the first study it was shown that at application of the ultrasound at the first harmonic (1.8 MHz), the encapsulated particles were focused to the centre of the droplets i.e. the pressure node. It was shown that both red blood cells and polystyrene microbeads could be aligned in the centre of the droplets. The usefulness of the technology was proved by combining acoustophoresis with a trident-shaped droplet split to allow for particle enrichment. At application of the ultrasound at the first harmonic close to 90% of the particles were positioned in the centre daughter droplets when approximately 2/3 of the original droplet volume was removed. To better understand the physics of the system, in the second study a theoretical model was developed where the acoustic field inside droplets was investigated. In the third study, switching of encapsulated particles between different microfluidic pathways was shown. At application of the ultrasound at the first harmonic the encapsulated particles were directed into pathway 1 (the centre daughter droplets) while at application of the ultrasound at the second harmonic the encapsulated particles were directed into pathway 2 (the side daughter droplets). In the fourth study, two-dimensional acoustophoresis was used to increase the detectability of particles encapsulated inside droplets by pre-aligning the particles before the droplet generation site. In the fifth and last study, it was demonstrated that acoustophoresis can be used to separate two different particle species originally encapsulated in the same droplet into different daughter droplets based on the acoustic properties of the particles.</p> <p>This thesis proves that acoustophoresis is a versatile technology that can find various applications in droplet microfluidics. The combination of droplet microfluidics and acoustophoresis opens up for new possibilities for miniaturisation of biological assays on-chip.</p> |                         |  |
| Key words: Acoustophoresis, Droplet microfluidics, Enrichment, Lab-on-a-chip, Particle manipulation, Ultrasound  |                         |  |
| Classification system and/or index terms (if any)  |                         |  |
| Supplementary bibliographical information<br>ISRN: LUTEDX/TEEM-1115-SE<br>Report: 4/18   |                         | Language: English  |
| ISSN and key title   |                         | ISBN: 978-91-7753-726-7 (print)<br>ISBN: 978-91-7753-727-4 (pdf)   |
| Recipient's notes  | Number of pages: 134    | Price  |
|  | Security classification |  |

I, the undersigned, being the copyright owner of the abstract of the above-mentioned dissertation, hereby grant to all reference sources permission to publish and disseminate the abstract of the above-mentioned dissertation.

Signature: *Anna Fornell*

Date: 2018-05-21



# List of publications

This thesis is based on the following papers, which will be referred by their roman numerals in the text. The papers are appended at the end of the thesis.

**I    Controlled Lateral Positioning of Microparticles Inside Droplets Using Acoustophoresis**

A. Fornell, J. Nilsson, L. Jonsson, P. K. Periyannan Rajeswari, H. N. Joensson, and M. Tenje

Analytical Chemistry, 87(20), 10521-10526 (2015)

Author's contribution: Part of developing the idea, fabrication of the microfluidic chip, planned and performed the experiments, analysed the results and major part of writing.

**II    Intra-droplet acoustic particle focusing: simulations and experimental observations**

A. Fornell, F. Garofalo, J. Nilsson, H. Bruus, and M. Tenje

*Submitted*

Author's contribution: Formulated the research question, fabrication of the microfluidic chips, planned and performed the experiments and major part of writing.

**III    An intra-droplet particle switch for droplet microfluidics using bulk acoustic waves**

A. Fornell, M. Ohlin, F. Garofalo, J. Nilsson, and M. Tenje

Biomicrofluidics, 11(3), 031101 (2017)

Author's contribution: Developed the idea, planned and performed the experiments, analysed the results and major part of writing.

**IV Improved positioning and detectability of microparticles in droplet microfluidics using two-dimensional acoustophoresis**

M. Ohlin, A. Fornell, H. Bruus, and M. Tenje

Journal of Micromechanics and Microengineering, 27(8), 084002 (2017)

Author's contribution: Part of fabrication of the microfluidic chip and part of writing.

**V Binary particle separation in droplet microfluidics using acoustophoresis**

A. Fornell, K. Cushing, J. Nilsson, and M. Tenje

Applied Physics Letters, 112(6), 063701 (2018)

*Selected as "Featured Article" by the editor*

Author's contribution: Developed the idea, planned and performed the experiments, analysed the results and major part of writing.

**Related publication by the author:**

**VI Particle manipulation methods in droplet microfluidics**

M. Tenje, A. Fornell, M. Ohlin, and J. Nilsson

Analytical Chemistry, 90(3), 1434-1443 (2018)

# List of abbreviations

|           |                                 |
|-----------|---------------------------------|
| BAW       | bulk acoustic wave              |
| DRIE      | deep reactive-ion etching       |
| MEMS      | microelectromechanical system   |
| PC        | polycarbonate                   |
| PCR       | polymerase chain reaction       |
| PDMS      | polydimethylsiloxane            |
| PEG       | polyethylene glycol             |
| PMMA      | polymethylmetacrylate           |
| PZT       | lead zirconate titanate         |
| SAW       | surface acoustic wave           |
| SEM       | scanning electron microscopy    |
| $\mu$ PIV | microparticle image velocimetry |
| $\mu$ TAS | micro total analysis system     |



# List of symbols

|            |   |
|------------|---|
| $a$        | radius                                  |
| $c$        | speed of sound                          |
| $Ca$       | capillary number                        |
| $\gamma$   | interfacial tension                     |
| $\eta$     | viscosity                               |
| $E_{ac}$   | acoustic energy density                 |
| $f$        | frequency                               |
| $F_{drag}$ | Stokes' drag force                      |
| $F_{rad}$  | primary acoustic radiation force        |
| $K$        | bulk modulus                            |
| $k$        | number of particles in a droplet        |
| $k$        | wave number                             |
| $\kappa$   | compressibility                         |
| $\lambda$  | average number of particles per droplet |
| $\lambda$  | wavelength                              |
| $L$        | characteristic length scale             |
| $p$        | pressure                                |
| $P$        | Poisson distribution                    |
| $\rho$     | density                                 |
| $Re$       | Reynolds number                         |
| $V$        | volume                                  |
| $v$        | velocity                                |

|        |                          |
|--------|--------------------------|
| $w$    | width                    |
| $y$    | distance                 |
| $z$    | acoustic impedance       |
| $\Phi$ | acoustic contrast factor |

# Contents

|   |     |
|---|-----|
| List of publications.....                                       | i   |
| List of abbreviations.....                                      | iii |
| List of symbols .....   | iv  |
| Contents.....   | vi  |
| 1. Introduction.....  | 1   |
| 1.1 A new tool for biological and medical research.....         | 1   |
| 1.2 Motivation for droplet microfluidics .....                  | 2   |
| 1.3 Research aim .....  | 3   |
| 2. Droplet microfluidics.....                                   | 5   |
| 2.1 General microfluidic concepts.....                          | 5   |
| 2.2 Droplet physics.....  | 8   |
| 2.3 Droplet chemistry .....                                     | 11  |
| 2.4 Droplet unit operations.....                                | 12  |
| 3. Intra-droplet particle manipulation.....                     | 19  |
| 3.1 General aspects on particle manipulation.....               | 19  |
| 3.2 Hydrodynamic methods.....                                   | 20  |
| 3.3 Magnetophoresis.....  | 21  |
| 3.4 Acoustophoresis .....                                       | 22  |
| 3.5 Dielectrophoresis .....                                     | 23  |
| 4. Acoustics.....   | 25  |
| 4.1 Sound waves and acoustic resonance .....                    | 25  |
| 4.2 Generation of acoustic waves .....                          | 27  |
| 4.3 Acoustic forces on particles.....                           | 28  |
| 4.4 Acoustic forces acting on immiscible fluid interfaces ..... | 32  |
| 4.5 Biocompatibility of acoustophoresis .....                   | 34  |

|  |    |
|--|----|
| 5. Microfluidic chip fabrication.....        | 35 |
| 5.1 Microfluidic chip materials.....         | 35 |
| 5.2 Silicon etching methods .....            | 36 |
| 5.3 Microfabrication.....                    | 37 |
| 6. Experimental methods .....                | 43 |
| 6.1 Fluids and particles .....               | 43 |
| 6.2 Experimental setup .....                 | 44 |
| 6.3 Droplet volume estimation.....           | 46 |
| 6.4 Particle counting.....                   | 47 |
| 7. Summary of included papers .....          | 49 |
| Paper I.....                                 | 50 |
| Paper II.....                                | 51 |
| Paper III .....                              | 52 |
| Paper IV .....                               | 53 |
| Paper V.....                                 | 54 |
| 8. Concluding remarks .....                  | 55 |
| 8.1 System improvements and integration..... | 55 |
| 8.2 Biological applications.....             | 56 |
| 8.3 Commercialisation.....                   | 56 |
| 8.4 Conclusion.....                          | 57 |
| Popular scientific summary .....             | 59 |
| Populärvetenskaplig sammanfattning.....      | 63 |
| Acknowledgements.....                        | 67 |
| References.....                              | 69 |



# 1. Introduction

The methods to analyse cells have improved tremendously since the first microscopy studies of cells in the middle of the 17<sup>th</sup> century.<sup>1,2</sup> This has enabled many important discoveries in the biological and medical sciences, but many fundamental questions still need to be answered such as why some bacteria do not respond to antibiotic treatments and what regulates how cancer spreads. In order to study these complex questions new methods where single cells can be studied at high throughput are required, and here droplet microfluidics has emerged as a promising technology.<sup>3-7</sup> Moreover, droplet microfluidics can be a useful tool for faster and more sensitive detection of diseases and for the development of new drugs. In this PhD project, a microfluidic system for manipulation of cells and microbeads encapsulated inside droplets has been developed.

## 1.1 A new tool for biological and medical research

Traditionally, cells are cultured and studied in systems such as Petri dishes or micro well plates, but these systems have several shortcomings such as low throughput and high cost. Moreover, in these systems entire populations of cells are studied, and the response is the average response of thousands of cells, and it is not possible to probe the response from single cells. This is a major obstacle as recent findings have shown that cells within a population show a high degree of heterogeneity, and that the cell-cell variability has important biological implications.<sup>8,9</sup> In addition, by studying populations of cells it is hard to detect rare cells or rare events.

To meet the limitations of these traditional cell analysis systems, lab-on-a-chip systems or sometimes also called micro total analysis systems ( $\mu$ TAS) have emerged as promising alternatives. In these systems the sample is handled and analysed in small microfluidic channels. The overall vision of lab-on-a-chip technology is to miniaturise an entire laboratory and all its functions onto a small so-called microfluidic chip, Figure 1.

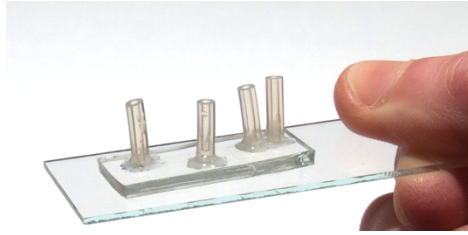


Figure 1. A photograph of a microfluidic chip.

In the early 2000s, a subfield of microfluidics called droplet microfluidics emerged as a suitable technology for further miniaturisation of biological assays.<sup>10</sup> In droplet microfluidics small droplets surrounded by an immiscible carrier fluid are generated with high throughput, Figure 2. The fluid making up the droplets is called the *dispersed phase* and the surrounding fluid is called the *continuous phase*. Typically, the dispersed phase is a water-based solution and the continuous phase some type of oil. The basis of the technology is the generation of monodisperse droplets in which particles can be encapsulated. In this thesis the term particle is used to describe various types of microscale objects such as cells or microbeads. In the initial experiments plastic microbeads are often used as “cell-mimics” to optimise the systems, and after that cells may be used. The idea is that each of these cell- or bead-containing droplets can be used as isolated reaction chambers, “mini test-tubes”, for biological experiments.

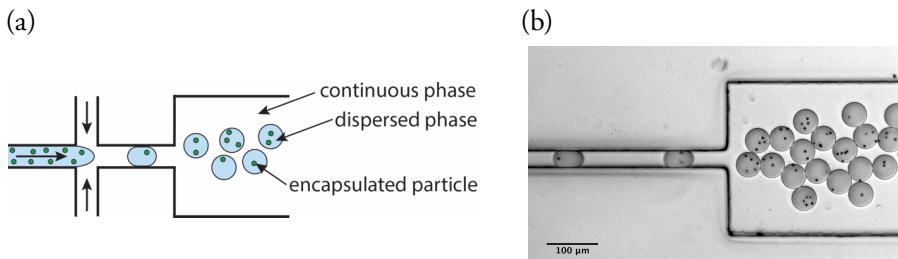


Figure 2. (a) In microfluidic channels water droplets containing cells or microbeads can be generated. Each droplet can be used as a “mini test-tube” for biological experiments. (b) Photograph of water-in-oil droplets (50  $\mu\text{m}$  diameter) containing polystyrene microbeads (3  $\mu\text{m}$  diameter).

## 1.2 Motivation for droplet microfluidics

Droplet microfluidic systems have several advantages compared with traditional cell analysis systems. The most striking advantage is that the volumes are reduced. The

---

generated droplets have typically volumes in the nL-pL range, meaning that the amount of biological sample and chemicals needed are reduced by several orders of magnitude compared with traditional systems. This leads to a huge decrease in cost and environmental impact for each analysis.<sup>11</sup> Another advantage of droplet microfluidics is that thousands of droplets can be generated and analysed per second, and this opens up for new possibilities for high throughput screening of biological samples.<sup>7,12</sup>

The small size of the droplets makes them perfectly suited for encapsulation of single cells.<sup>5</sup> As mentioned in section 1.1, measuring the response from single cells instead of the average response of a whole population of cells gives more sensitive analyses.<sup>8,9</sup> In addition to studying the encapsulated cells themselves, biomolecules that the cells secrete into the droplet volume can be studied.<sup>13</sup> Since the biomolecules are secreted into a small volume the concentration becomes high and it becomes much easier to detect and measure the biomolecules compared with traditional systems.

One of the main drawbacks of droplet microfluidics is that the fabrication of microfluidic systems with integrated and automated sample handling and analysis is not trivial and often requires advanced microfabrication methods. Since the amount of sample is reduced, very sensitive read-out methods able to handle and detect small amount of sample are also required.

Overall, droplet microfluidics holds great expectations to be a powerful technology for biological and medical sciences. It should be noted that many of the advantages of droplet microfluidic systems are also valid for single-phase microfluidic systems, however using droplets often leads to further reduction in volume, faster mixing and higher throughput compared with single-phase microfluidic systems.

Since droplet microfluidics is a rather new research field, most of the systems presented so far in the literature are mainly showing proof of concept, and to reach the full potential of the technology more research is needed.

### 1.3 Research aim

To allow for the full implementation of droplet microfluidics in biological and medical research all standard laboratory processes should be possible to perform on a microfluidic chip. For example, one of the most frequently occurring process steps in cell-based assays is centrifugation as this allows for enrichment and separation of cells. Consequently, methods to perform such steps in droplet microfluidic systems are also required.



## 1. Introduction

---

The aim of this PhD project has been to develop a new droplet unit operation for label-free handling of cells and microbeads inside droplets. To accomplish this, a microfluidic system where ultrasonic standing waves, also called acoustophoresis, is used to manipulate particles inside droplets is fabricated and evaluated. The development of such particle manipulation method expands the droplet microfluidic toolbox, and opens up for new possibilities for droplet-based biological assays.

## 2. Droplet microfluidics

Droplet microfluidics has emerged as a subfield of microfluidics, and proven to be a promising technology in a wide range of applications. In this chapter the most central droplet microfluidic concepts and the important technical advancements in the field are described.

### 2.1 General microfluidic concepts

Many microfluidic concepts that apply in single-phase microfluidics are also highly relevant in droplet microfluidics, and these concepts are discussed in this section.

#### Dimensionless numbers in microfluidics

To characterise various fluid dynamic phenomena several dimensionless numbers have been defined such as the Bond number, the capillary number, the Péclet number and the Reynolds number. Of these, the capillary number and the Reynolds number are the most commonly mentioned dimensionless numbers in droplet microfluidics.

The Reynolds number ( $Re$ ) describes the ratio between the inertial and viscous forces and is defined as,

$$Re = \rho v L / \eta \quad (1)$$

where  $\rho$  is the density of the fluid,  $v$  is the average velocity of the fluid,  $L$  is the characteristic length and  $\eta$  is the viscosity of the fluid.<sup>14</sup> The capillary number ( $Ca$ ) describes the ratio between the viscous and interfacial forces and is defined as,

$$Ca = \eta v / \gamma \quad (2)$$

where  $\gamma$  is the interfacial tension between the dispersed and the continuous phase.<sup>14</sup>

### Laminar flows

In microfluidic channels the fluid flow is generally laminar, meaning that the fluid flows in parallel layers, Figure 3. The opposite to laminar flow is turbulent flow.



*Figure 3. The illustration shows the difference between laminar and turbulent flow. In microfluidics the flow is typically laminar.*

If a flow is laminar or turbulent depends on the Reynolds number of the system. At low Reynolds numbers the flow is laminar while at higher Reynold numbers ( $\sim 2000-3000$ ) the flow becomes turbulent.<sup>14</sup> In microfluidic systems the Reynolds number is often between  $10^{-6}$  and 10, thus the flow is laminar.<sup>14</sup>

The laminar flow has the consequence that mixing of fluids and molecules are much slower in microsystems compared to macrosystems. In microsystems mixing occurs mainly by diffusion which is typically a very slow process.<sup>14</sup>

In experiments aiming to focus particles in microfluidic channels the laminar flow is often advantageous as it enables precise control over the suspended particles. For instance, if a particle is positioned in a flow stream in the beginning of the channel, the particle will maintain its position and follow the flow stream throughout the entire channel.

### No-slip boundary condition and flow profiles in microchannels

Another fundamental fluid dynamic concept is the so-called no-slip boundary condition. This boundary condition states that close to a solid boundary such as a channel wall the velocity of the fluid is zero. This has implications on the flow profile in both single-phase and droplet microfluidic systems when the flow of the fluids are generated by a pressure difference.

Taken the simplest case with only one fluid, the no-slip boundary condition results in that the flow will have a parabolic flow profile where the flow velocity is highest in the centre of the channel and zero at the walls, Figure 4.<sup>15</sup>

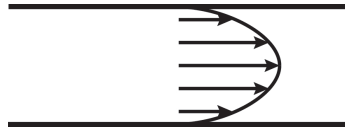


Figure 4. Parabolic flow profile. The flow velocity is highest in the centre of the channel and zero at the walls.

Regarding the flow profile in droplet microfluidic systems, these systems can be divided into two cases: the droplet is small in relation to the channel and when the droplet (plug) fills most of the channel, Figure 5.



Figure 5. (a) The droplets are small in relation to the channel dimensions. (b) The droplets (plugs) fill the channel width.

The first case (Figure 5(a)) is similar to single-phase systems. Here the continuous phase is having a parabolic flow profile and the droplets will follow the flow streams of the continuous phase, meaning that the droplets will move fastest in the centre of the channel and slower closer to the walls.<sup>16</sup> However, for the second case (Figure 5(b)) when the droplet fills the channel, the situation is more complex. Here the droplet will have a different velocity compared to the continuous phase and there will be recirculating flows in the continuous phase.<sup>16</sup>

For droplet microfluidic systems it is not only the flow profile of the continuous phase that is of interest, but also the flow profile inside the droplets. The no-slip boundary condition and the fact that the two phases cannot mix do influence the flow fields inside the droplets both in small and large droplets.<sup>16</sup> As a result of these effects, there will be recirculating flows inside the droplets, and this is discussed in section 2.2.

## Stokes' drag force

A particle that is moved in a fluid or when the fluid is moved relative to the particle, will experience a drag force. This occurs for example when external forces such as acoustic or magnetic forces are used to manipulate particles in microfluidic channels. For low Reynolds numbers and spherical particles this force, also known as Stokes' drag force ( $F_{\text{drag}}$ ), is given by

$$F_{\text{drag}} = 6\pi\eta av \quad (3)$$

where  $\eta$  is the viscosity of the fluid,  $a$  is the radius of the particle and  $v$  is the velocity of the fluid relative to the particle.<sup>15</sup> The direction of this force is in the opposite direction to the movement induced by the external force.

## 2.2 Droplet physics

### Droplet generation

The common component in every droplet microfluidic system is the droplet generation, and it exists both passive and active droplet generation methods.<sup>17</sup> Passive methods relies on the spontaneous break-up of droplets when two immiscible fluid flows meet in a channel junction<sup>10,18,19</sup> whereas in active methods external components such as valves,<sup>20</sup> acoustic fields<sup>21</sup> or electric fields<sup>22,23</sup> are used to control the droplet generation process. Active methods can find uses in certain applications such as on-demand control of droplet generation, but generally passive methods are favoured due to simpler microfabrication and easier operation.

Three channel geometries for passive droplet generation are shown in Figure 6: T-junction,<sup>10</sup> flow-focusing,<sup>18</sup> and co-flow.<sup>19</sup> Of these, the T-junction and flow-focusing are the most commonly used since they can be fabricated by standard microfabrication processes such as soft lithography and etching. The co-flow design is typically realised by insertion of a small capillary inside a larger capillary and this design is thus more difficult to integrate with other droplet unit operations. In the experiments described in Paper I, II and IV the droplets were generated using a flow-focusing geometry and in the experiments described in Paper III and V the droplets were generated using a T-junction.

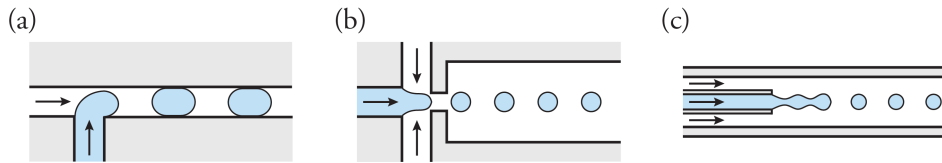


Figure 6. Three channel geometries for droplet generation: (a) T-junction, (b) flow-focusing and (c) co-flow. The arrows indicate the flow directions.

There are several physical concepts that play a role in the break-up of droplets. The interfacial tension strives to minimise the surface energy by reducing the surface area between the two fluids, and droplets are produced since for a given volume a sphere

---

(droplet) is the shape having the minimum surface area.<sup>16</sup> Sometimes the droplet is constricted in space by the channel dimensions and hence the droplet is taking a plug-like shape. In this thesis the term droplet is used to describe both spherical droplets and plugs. The droplet break-up process can be described as a competition between forces acting to deform the interface between the two fluids and forces counteracting the deformation.<sup>24,25</sup>

To explain the droplet break-up process various models have been developed, and the exact model depends for example on the channel geometry and the flows. Common to all is that the droplet generation process is divided into three flow regimes: squeezing, dripping and jetting, Figure 7, and which flow regime the droplet generation takes place in, depends on the capillary number of the system.

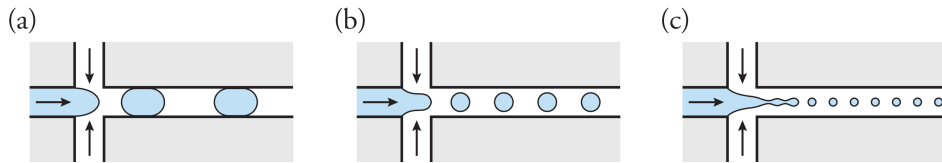


Figure 7. Droplet generation regimes: (a) squeezing, (b) dripping and (c) jetting. The arrows indicate the flow directions.

At low capillary numbers droplet generation occurs by squeezing, and in this regime the droplet blocks the channel causing the build-up of a pressure upstream, and this pressure difference is what makes the dispersed phase break up into droplets.<sup>25</sup> In the dripping regime (intermediate capillary numbers) the droplet does not constrict the channel and shear forces are reported to play a role in the droplet break-up.<sup>25</sup> At even higher capillary numbers droplet generation occurs by jetting, and in this regime droplet break-up is primarily driven by the Rayleigh-Plateau instabilities.<sup>25</sup>

The ability to generate monodisperse droplets of a specific size is one of the key advantages of droplet microfluidics, and the size of the droplets can be controlled by several means. The channel geometry and the dimensions of the channels influence the droplet size, but the flow rates and the fluid properties of the dispersed and continuous phase also have an impact.<sup>26</sup> For example, if small droplets are aimed for, the flow rate of the continuous phase should be much higher than the dispersed phase. However, changing the flow rates does not only affect the droplet size, but the droplet generation frequency as well. In some applications high droplet generation frequency is essential, whereas in some applications the detection or manipulation operations may set the throughput limit.

### Flow fields inside droplets

When a droplet is moving in a microfluidic channel internal circulating flows arise in the droplet, and these flows are related to the no-slip boundary condition and the presence of the immiscible interface between the dispersed and continuous phase.<sup>16</sup>

To characterise the circulating flows that occur inside moving droplets different methods can be employed such as microparticle image velocimetry ( $\mu$ PIV).<sup>27,28</sup> Hein *et al.* investigated the flow profile inside moving droplets in rectangular channels, Figure 8, and they observed that where the droplet almost contacts the walls the flow inside the droplet is directed backwards relative to the droplet direction.<sup>27</sup> However, in rectangular channels there are gutters in the corners of the channel where the continuous phase can bypass, and they noticed that close to these gutters the flow is directed forward in the droplet. In addition to this, they observed that fluid vortices occur in the front and end of the droplets.

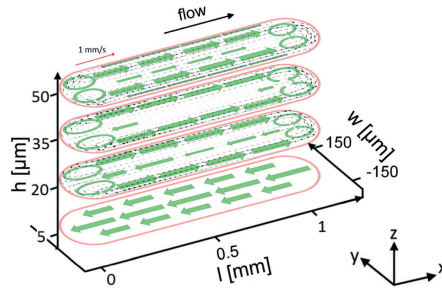


Figure 8. Hein *et al.* investigated the flow fields inside droplets using  $\mu$ PIV. The green arrows represent the internal flows that occur when the droplet is moving, and the red arrow indicates the droplet flow direction. Note that only half of the droplet height is shown due to symmetry reasons:  $z=0 \mu\text{m}$  is the bottom of the channel and  $z=50 \mu\text{m}$  is half the height of the channel. Reproduced from Ref. 27 with permission from the Royal Society of Chemistry.

It should be noted that Figure 8 shows the flow fields inside droplets for a particular system, and there are many parameters that affect the flows inside droplets such as the fluid properties, the flow rates and the microfluidic channel design.<sup>27</sup> Consequently, to get a correct picture of the flow fields inside droplets for a specific system all these factors must be taken into consideration.

The internal circulating flows result in that mixing occurs much faster in droplets compared with single-phase systems,<sup>29</sup> and the fast mixing is one of the main advantages of droplet microfluidics compared with single-phase systems. The internal circulating flows also affect the position of particles inside droplets and play an important role in experiments aiming to focus particles inside droplets. Depending on the system the internal flows can either be employed in combination

---

with sedimentation to position particles inside droplets or need to be competed with, for more details see Chapter 3.

## 2.3 Droplet chemistry

### Fluids

Various combinations of immiscible fluids can be used to create droplets in microfluidic systems. One of the main applications of droplet microfluidics is the encapsulation of cells and biomolecules, and therefore aqueous solutions such as water or cell medium are often selected as the dispersed phase. For the continuous phase the options are broader. The most commonly used continuous phase in droplet microfluidics is fluorinated oil (e.g. HFE-7500 or FC-40), but for example mineral oil, silicone oil and vegetable oil have also been reported in several studies.<sup>30</sup> Ideally, the continuous phase should provide high droplet stability, low cross-contamination, have high gas solubility and be biocompatible. In specific applications, other aspects may be important. For example in Paper II it is shown that the acoustic properties of the fluids are important to consider in applications where acoustic forces are used to manipulate particles inside droplets.

### Surfactants

Emulsions (such as water droplets in oil) have higher surface energy compared with the two separate phases, and accordingly, due to the principle of minimisation of energy emulsions degrade with time.<sup>31</sup> This is manifested by two droplets that come in close contact tend to coalesce. In addition to coalescence, emulsions can be degraded by Ostwald ripening.<sup>31</sup>

In most applications high droplet stability and no cross-contamination between the individual droplets are of importance, and to increase the droplet stability surfactants are often added to the fluids.<sup>30</sup> A surfactant is an amphiphilic molecule, that has one hydrophilic part and one hydrophobic part. In a two-phase system the surfactant molecules migrate to the interface between the fluids. The hydrophilic parts are positioned in the water phase whereas the hydrophobic parts are positioned in the oil phase, Figure 9. This results in a decrease in the surface energy and stabilisation of the droplets. In addition, the surfactants hinder coalescence by steric repulsions between the droplets and by inducing Marangoni stresses at the



## 2. Droplet microfluidics

---

interface.<sup>30</sup> Several different surfactants have been used in droplet microfluidics,<sup>30</sup> and which surfactant to choose in a particular system depends on which fluids that are being used. For example, in the experiments described in Paper II and IV perfluoropolyether (sold as “Krytox”) was added to the fluorinated oil to increase the droplet stability.

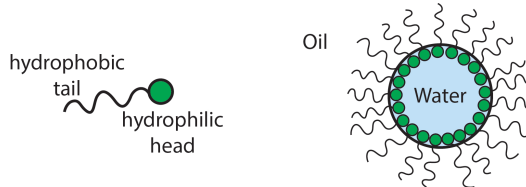


*Figure 9. Surfactants are commonly added to the continuous phase and/or dispersed phase to increase the droplet stability. A surfactant molecule (shown to the left) has one hydrophilic part and one hydrophobic part. The surfactant molecules are positioned at the interface between the water and the oil.*

As an alternative to standard surfactants, droplets can be stabilised using Pickering emulsions in which small solid particles are adsorbed at the fluid interface.<sup>32</sup> Pan *et al.* used polyethylene glycol (PEG) adsorbed nanoparticles to stabilise droplets and observed much lower leakage of small molecules compared with the use of standard surfactants.<sup>32</sup>

## 2.4 Droplet unit operations

### A toolbox for droplet microfluidics

To perform biological assays in droplets different droplet unit operations have been developed that allow for example of addition of reagents, sample enrichment and analysis of the content inside the droplets. Typically, multiple unit operations are combined into complex microfluidic circuits, and for example in the experiments described in Paper I, III and V the acoustic particle focusing was combined in series with a droplet split to enable particle enrichment. However, the integration of several unit operations onto a single microfluidic chip can be a practical challenge,<sup>33</sup> and sometimes this is solved by combining on-chip unit operations with off-chip processing steps or by having more than one microfluidic chip. In the following section some of the most common droplet unit operations are described.

---

## Particle encapsulation

In the droplet generation process, cells and microbeads can be encapsulated in the droplets. Typically, the number of particles encapsulated in each droplet is determined by the Poisson distribution which is given by,

$$P(k, \lambda) = \frac{\lambda^k e^{-\lambda}}{k!} \quad (4)$$

where  $P(k, \lambda)$  is the portion of droplets containing  $k$  particles and  $\lambda$  is the average number of particles per droplet.<sup>34</sup> For example if  $\lambda = 1$  only 37% of the droplets will contain a single particle while the rest of the droplets will be empty (37%) or contain multiple particles (26%).

In applications aiming to study single cells, overcoming the Poisson distribution is a major challenge as in these applications it is important to ensure that the result comes from a single cell and not from an empty droplet or from multiple encapsulated cells. However, in applications where many cells are encapsulated in each droplet the variability in the number of encapsulated cells is a minor problem because at high cell concentrations the number of cells in each droplet can be approximated by the normal distribution.<sup>34</sup>

Several strategies to increase the probability that each droplet contains exactly one particle have been reported. The most common approach is to dilute the sample concentration but this comes at the expense of a large number of empty droplets.<sup>34</sup> However, these empty droplets can either be used as controls in the experiments<sup>5</sup> or be removed in a subsequent sorting step.<sup>35,36</sup>

One method to increase the likelihood of encapsulating single cells was presented by Edd *et al.*, Figure 10.<sup>37</sup> In this method, called ordered encapsulation, a high aspect ratio channel was used where, at high cell concentrations, the cells were self-organised with uniform spacing before the droplet generation. By matching the flow rates with the cell spacing a high amount of droplets containing single cells were obtained.

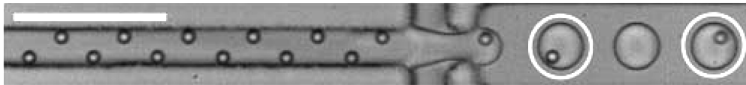


Figure 10. Ordered encapsulation of particles increases the probability that the droplets contain single particles. The scale bar is 100  $\mu\text{m}$ . Reproduced from Ref. 37 with permission from the Royal Society of Chemistry.

### Addition of reagents

One frequently occurring step in biological assays is the addition of reagents, and on the macroscale this is done by pipetting. Accordingly, an equivalent operation is required in droplet microfluidic systems.

Addition of reagents to droplets can be realised by merging two droplets with different content. Droplets that are not stabilised or only weakly stabilised by surfactants only need to come in close contact with each other to merge, and by smart channel design two individual droplets can be brought in close contact under controlled conditions resulting in droplet merging and mixing of the reagents, Figure 11(a).<sup>38</sup> Likewise, Sesen *et al.* developed a system where acoustic forces were used to immobilise a droplet, and when another droplet arrived the two droplets were merged.<sup>39</sup>

However, generally droplets are stabilised with surfactants and the droplets do not merge easily, thus special technical solutions have been developed to control merging of surfactant stabilised droplets such as electrocoalescence where an electric field is applied to induce merging of droplets.<sup>40</sup>

An alternative method to add reagents to droplets was reported by Abate *et al.* where they developed a microfluidic chip implementing a so-called pico-injector to add fluid into existing droplets, Figure 11(b).<sup>41</sup> In this method the injection of fluid into the droplets was triggered by the application of an electric field which destabilised the fluid interface and allowed fluid to be injected.

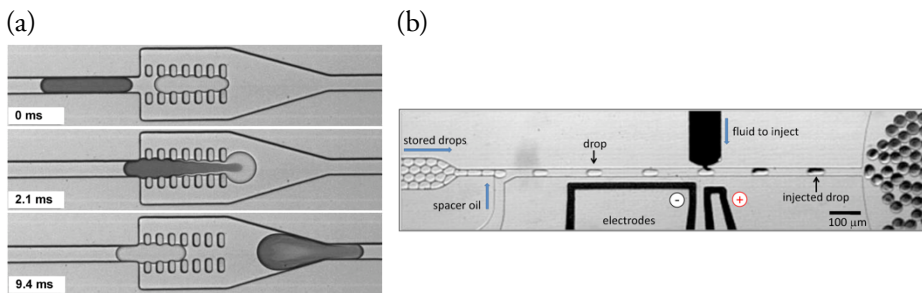


Figure 11. (a) Droplet merging. (b) Addition of fluid into droplets using a pico-injector. (a) Reproduced from Ref. 38 with permission from the Royal Society of Chemistry. (b) Reproduced from Ref. 41 with permission from the National Academy of Sciences.

---

## Droplet splitting

In contrast to adding fluid and reagents into existing droplets, a unit operation to divide one droplet into two or more daughter droplets is also required to reduce the droplet volume. Droplet splitting can be used for example to create replicates or control droplets, or it can be used in combination with particle manipulation to accomplish particle enrichment. Splitting is often induced using some type of channel branching such as a bifurcation.<sup>42</sup> However, in some applications, such as acoustic particle enrichment as described in Paper I, III and V a trifurcation is better suited for droplet splitting than a bifurcation. The size of the resulting daughter droplets depends on the channel geometry as well as on the flow rates in the respective outlets. As shown in Figure 12 Link *et al.* developed a microfluidic chip where several droplet splits were placed in series with the result that one droplet was split into multiple daughter droplets.<sup>42</sup> In addition to splitting droplets using channel branches, external forces such as acoustics can be used to split droplets.<sup>43</sup>

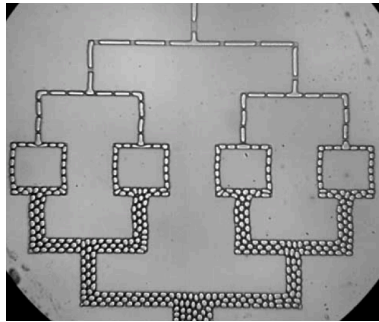


Figure 12. Droplet splitting in multiple T-junctions. Reproduced from Ref. 42 with permission from the American Physical Society.

## Droplet handling

Methods to handle whole droplets such as sorting and trapping as well as methods to handle cells and microbeads encapsulated inside droplets have been developed.<sup>44</sup> The latter is the main theme of this PhD project, and the available methods for manipulation of cells and microbeads encapsulated inside droplets are reviewed in Chapter 3.

Droplet sorting can be employed to retrieve or separate certain droplets from a large population of droplets. Sorting of droplets is often divided into passive and active methods. Two examples of passive droplet sorting methods are pinched flow fractionation<sup>45</sup> and deterministic lateral displacement,<sup>36</sup> and in both these methods

## 2. Droplet microfluidics

---

the droplets are sorted based on size. Passive sorting can be useful in certain applications, however, active methods are generally preferred since these methods have the advantage that sorting can be triggered on-demand. Baret *et al.* developed an active droplet sorter where the droplets were sorted using dielectrophoresis based on the fluorescence signal from the droplets. With this droplet sorter they showed sorting of cells encapsulated inside droplets based on the enzymatic activity of the cells, Figure 13(a).<sup>46</sup> Another fluorescence-activated droplet sorter was presented by Schmid *et al.* where they instead of electric fields used surface acoustic waves (SAW) to sort droplets, Figure 13(b).<sup>47</sup> In addition to SAW, bulk acoustic waves (BAW) can also be employed to sort droplets in microfluidic channels, Figure 13(c).<sup>48</sup>

To enable investigation of encapsulated cells and reactions inside droplets that evolves over time, methods to trap and immobilise droplets on-chip have been developed. For example, Huebner *et al.* presented a droplet trapping array where droplets could be trapped, the encapsulated cells monitored, and later the droplets could be released, Figure 13(d).<sup>49</sup>

### **Droplet detection and analysis**

Different methods to detect and analyse the content inside the droplets exist. In cell-based assays both the encapsulated cells and biomolecules that the cells secrete are of biological interest. The dominating read-out methods are fluorescence detection and microscopy,<sup>11,49,50</sup> but other methods such as matrix-assisted laser desorption/ionization mass spectrometry can also be used.<sup>51</sup> Brouzes *et al.* developed a microfluidic system for cytotoxicity screening using fluorescence based read-out.<sup>50</sup> To evaluate the cell viability the encapsulated cells were stained using fluorescent live and dead stains, and the fluorescent signals were detected using laser illumination and photomultiplier tubes.

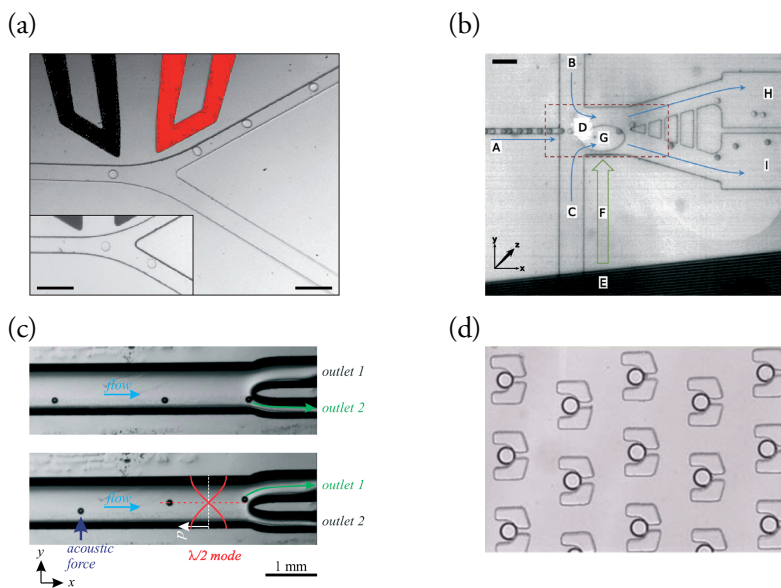


Figure 13. (a) Droplet sorting using dielectrophoresis. Without an electric field applied (the inset) the droplets flow into the lower channel while with the electric field applied the droplets are deflected into the upper channel. The scale bar is  $100\ \mu\text{m}$ . (b) Droplet sorting using surface acoustic waves. The default route for the droplets is into the lower channel, but if a fluorescent signal is detected the acoustics is triggered and the droplet is directed into upper channel. The scale bar is  $100\ \mu\text{m}$ . (c) Droplet sorting using bulk acoustic waves. Without acoustics (upper photo) the droplets flow into the lower channel while in the acoustic standing wave-field the droplets are deflected into the upper channel. (d) Droplet trapping array. (a-d) Reproduced from Ref. 46–49 with permission from the Royal Society of Chemistry.



# 3. Intra-droplet particle manipulation

In this PhD project particles encapsulated inside droplets have been manipulated using acoustic forces (i.e. acoustophoresis). This particle manipulation method was selected as it is a label-free and biocompatible method, thus well-suited for life science applications. Acoustic particle manipulation has other advantages such as it can be used for separation of particles based on the material properties of the particles and for on-demand switching of particles between different fluidic pathways. However, acoustic forces are not the only forces that can be used to manipulate particles inside droplets, and in this chapter the different methods for manipulation of particles encapsulated inside droplets are reviewed.

## 3.1 General aspects on particle manipulation

Manipulation of cells and microbeads in droplets can serve many purposes such as enrichment, separation and washing.<sup>44</sup> All these operations were first implemented in single-phase microfluidic systems,<sup>52</sup> and have later been implemented in droplet microfluidic systems.

Several different intra-droplet particle manipulation methods exist. All methods have their advantages and disadvantages, and no “force fits all” exists. Instead the choice of method should be based on the intended application and on the available microfabrication processes and equipment. In addition, in biological applications the biocompatibility of the method should be considered.

Particle manipulation methods are typically divided into active and passive methods depending on if external forces are employed or not. Active methods have the advantage that they can be regulated on-demand, but have the drawback that the experimental setup is often more complex. Another way to divide particle manipulation methods is whether the method is label-free or not. In Table 1 a summary of the available methods for manipulation of particles inside droplets is shown. It should be mentioned as droplet microfluidics and especially manipulation of encapsulated particles is a new research field, most of the presented papers are



### 3. Intra-droplet particle manipulation

mainly showing proof of concept and hence advances in such as throughput and the smallest particles that can be manipulated are likely to come.

Table 1. Methods for manipulation of particles encapsulated inside droplets.

| Manipulation method     | Sorting criteria                 | Active/passive | Label-free | Particle species                        | Comments                     | Ref.          |
|-------------------------|----------------------------------|----------------|------------|---|------------------------------|---------------|
| Hydrodynamics (gravity) | size, density                    | passive        | yes        | 5-38 $\mu\text{m}$ microbeads and cells | low flows or heavy particles | 27,53,54      |
| Magnetophoresis         | size, magnetic susceptibility    | active         | no         | 1 $\mu\text{m}$ microbeads              | magnetic microbeads          | 55,56         |
| Acoustophoresis         | size, density, compressibility   | active         | yes        | 5-10 $\mu\text{m}$ microbeads and cells | complex fabrication          | Paper I-V, 57 |
| Dielectrophoresis       | size, permittivity, conductivity | active         | yes        | 5 $\mu\text{m}$ microbeads and cells    | low flows                    | 58            |

## 3.2 Hydrodynamic methods

Hydrodynamic interactions occur in all droplet microfluidic systems and affect particles encapsulated inside the droplets. The hydrodynamic forces are related to the internal flows that occur inside the droplets (section 2.2).

There are several reports on passive particle manipulation where hydrodynamics and sedimentation are used to position particles at certain locations inside the droplets. For example, Kurup and Basu reported on a system where glass beads with a diameter of 38  $\mu\text{m}$  were efficiently accumulated in the end of the droplets in a circular tubing, Figure 14(a).<sup>53</sup> In this method, the particles did sediment to the bottom of the droplets and were then accumulated in the end of the droplets by the internal flows. In this method the particles should preferably be large and have high density. A biological application of a similar system was presented by Sun *et al.* where they showed separation of plasma from blood in long droplets.<sup>54</sup>

Hydrodynamics and sedimentation do not necessarily result in that the particles accumulate in the end of the droplets. Hein *et al.* showed that in rectangular channels and at low capillary numbers plastic microbeads with a diameter of 8  $\mu\text{m}$  could be accumulated at the sides of the droplets.<sup>27</sup> Moreover, they integrated a trident-shaped droplet split which enabled concentration of microbeads in the side daughter droplets, Figure 14(b).

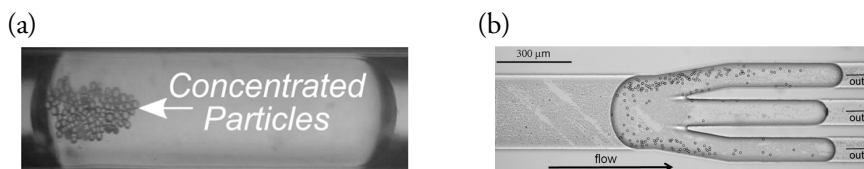


Figure 14. (a) Glass beads ( $38\ \mu\text{m}$ ) accumulate in the end of the droplet in a circular tubing due to the sedimentation and internal flows. (b) In a rectangular channel microbeads ( $8\ \mu\text{m}$ ) accumulate at the sides of the droplet, and in the trifurcation the microbeads are accumulated in the side daughter droplets. (a) Reproduced from Ref. 53 with the permission of AIP Publishing. (b) Reproduced from Ref. 27 with permission from the Royal Society of Chemistry.

### 3.3 Magnetophoresis

The first active particle manipulation method that was applied to manipulate particles inside droplets was magnetophoresis. The magnetic force on a particle depends on the size of the particle, the magnetic susceptibility of the particle and the surrounding fluid and the strength and gradient of the magnetic field.<sup>59</sup> Magnetophoresis is a useful method, but has the limitation that it only works with magnetic particles. Manipulation of biological particles can be accomplished by coupling the bioparticles to magnetic affinity beads.<sup>56</sup>

Lombardi and Dittrich developed a system where magnetic microbeads were encapsulated inside droplets, and magnetic forces in combination with a droplet split were used to concentrate all microbeads into one of the two formed daughter droplets, Figure 15.<sup>55</sup> Moreover, they showed that the system could be used to investigate drug-protein interactions, and tested the system for determination of the association constant between warfarin and human serum albumin.

### 3. Intra-droplet particle manipulation

---

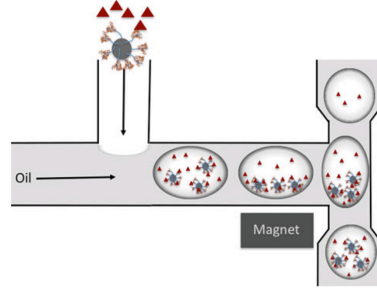


Figure 15. Droplets containing human serum albumin coated magnetic beads (circles) and the drug warfarin (triangles) are generated. A magnet is used to position the magnetic beads on one side of the droplets, and after the droplet split the magnetic beads are accumulated in the lower daughter droplets. Reproduced from Ref. 55 with permission from Springer Nature.

## 3.4 Acoustophoresis

In all experiments described in the papers included in this thesis, bulk acoustic standing waves (BAW) were used to manipulate particles inside droplets. In an acoustic standing wave-field micrometre-sized particles are moved to the pressure nodes or anti-nodes by the primary acoustic radiation force ( $F_{\text{rad}}$ ). The primary acoustic radiation force depends on the size of the particle, the density and compressibility of the particle and the surrounding fluid and the gradient of the acoustic pressure and acoustic velocity fields. In Chapter 4, the physics of acoustophoresis is described in more detail.

Acoustophoresis has the advantage of being label-free, and for example in Paper III it was shown that cells can be manipulated and enriched in droplets, Figure 16(a). Other advantages using bulk acoustic waves are that it allows for switching of particles between different daughter droplets (Paper III), as well as binary separation of particles based on the acoustic properties of the particles (Paper V). The main drawback of the method is that the microfluidic chips should be fabricated in a material with high acoustic impedance (section 4.1).<sup>60</sup>

In addition to bulk acoustic waves also surface acoustic waves (SAW) can be used to move particles inside droplets. Park *et al.* developed a system for separation of 5  $\mu\text{m}$  and 10  $\mu\text{m}$  polystyrene particles encapsulated inside droplets by using travelling surface acoustic waves at two separate frequencies, Figure 16(b).<sup>57</sup>

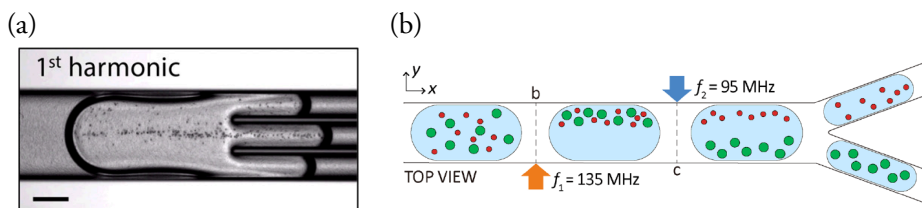


Figure 16. (a) In a bulk acoustic standing wave-field yeast cells are focused to the centre of the droplet, and in the droplet split the cells are enriched the centre daughter droplet. The scale bar is 150  $\mu\text{m}$ . (b) Separation of 5  $\mu\text{m}$  and 10  $\mu\text{m}$  particles inside droplets using travelling surface waves by first applying one frequency (135 MHz) in one direction and then a second frequency (95 MHz) in the opposite direction. (a, b) Reproduced from Ref. 61, 57 with the permission of AIP Publishing.

### 3.5 Dielectrophoresis

Another commonly used label-free particle manipulation method in microfluidics is dielectrophoresis. In this method, a non-uniform electric field is applied, and that induces a force on the particles.<sup>62</sup> It should be emphasised that since a non-uniform electric field is used, the particles do not need to be charged but only to have dielectric properties to be affected by the force. The dielectric force on a particle depends on the size of the particle, the permittivity and conductivity of the particle and the surrounding fluid and the gradient of the electric field.

Recently, Han *et al.* used dielectrophoresis in combination with an asymmetric droplet split to enrich particles as well as cells inside droplets, Figure 17.<sup>58</sup> Using this system, they achieved nearly 6 times enrichment of polystyrene microbeads into one of the daughter droplets and on average 90% recovery of particles, although the throughput of the system was less than 1  $\mu\text{L}/\text{min}$ .

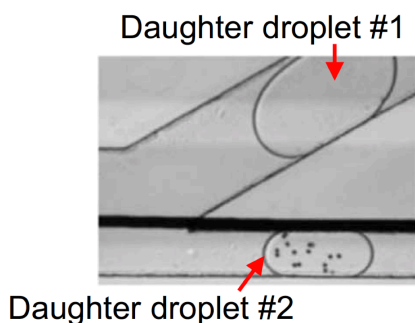


Figure 17. Dielectrophoresis is used in combination with a droplet split to enrich microbeads into one of the formed daughter droplets. Reprinted from Ref. 58. Copyright 2017, with permission from Elsevier.



## 4. Acoustics

The first report of manipulation of particles using acoustic standing waves dates back to 1866 when the German physicist August Kundt observed that dust particles in a tube could be positioned at specific locations by applying sound at certain frequencies.<sup>63</sup> Likewise, acoustic standing waves can be used to manipulate suspended particles in microfluidic channels. There are numerous studies where acoustophoresis is applied to focus, enrich and separate particles in single-phase microfluidic systems.<sup>64–67</sup> In this thesis it is shown for the first time that acoustophoresis can be used to manipulate particles encapsulated inside droplets. This chapter presents the basic physics of acoustic particle manipulation in microfluidic systems.

### 4.1 Sound waves and acoustic resonance

Sound is mechanical waves that propagate through a medium. When a sound wave meets a medium with different acoustic impedance ( $z$ ) part of the wave is transmitted and part of the wave is reflected, Figure 18(a). The ratio between the reflected wave and the incident wave is given by,

$$\frac{p_r}{p_i} = \frac{z_2 - z_1}{z_2 + z_1} \quad (5)$$

where  $p_i$  and  $p_r$  are the pressure amplitudes of the incident and the reflected waves and  $z_1$  and  $z_2$  are the acoustic impedances of the two different media.<sup>68</sup> The acoustic impedance is related to the material properties of the medium, and is calculated as  $z = \rho c$  where  $\rho$  is the density and  $c$  is the speed of sound of the medium.

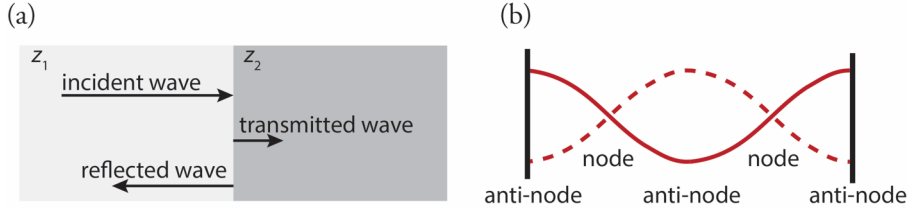


Figure 18. (a) At an interface part of the sound wave is reflected and part of the sound wave is transmitted. (b) A standing wave with pressure nodes and pressure anti-nodes results when two waves with the same frequency and amplitude but with the opposite travelling directions are superimposed.

When two sound waves meet, such as the incident wave and the reflected wave, the two waves are superimposed. If the two waves travel in the opposite directions and have the same frequency and amplitude a standing wave results. A standing wave is characterised by that the wave is not moving in any direction. Some points on the wave have minimal pressure amplitude (nodes) and other points have maximal pressure amplitude (anti-nodes), Figure 18(b).

In the experiments described in Paper I-V an acoustic standing wave-field was generated in the channels by vibrating the entire microfluidic chip using bulk acoustic waves (BAW). To generate an acoustic standing wave-field in a microchannel using BAW basically two requirements should be fulfilled. First, the microfluidic chip should be fabricated in a high acoustic impedance material.<sup>60</sup> Having a large difference in the acoustic impedance between the fluid and the chip material has the consequence that most of the wave is bounced back and forth between the channels walls (Equation (5)). Secondly, the frequency of the sound ( $f$ ) should be matched to the dimensions of the channel so that acoustic resonance occurs. To generate resonance between the channel walls the width of the channel ( $w$ ) should be a multiple half wavelengths,

$$w = n\lambda/2 \quad (6)$$

where  $\lambda$  is the wavelength of the sound and  $n = 1,2,3 \dots$  corresponds to the first harmonic (sometimes called the fundamental resonance), second harmonic and third harmonic. The wavelength of the sound is related to the frequency and the speed of sound ( $c$ ) in the material according to

$$f = c/\lambda \quad (7)$$

Fulfilment of Equation (6) yields a standing wave across the channel width. As shown in Paper IV a standing wave can also be created from the top to the bottom of channel by using a second frequency that is matched to the channel height

---

instead. Alternatively, a standing wave can be created in both the height and width direction by using a square microchannel.

## 4.2 Generation of acoustic waves

In microfluidics the channels are typically a couple of hundred micrometres in width and for example the speed of sound of water is  $\sim 1500$  m/s, thus the frequency for generation of a bulk acoustic standing wave-field in the channel is typically in the MHz range (Equation (6) and (7)). Sound waves in that frequency range are called ultrasound, and are commonly generated using piezoelectric transducers.

A piezoelectric material is characterised by that when a voltage is applied it will cause the material to be compressed or stretched, Figure 19.<sup>68</sup> Likewise, if an external force is applied that compress or stretch the material a voltage will be generated.

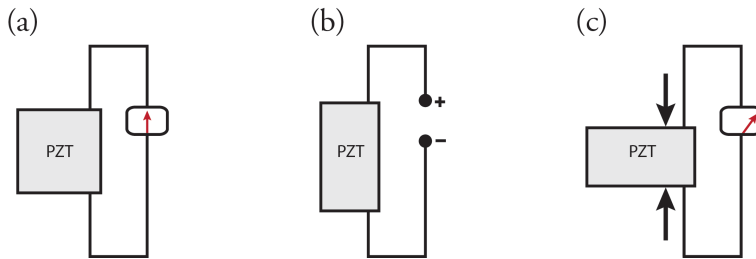


Figure 19. (a) No voltage or stress is applied over the piezoelectric material. (b) When a voltage is applied, the piezoelectric material will be stretched (or compressed). (c) When the material is compressed (or stretched), a voltage will be generated instead.

The most common material used for the fabrication of ultrasonic transducers is a ceramic material consisting of lead zirconate titanate (PZT).<sup>68</sup> The piezoelectric effect of PZT is related to the presence of dipoles in the material which in turn is related to the crystal structure of the material (perovskite crystal structure). Inherently the material shows no piezoelectricity as the dipoles are distributed randomly, Figure 20(a). However, the material can be made piezoelectric by orienting all the dipoles in the same direction by applying a strong electric field at elevated temperature, Figure 20(b).<sup>69</sup> After removing the electric field and decreasing the temperature the alignment of the dipoles remains and the material shows piezoelectric properties.



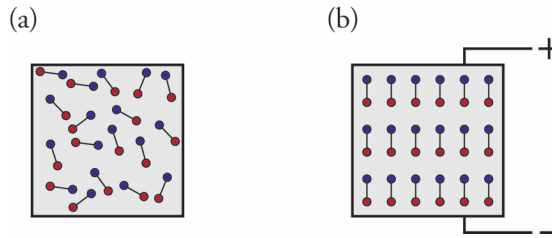


Figure 20. (a) Inherently random distribution of dipoles in the material, and the material shows no piezoelectric properties. (b) By applying a strong electric field at elevated temperature the dipoles are aligned. This alignment remains after the electric field is removed and the temperature is decreased, and gives the material piezoelectric properties.

In the experiments described in this thesis a piezoelectric plate made of PZT (the transducer) was glued to the microfluidic chip, and a high frequency (MHz) AC signal was applied over the transducer. This caused the entire chip to vibrate, and enabled the build-up of a standing wave in the channel when the frequency was matched to the channel dimensions. The thickness of the piezoelectric transducer is of importance as the piezoelectric transducer vibrates most strongly when the thickness corresponds to a half wavelength in the piezoelectric material.<sup>68</sup> Thus, to generate a strong acoustic wave-field in the channel the thickness of the transducer should be carefully selected depending on the operation frequency of the system.

In addition to BAW which have been used in this PhD project, surface acoustic waves (SAW) can be used to manipulate particles in microfluidic channels.<sup>70</sup> In contrast to BAW systems where the sound waves propagate throughout the entire microfluidic chip, in SAW systems the acoustic waves are generated by actuating interdigital transducers placed on a piezoelectric substrate and then the generated acoustic waves propagate along the surface and are coupled into the microfluidic channel.

### 4.3 Acoustic forces on particles

#### Primary acoustic radiation force

A particle in an acoustic standing wave-field is moved to the pressure nodes or anti-nodes by the primary acoustic radiation force, Figure 21. This force results from the scattering of sound waves on the particle. Assume the simplest case, a one-dimensional standing wave-field and half wavelength resonance (i.e. the first

harmonic), then the primary acoustic radiation force,  $F_{\text{rad}}$ , on a small particle ( $a \ll \lambda$ ) is given by,<sup>71</sup>

$$F_{\text{rad}} = 4\pi\Phi(\tilde{\kappa}, \tilde{\rho})ka^3E_{\text{ac}}\sin(2ky) \quad (8a)$$

$$\Phi = \frac{1}{3}\left(\frac{5\tilde{\rho}-2}{2\tilde{\rho}+1} - \tilde{\kappa}\right) \quad (8b)$$

$$\tilde{\rho} = \frac{\rho_{\text{particle}}}{\rho_{\text{fluid}}} \quad (8c)$$

$$\tilde{\kappa} = \frac{\kappa_{\text{particle}}}{\kappa_{\text{fluid}}} \quad (8d)$$

where  $a$  is the radius of the particle,  $\lambda$  is the wavelength of the sound,  $\Phi$  is the acoustic contrast factor,  $k$  is the wave number ( $k = 2\pi/\lambda$ ),  $E_{\text{ac}}$  is the acoustic energy density,  $y$  is the distance from the channel wall,  $\rho$  is the density of the particle and the surrounding fluid and  $\kappa$  is the compressibility of the particle and the surrounding fluid. The compressibility of a fluid is calculated as  $\kappa = 1/(c^2\rho)$  and the compressibility of a solid is calculated as  $\kappa = 1/K$  where  $K$  is the bulk modulus of the material.

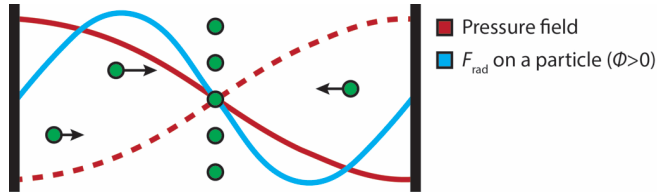


Figure 21. The primary acoustic radiation force ( $F_{\text{rad}}$ ) on a positive acoustic contrast particle (green circle) in a half wavelength standing wave-field.

The primary acoustic radiation force causes a movement of the suspended particles, and the velocity of a particle ( $v$ ) can be calculated by balancing the primary acoustic radiation force (Equation (8a)) and the drag force (Equation (3)),

$$F_{\text{rad}} = F_{\text{drag}} \quad (9a)$$

$$v = \frac{2\Phi(\tilde{\kappa}, \tilde{\rho})ka^2E_{\text{ac}}\sin(2ky)}{3\eta} \quad (9b)$$

where  $\eta$  is the viscosity of the fluid. The direction of the primary acoustic radiation force on a particle depends on the sign of the acoustic contrast factor (Equation (8b)), which in turn depends on the acoustic properties of the particle in relation to the surrounding fluid. If the sign of the acoustic contrast factor is positive ( $\Phi > 0$ ) the particle is moved to the pressure node whereas if the sign is negative ( $\Phi < 0$ ) the particle is moved to the pressure anti-nodes.

Typically, cells and plastic microbeads have positive acoustic contrast in water, but it also exists some particle species that have negative acoustic contrast such as lipid particles<sup>64,72</sup> or particles made of polydimethylsiloxane (PDMS).<sup>73,74</sup> By using particles with opposite acoustic contrast it is possible to separate two different particle species from each other.<sup>64,72–74</sup> In Paper V a system was developed where two particle species (polystyrene microbeads and in-house synthesised PDMS particles) originally encapsulated in the same droplet were separated into different daughter droplets based on the acoustic properties of the particles.

In addition to aligning particles in the lateral direction, acoustophoresis can also be used to position particles in the vertical direction by matching the frequency to the channel height instead (Equation 6). As shown in Paper IV by implementing two-dimensional acoustophoresis particles can be aligned in both the lateral and vertical direction. Assuming positive acoustic particles and the first harmonic, this results in that the particles are focused into a narrow beam in the centre of the channel, Figure 22. By implementing two-dimensional acoustophoresis all particles are placed in the same flow stream.

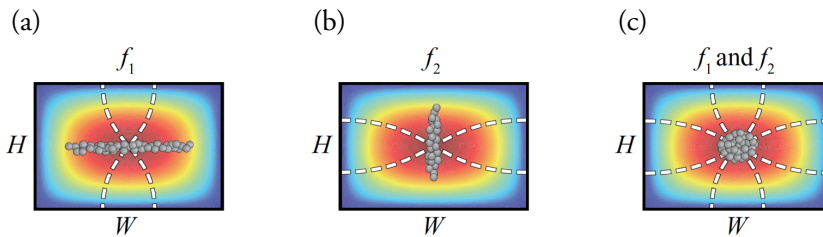


Figure 22. (a) Acoustic particle focusing in the vertical direction. The colour plot shows the parabolic flow velocity profile in a microchannel. The red colour represents maximum fluid velocity and the blue colour represents zero fluid velocity. (b) Acoustic particle focusing in the lateral direction. (c) Combining vertical and lateral acoustic particle focusing (i.e. two-dimensional acoustophoresis) result in that positive acoustic contrast particles are focused into a narrow beam in the centre of the channel. Reproduced from Ref. 75 with the permission of IOP Publishing.

Moreover, acoustic particle manipulation is not limited to the first harmonic, but higher harmonics can be used as well (Equation 6). For example, at the second harmonic there are two pressure nodes, one located at  $y = w/4$  and one located at  $y = 3w/4$ , thus positive acoustic contrast particles are positioned in two lines instead of only one, Figure 23. In Paper III the frequency was switched between the first and second harmonic to direct particles into either the centre outlet or the side outlets.

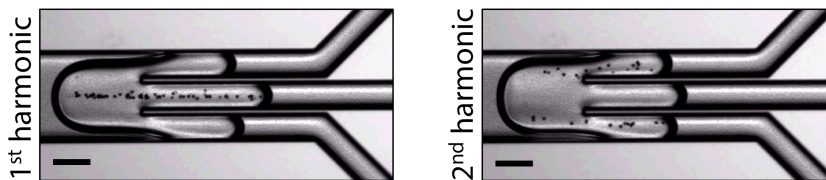


Figure 23. Acoustic focusing of polystyrene microbeads inside droplets at the first and second harmonic. The scale bars are 150  $\mu\text{m}$ . Reproduced from Ref. 61 with the permission of AIP Publishing.

## Particle-particle interaction and acoustic streaming

Particles having a diameter above 1-2  $\mu\text{m}$  are mainly affected by the primary acoustic radiation force, but the particles are affected by the acoustic field in other ways as well such as particle-particle interaction and acoustic streaming.

The particle-particle interaction is sometimes called the secondary acoustic radiation force, and this force is most important at high particle concentrations.<sup>76</sup> As the particle concentrations in the experiments described in the included papers are low, it is assumed that particle-particle interaction does not play a dominant role in these experiments. Related, in Paper III it was observed that no significant difference in the particle enrichment performance was measured when the number of particles per droplet was varied, which is a further indication that particle-particle interaction does not play a significant role in that particular experiment.

The acoustic field does not only affect the particles directly, but also induces acoustic streaming in the fluid. In single-phase systems acoustic streaming has been studied extensively,<sup>77</sup> but the particular effects of acoustic streaming in droplet microfluidic systems have not been investigated in any detail. Generally, acoustic streaming becomes most important for small particles and sets the limit for how small particles that can be focused.<sup>78</sup> In the papers included in this thesis the particles and cells are at least a few micrometre in size, and hence it is assumed that acoustic streaming does not play a dominant role in the described experiments. Furthermore, the internal motions inside droplets are probably more dominating than the acoustic streaming.

## Numerical simulations

Simulations are often very valuable to understand the governing physical principles, and in the studies described in Paper II and IV numerical simulations were performed using the finite-element solver COMSOL Multiphysics.

The physical model behind acoustic particle manipulation is very complex and there are many aspects that need to be considered. The acoustic field and the resulting force on a particle depends on several factors such as the actuation mode, the material and size of the chip and the transducer, the channel dimensions, the fluid and particle properties etc. In the study described in Paper II the acoustic field inside a water droplet confined in a microfluidic channel was simulated. The results showed that to achieve good quality acoustic focusing of the encapsulated particles it is important to match the acoustic properties of the dispersed and continuous phase.

As mentioned in section 2.2 particles inside droplets exposed to an acoustic standing wave-field are not only affected by the acoustic forces but by the internal fluid flows arising from the movement of the droplets in the channel as well. These internal fluid flows can be simulated, and in the study described in Paper IV the positioning of encapsulated particles inside moving droplets with and without prior acoustic particle focusing was investigated. First the flow velocity field inside the droplets was determined, and then a particle trajectory model was used to study the particle positioning within the droplets.

These two examples described in Paper II and IV show how simulations can be useful to increase the physical understanding and explain experimental observations. Numerical simulations can also provide guidance in the design of the microfluidic systems and when setting up the experiments.

### 4.4 Acoustic forces acting on immiscible fluid interfaces

The interaction of acoustic forces with the fluid interface in immiscible systems was studied long before the emergence of droplet microfluidics. Already in 1939 Hertz and Mende showed that when a sound beam hits an immiscible fluid interface where the two fluids have different speed of sound the interface is deflected upwards or downwards, Figure 24.<sup>79</sup>

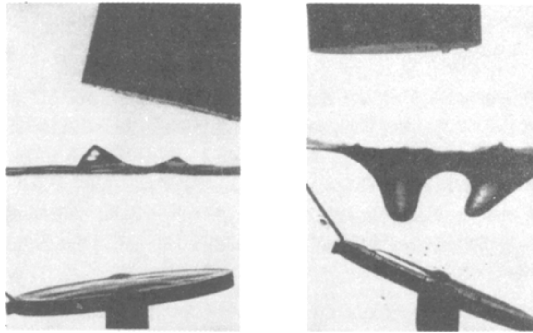


Figure 24. Deflection of fluid interfaces caused by a sound beam. In the left photograph it is water on top of  $\text{CCl}_4$  and in the right photograph it is water on top of aniline. The direction of the deflection of the interface depends on the speed of sound of the fluids. The speed of sound of  $\text{CCl}_4$  is lower than water causing the interface to be deflected upwards while the speed of sound of aniline is higher than water causing the interface to be deflected downwards. Note that the deflection is independent of the direction of the sound beam. Reproduced from Ref. 79.

In the experiments performed in this PhD project deflection of immiscible fluid interfaces has been observed in droplets confined in microfluidic channels, Figure 25. In the experiment it was observed that at application of the ultrasound at certain frequencies the fluid interface was deformed by the ultrasound. This effect was only observed for water droplets surrounded by fluorinated oil and not for water droplets surrounded by olive oil. This is probably related to the fact that there is a large difference in the acoustic properties between fluorinated oil and water but not between olive oil and water (Table 2 in section 6.1). Further, it should be noted that the deformation of the fluid interface was only observed at application of the ultrasound at certain frequencies and not the same as the frequency for particle focusing. However, to explain the physics of the observed phenomenon more research is needed.

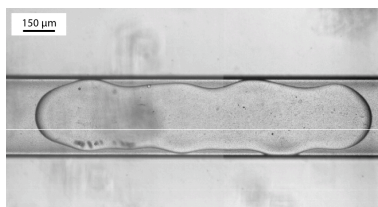


Figure 25. Deformation of the droplet interface caused by the application of the ultrasound. The dispersed phase is water having a speed of sound of 1497 m/s and the continuous phase is fluorinated oil with 2% surfactant (Krytox) having a speed of sound of 659 m/s. The frequency of the applied ultrasound in this experiment is 2.15 MHz. The deformation of the fluid interface is only observed at certain frequencies. The white line in the photograph is an artefact from the camera.

There are several reports on droplet microfluidic systems based on the interaction of acoustic forces with the interface between the dispersed and continuous phase. Schmid and Franke developed a microfluidic system where SAW were used to control the length of droplets generated in a flow focusing device.<sup>80</sup> It was shown that higher power of the SAW resulted in shorter droplets. Jung *et al.* developed a system where SAW was used to split one droplet into two daughter droplets, and they observed that in the splitting event particles inside the droplets were pushed backwards and always ended up in the last daughter droplets.<sup>43</sup>

### 4.5 Biocompatibility of acoustophoresis

From a biological perspective, acoustophoresis has two clear advantages namely that the method requires no labelling of biological sample and that the method is gentle to cells. Burguillos *et al.* tested several cell types and showed that acoustophoresis did not change cell viability and proliferation, and that the cells kept their normal cellular functions.<sup>81</sup> However, when comparing such results one should be careful as different cell types, microfluidic systems and experimental conditions may perform differently.<sup>82</sup>

For example, one aspect that is very much dependent on the microfluidic chip and the experimental conditions is the temperature rise caused by actuation of the transducer. The amount of heating depends on the applied voltage over the transducer, thus in cell experiments the applied voltage needs to be limited to not generate temperatures above 37°C in the channel. One way to improve the temperature control is by integrating active cooling to the system.<sup>83,84</sup>

Another chip related aspect is that BAW systems are often made in silicon or glass that do not allow for gas exchange, and this aspect need to be considered in long-term cell experiments.

# 5. Microfluidic chip fabrication

In this chapter the material considerations and the methods used to fabricate the microfluidic chips used in the experiments described in Paper I-V are discussed.

## 5.1 Microfluidic chip materials

Droplet microfluidic chips can be fabricated in various materials, such as polymers, glass and silicon.<sup>85</sup> In academic research an elastic polymer called polydimethylsiloxane (PDMS) is often used to make microfluidic chips through a process called soft lithography.<sup>86</sup> This fabrication method is often preferred in research as it allows for rapid and cheap prototyping. Other advantages of using PDMS as chip material includes that it is a transparent material and has high gas permeability which is important in biological assays with living cells.<sup>87</sup> As an alternative to soft lithography, polymer microfluidic chips can be made of thermoplastics such as polymethylmetacrylate (PMMA) or polycarbonate (PC).<sup>85</sup> Microfluidic chips made of thermoplastics have the advantage that they can be fabricated using for example injection molding which is a fabrication process well-suited for mass production.

However, certain applications require materials with specific properties such as high mechanical stability or high resistance to chemicals, and in these applications polymers may not be suitable materials. For example bulk acoustic wave (BAW) systems are preferentially fabricated in rigid materials that have high acoustic impedance to allow for the build-up of a strong acoustic standing wave-field in the channel (section 4.1).<sup>60</sup> Accordingly, BAW systems are often etched in silicon or glass and sealed with glass lids. Figure 26 shows acoustic particle focusing in droplets in a silicon and glass channel, respectively.



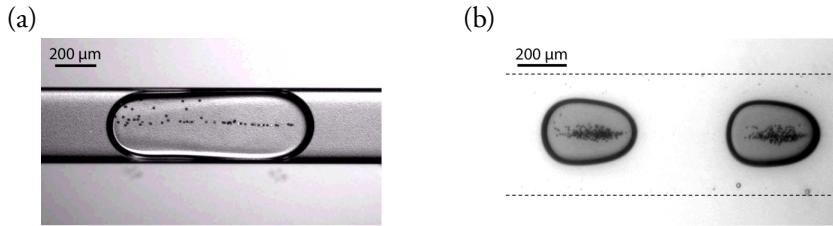


Figure 26. (a) Acoustic particle focusing in a water droplet in a silicon channel. (b) Acoustic particle focusing in a water droplet in a glass channel. The dashed lines indicate the width of the channel at the top.

Of these two materials, silicon has the advantage that it is a crystalline material and channels with vertical walls can be fabricated by wet etching. Glass on the other hand is a non-crystalline material, and wet etching of glass is an isotropic process yielding channels with rounded walls. The advantage using glass is that it is an optical transparent material, and for example in some microscopy techniques it is advantageous to look at the transmitted light instead of the reflected light. In the experiments described in Paper I-V silicon-glass microfluidic chips were used, where the channels were etched in silicon and sealed with transparent glass lids.

### 5.2 Silicon etching methods

Methods to etch structures in silicon are used extensively in the microelectronic and microelectromechanical systems (MEMS) industry, and the same microfabrication processes can be applied to fabricate microfluidic systems.<sup>88</sup> Silicon can be etched using either wet etching or dry etching.<sup>89</sup>

Wet etching of silicon can be accomplished using a few different chemicals where some etchants are crystalline dependent whereas others are crystalline independent.<sup>90</sup> For example KOH as used to fabricate the chip described in Paper I, etches the (100)-plane of single-crystal silicon much faster than the (111)-plane which is almost not etched at all.<sup>90</sup> For acoustic particle manipulation, channels with vertical walls are often preferred, and this can for example be realised by KOH wet etching on a (100) silicon wafer by orientating the channels 45° with respect to the primary flat (Figure 27), but this comes at the expense that the channels parallel or vertical with the primary flat will have a V-shape or trapezoidal-shape. Consequently, the orientation-dependence of KOH wet etching limits the design possibilities, and instead dry etching such as deep reactive-ion etching (DRIE) is often favoured in microfluidic applications. DRIE has the advantage that channels with vertical walls can be fabricated independent of the crystal planes. However, the

---

main disadvantage with DRIE is that it requires expensive equipment not found in every cleanroom.

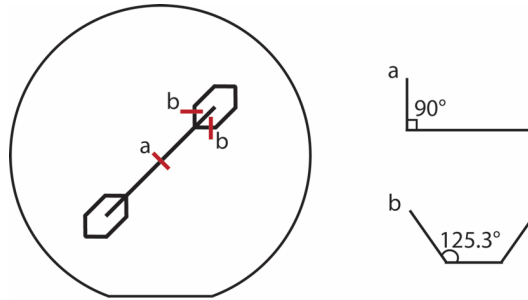


Figure 27. KOH wet etching of (100) silicon. Channels oriented  $45^\circ$  to the primary flat (line a) will have a rectangular cross-section while the channels parallel or vertical with the primary flat (line b) will have a V-shape or trapezoidal-shape.

## 5.3 Microfabrication

In this section the steps for fabricating the silicon-glass microfluidic chips used in the experiments included in this thesis are described. The chip used in the experiments described in Paper I was fabricated by KOH wet etching and the chips used in the experiments described in Paper II-V were fabricated by DRIE. The two different fabrication processes are summarised in Figure 28.

### Photomask

The first step in both the processes was the fabrication of photomasks that could be used to define the channels on the silicon wafers in the UV-photolithography step. The design of each photomask was drawn in a CAD program. Channels etched with KOH do not necessarily have the same final dimensions as the photomask, and consequently this needed to be taken into consideration in the design process. As an example, the final width of the main channel etched on a (100) silicon wafer where the main channel is orientated  $45^\circ$  to the primary flat (Paper I, Figure 27(a)) is the width of the main channel on the mask plus twice the depth of the channel. However, channels fabricated using DRIE have the same final width as on the photomask (Paper II-V).

## 5. Microfluidic chip fabrication

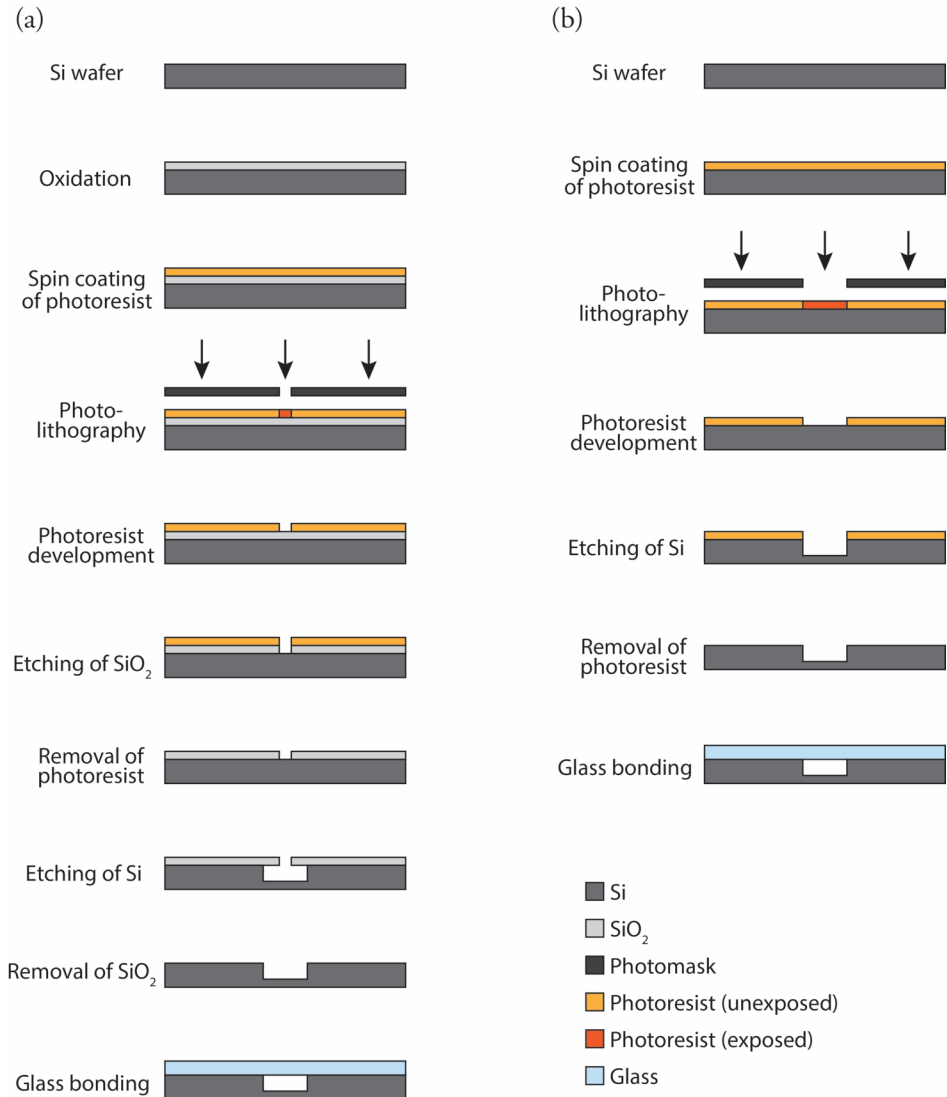


Figure 28. The process steps for fabrication of silicon-glass microfluidic chips using (a) KOH wet etching and (b) DRIE.

---

After designing the photomask, a mask writer was used to transfer the design onto a glass-chromium plate covered with a layer of light sensitive polymer (in this case a positive photoresist). A positive photoresist has such properties that it becomes more soluble in the response to light.<sup>90</sup> The mask writer uses a technology called direct writing lithography where a laser is used to create the pattern in the photoresist by illuminating certain areas of the photoresist according to the design in the CAD file. The glass-chromium plate was then developed using a photoresist developer, and the illuminated areas of the photoresist were dissolved while the unilluminated photoresist remained. This resulted in areas on the glass-chromium plate with bare chromium, and these areas were then removed by etching, and a transparent pattern where light could shine through was obtained.

## **Photolithography**

For transferring the pattern defined by the photomask onto the silicon wafer UV-photolithography was used. A thin layer (1-2  $\mu\text{m}$ ) of positive photoresist was spin coated onto the wafer, and the patterns were defined in the photoresist layer by UV-light exposure through the photomask. The exposed areas were then dissolved using a photoresist developer. Since KOH wet etching is a crystalline dependent etch method the mask orientation and alignment on the silicon wafer was crucial for the final result, but in DRIE the mask orientation and alignment was not of importance.

## **Etch mask**

In order to define the structures to be etched on the silicon wafers etch masks were needed. As the etch mask is exposed to the etchants, it is important that the etch mask withstand the etchants. For the KOH wet etching process,  $\text{SiO}_2$  was used as the etch mask. An extremely thin layer of  $\text{SiO}_2$  forms spontaneously on silicon wafers (native oxide), but to create a slightly thicker layer of  $\text{SiO}_2$  thermal oxidation was employed. The  $\text{SiO}_2$  etch mask was realised, after the photolithography step, by etching using buffered-HF. In DRIE no additional etch mask needed to be fabricated as the photoresist itself functioned as the etch mask.

## **Etching**

After defining the etch mask on the wafer the channels were etched. The microfluidic chips described in Paper I were fabricated on a (100) silicon wafer using KOH wet etching where the main channels were orientated  $45^\circ$  to the primary flat.

## 5. Microfluidic chip fabrication

---

As KOH etches the (100)-plane but not the (111)-plane to any significant degree, channels with vertical walls were created, Figure 29(a). The KOH etch rate depends on the KOH concentration and the temperature,<sup>91</sup> thus these two parameters as well as the etch time needed to be carefully monitored to obtain channels with the desired depth and width.

The microfluidic chips described in Paper II-V were fabricated using DRIE.<sup>92</sup> In this process a plasma (in my experiments  $\text{SF}_6$  ions) was used to etch the channels, however to protect the channel walls the plasma etching step was repeatedly cycled with the deposition of a passivation layer (in my experiments  $\text{C}_4\text{F}_8$ ). These repeated cycles of etching and passivation make it possible to fabricate deep channels with vertical walls irrespective of the crystal orientation of the silicon wafer, and in Figure 29(b) a photograph of one of the fabricated channels is shown. In Figure 29(c) a more detailed photograph of the channel wall is shown, and here the traces of the repeated cycles of etching and passivation can be observed.

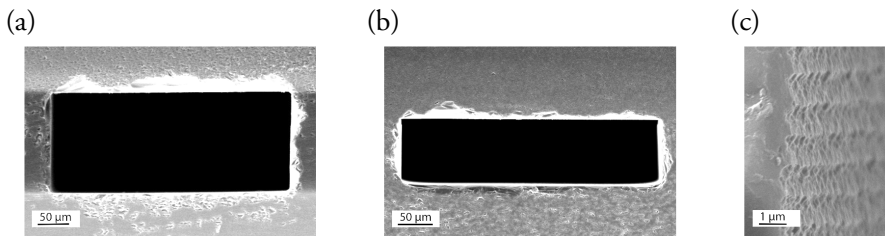


Figure 29. (a) A scanning electron microscopy (SEM) image of a channel fabricated using KOH wet etching. The channel is fabricated on a (100) silicon wafer where the channel is oriented  $45^\circ$  to the primary flat. (b) SEM image of a channel fabricated using DRIE. (c) SEM image showing the channel wall fabricated using DRIE. The wavy structure is a result of the etching and passivation cycles. Image courtesy M. Andersson and K. Svensson.

### Glass bonding

After etching, the silicon channels were sealed, and this was accomplished by anodic bonding of glass lids.<sup>93</sup> The silicon and glass surfaces were put in close contact at elevated temperature ( $\sim 500^\circ\text{C}$ ) and a DC voltage ( $\sim 1$  kV) was applied over the surfaces (silicon-anode and glass-cathode). The applied electric potential caused the formation of a strong electrostatic bond between the silicon and the glass surfaces. However, it should be noted that a pre-requisite for this to occur is that the surfaces are extremely clean.

---

## World-to-chip connection

Before bonding the glass wafer to the silicon, fluidic inlet and outlet holes were made either by etching holes through the silicon wafer from the backside or by drilling holes. After bonding of the glass lid, short pieces (~1 cm) of silicone tubing were glued to the inlet and outlet holes as fluid connectors.

## Surface modification

To allow for the generation of water droplets surrounded by oil and high droplet stability, the microfluidic channels need to be hydrophobic. This was accomplished in my experiments by flushing the channels with a solution of  $\text{Si}(\text{CH}_3)_2\text{Cl}_2$  in  $[(\text{CH}_3)_2\text{SiO}]_4$  (Repel-Silane).

## Acoustic actuation

The final step in the fabrication process was the attachment of the piezoelectric transducer. Electrical wires were soldered on the piezoelectric transducer, and the transducer was glued to the microfluidic chip using low viscosity cyanoacrylate glue. The piezoelectric transducer could be placed on either the silicon side or the glass side of the chip. In Figure 30 a photograph of the complete microfluidic chip is shown.

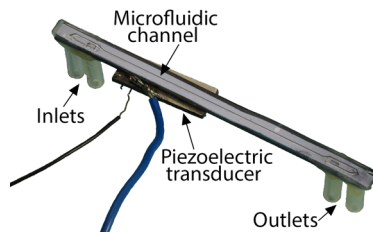


Figure 30. Photograph of a silicon-glass microfluidic chip. The length of the chip is 5.5 cm.



# 6. Experimental methods

This chapter aims to introduce the materials and experimental methods that have been used in the studies described in Paper I-V.

## 6.1 Fluids and particles

In this PhD project mainly two different two-phase systems were studied: water droplets in fluorinated oil (HFE-7500) and water droplets in olive oil. The properties of these fluids are presented in Table 2. A drop tensiometer was used to measure the interfacial tension between water and the oils. The viscosities of the fluids were measured using a falling ball microviscometer, except for the viscosity of water that is reprinted from CRC Handbook of Chemistry and Physics.<sup>94</sup> The density and speed of sound were measured using a Density and Sound Velocity Meter.

*Table 2. Fluid properties.*

| Fluid                                       | Interfacial tension to water (mN/m) | Viscosity (mPas) | Density (kg/m <sup>3</sup> ) | Speed of sound (m/s) |
|---|-------------------------------------|------------------|------------------------------|----------------------|
| Water                                       | -                                   | 0.89             | 997                          | 1497                 |
| Fluorinated oil (with 0% Krytox surfactant) | 41                                  | 1.20             | 1619                         | 660                  |
| Fluorinated oil (with 2% Krytox surfactant) | 15                                  | 1.32             | 1621                         | 659                  |
| Olive oil                                   | 16                                  | 60.8             | 910                          | 1450                 |

In the experiments described in Paper I-V various types of particles were used. As positive contrast particles polystyrene beads (5  $\mu\text{m}$  or 10  $\mu\text{m}$  in diameter) were used, and as negative acoustic particles PDMS particles were synthesised and used. For the cell experiments red blood cells and yeast cells were used. In Table 3 the acoustic properties and the calculated acoustic contrast factor for the particles used in the experiments are presented. Data for yeast cells are not included in the table as the speed of sound of yeast cells were not found in the literature, however the acoustic



## 6. Experimental methods

particle focusing experiments proved that yeast cells have positive acoustic contrast in water.

Table 3. Acoustic properties of particles.

| Particle          | Density (kg/m <sup>3</sup> ) | Speed of sound (m/s) | Calculated values for the acoustic contrast factor in water |
|-------------------|------------------------------|----------------------|---|
| Polystyrene beads | 1059 <sup>95</sup>           | 1493 <sup>95</sup>   | 0.038   |
| Red blood cells   | 1103 <sup>95</sup>           | 1510 <sup>95</sup>   | 0.070   |
| PDMS particles    | 965 <sup>60</sup>            | 1076 <sup>60</sup>   | -0.344  |

### 6.2 Experimental setup

The microfluidic chip (section 5.3) is the core component of the experimental setup, but the experimental setup consists of several other important parts. The exact setup differs slightly between the five papers, but in Figure 31 a schematic figure of a typical setup is shown.

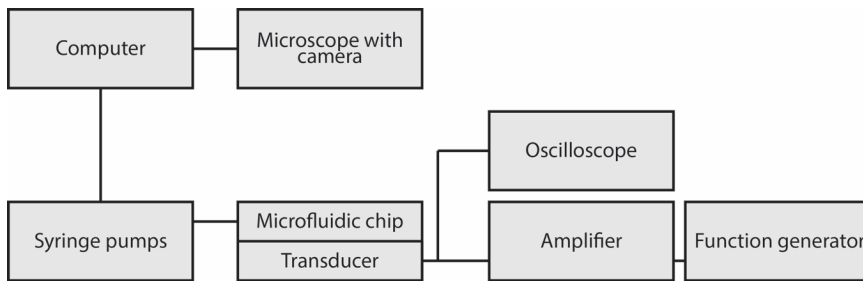


Figure 31. Schematic of the experimental setup.

#### Control of the fluids

Precise control of the fluids is crucial for stable operation of the microfluidic chip, and this is often realised by using syringe pumps or a pressure driven system. In the experiments described in Paper I-V syringe pumps were used to inject or withdraw the fluids. It is wise to consider the fluidic setup already in the design of the chip as this may simplify the setup. For example the microfluidic chips used in the experiments described in Paper I, III and IV were designed with the two side outlets joined on the chip to reduce the number of syringe pumps needed.

---

## Electrical setup

In the experiments the piezoelectric transducer was actuated by an AC signal, and the frequency of the signal was manually adjusted to find the resonance frequency where the particles were most strongly aligned. An oscilloscope was used to monitor the voltage over the transducer. From the function generator the maximum amplitude of the output signal was  $10 V_{\text{peak-peak}}$  at a load of  $50 \Omega$  and  $20 V_{\text{peak-peak}}$  when the load impedance goes to infinity. In Paper I-III and V the output signal from the function generator was amplified before connected to the transducer. However, depending on the flow rates amplification of the signal might not be needed. In Figure 32 the same chip design as described in Paper V is operated without amplification of the output signal, and as seen in the figure the particles are still aligned.

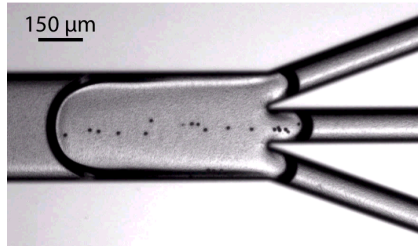


*Figure 32. Acoustic particle focusing in a droplet without amplification of the electrical signal. The output voltage from the function generator is  $10 V_{\text{peak-peak}}$  and the total flowrate in the experiment is  $3 \mu\text{L}/\text{min}$ .*

## Optical setup

The microfluidic chips were studied using an optical microscope equipped with a camera. In the experiments described in Paper I-III and V a non-inverted microscope was used while in the experiment described in Paper IV an inverted microscope was used. For the experiments performed in this thesis both microscope configurations works equally well, and it is more a matter of convenience regarding for example how to have space to connect fluidic tubings and the possibility to observe the channels with the eye.

When using optical microscopy there are some aspects to consider such as the resolution of the acquired images and the depth of field so that the critical features are not ignored. Another aspect that is especially important when continuous events are studied is the frame rate of the camera, and to display the events correctly and avoid aliasing the frame rate of the camera should be sufficiently high.

Another effect that may occur in droplet microfluidic systems that can hide important features is the dark border around the droplets, Figure 33. This dark border arises due to the different refractive indices of the dispersed and continuous phase.<sup>96</sup> For example water has a refractive index of 1.33 while olive oil has a refractive index of approximately 1.46-1.48,<sup>97</sup> and this large difference in refractive index gives rise to a very thick black border (Figure 33(a)). On the other hand the refractive index of fluorinated oil is only 1.29,<sup>98</sup> and a much thinner black border is observed for water droplets surrounded by fluorinated oil (Figure 33(b)).

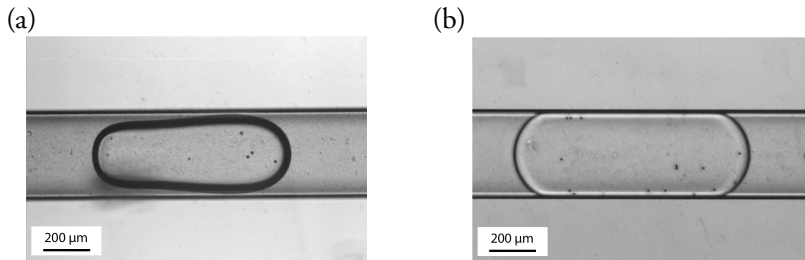


Figure 33. (a) A water droplet surrounded by olive oil. The dark border arises due to the different refractive indices of the dispersed and continuous phase. (b) A water droplet surrounded by fluorinated oil has a much thinner border.

### 6.3 Droplet volume estimation

For quantitative measurements and determination of particle concentration it is often important to know the volume of the droplets. The volume ( $V$ ) of a spherical droplet, such as the droplets described in Paper IV is easily calculated by measuring the radius ( $a$ ) and using the formula  $V = 4\pi a^3/3$ . In the experiments described in Paper I and III the droplets were confined by the channel dimensions and took a more plug-like shape. The volume of these droplets was calculated by measuring the area of the droplet from a top-view photograph, and then multiplying with the height of the channel. However, this volume estimation method introduces an error as the droplet is rounded. Musterd *et al.* have developed a method to more accurately estimate the volume of plug-like droplets from two-dimensional images in different channel geometries,<sup>99</sup> but that method is only validated for long droplets and therefore the method was not used here.

---

## 6.4 Particle counting

Quantification of the particle concentrations is the key characterisation step in particle enrichment experiments. In Paper I the concentration of particles was measured using a Coulter Counter instrument and in Paper III the number of particles was instead counted manually.

The Coulter Counter relies on the Coulter principle, in which two electrodes are used to measure the resistance change induced as particles flow through a narrow aperture one by one.<sup>100</sup> In addition, the Coulter Counter can also measure the size distribution of particles. This counting method has the advantage that it is an automatic operation and many particles can be counted easily, however it is an off-chip analysis method which may induce error in the manual collecting and handling steps. Alternatively, particles can be counted manually from the acquired microscope images, and this has the advantage that there are no further handling steps of the sample. However, to count particles manually is a laborious method if many particles are to be counted, and as it is a manual process there is a risk that some particles are accidentally not counted. Maybe more problematic is the dark ring around the droplet that may obscure particles so that they are not seen and hence not counted, section 6.2 and Figure 33. To conclude, both these counting methods have their advantages and disadvantages, and which method to choose depends on several factors such as the size and type of particles, the surface roughness of the channel and the throughput of the system.



## 7. Summary of included papers

The central theme of this PhD project has been manipulation of cells and microbeads encapsulated inside droplets using acoustophoresis, and this thesis is based on five papers (Figure 34). First I demonstrated the method and used it for particle enrichment (Paper I), and in the following paper the theoretical understanding of the system was expanded (Paper II). Next, the technology was applied for particle switching (Paper III), increased optical detection (Paper IV) and binary particle separation (Paper V) in droplets. This chapter aims to briefly introduce the five papers and highlight the most important advancements and results from each paper.

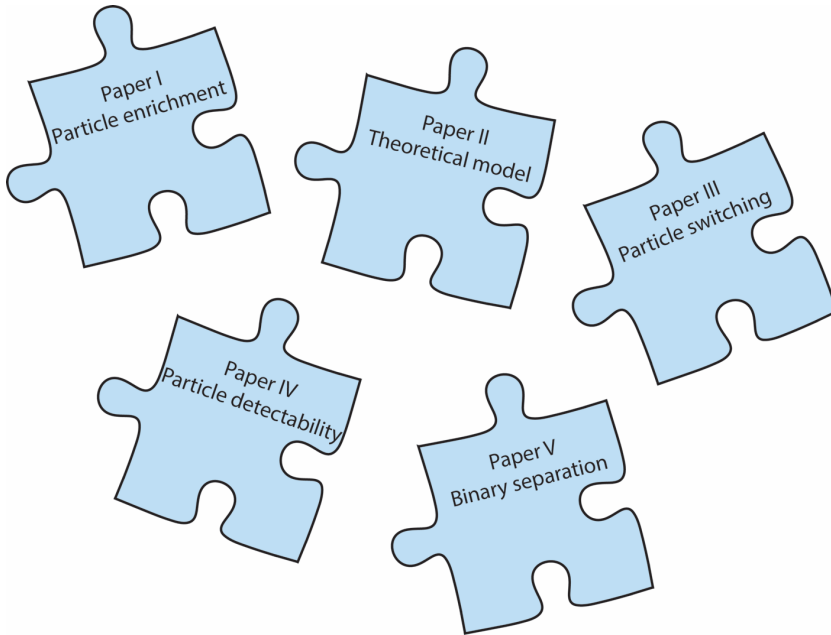


Figure 34. The five papers that constitute this thesis.

## Paper I: Controlled lateral positioning of microparticles inside droplets using acoustophoresis

One of the key bottlenecks in droplet microfluidics has been the lack of a method to control the position of cells and microbeads encapsulated inside droplets. In this paper focusing of polystyrene microbeads (5  $\mu\text{m}$ ) and red blood cells encapsulated in water-in-oil droplets using acoustophoresis is shown for the first time. The microfluidic chip was fabricated in silicon using KOH wet etching and sealed with a glass lid. To generate a standing wave-field in the channel a 2 MHz piezoelectric transducer was attached to the chip. In Figure 35(a) a schematic of the operation principle is shown. In the chip droplets containing particles were generated and acoustic forces were used to focus the encapsulated particles to the pressure node located along the centre-line of the droplet. A trident-shaped droplet split was integrated on the chip to allow for particle enrichment. With the ultrasound applied 89% of the particles were enriched in the centre daughter droplets when approximately two third of the original droplet volume was removed, Figure 35(b). The developed droplet unit operation has the potential to be integrated in a variety of droplet microfluidic systems as particle manipulation is one of the most common steps in biological assays.

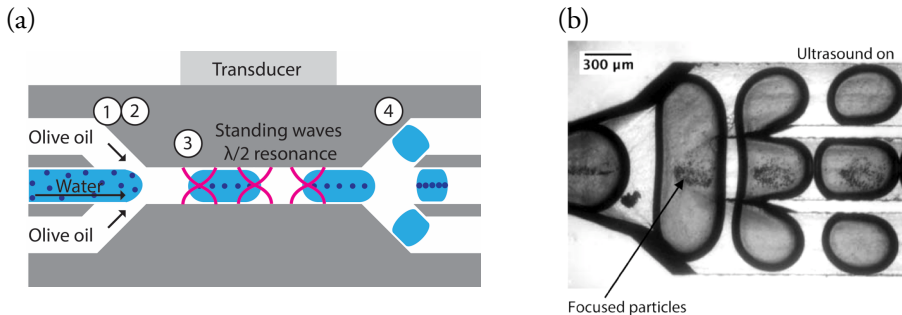


Figure 35. (a) Illustration of acoustic particle enrichment in droplets. There are four key steps: 1) Droplet generation 2) Encapsulation of particles 3) Acoustic particle focusing and 4) Droplet splitting. (b) Photograph of the droplet split. When the ultrasound is applied the particles are directed into the centre daughter droplets. Reprinted with permission from Ref. 101. Copyright 2015 American Chemical Society.

---

## Paper II: Intra-droplet acoustic particle focusing: simulations and experimental observations

In the first acoustic focusing experiments it was observed that it was difficult to focus particles in water droplets surrounded by fluorinated oil, but much easier to focus particles in water droplets surrounded by olive oil. Driven by this observation the aim of this paper was to study the influence of the acoustic properties of the continuous phase in relation to the dispersed phase on acoustic particle focusing for two systems: water droplets in fluorinated oil and water droplets in olive oil. Fluorinated oil and water have very different acoustic properties while the acoustic properties of olive oil and water are similar. As seen in Figure 36(a) at application of the ultrasound the encapsulated particles were affected in the two systems, but the particles in the droplet surrounded by olive oil were more strongly aligned. To study this effect in more detail numerical simulations were performed, Figure 36(b). The simulations showed that strong and uniform acoustic focusing only occurs when the dispersed and continuous phase are acoustically matched, while for the acoustically mismatched system focusing is only maintained near the centre of the droplet. The latter is problematic as the internal flows arising from the movement of the droplet along the channel tend to mix the encapsulated particles, thus resulting in bad alignment of the particles. Therefore it is the recommendation to use dispersed and continuous phases that are acoustically matched to achieve good intra-droplet particle focusing. However, it should be noted that in the choice of fluids other aspects often need to be considered as well, such as droplet stability and biocompatibility.

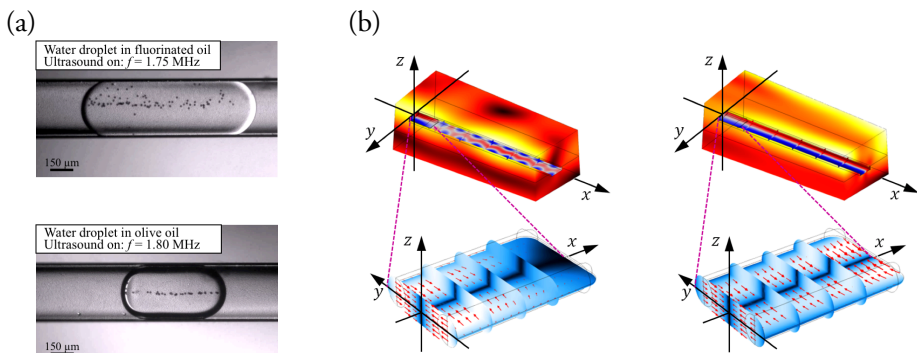


Figure 36. (a) Acoustic focusing is much stronger in a droplet where the dispersed and continuous phase are acoustically matched (water droplet in olive oil). (b) Simulations of the acoustic pressure field (upper images) and the acoustic radiation force (insets) in a water droplet surrounded by fluorinated oil (left) and in a water droplet surrounded by olive oil (right).



## Paper III: An intra-droplet particle switch for droplet microfluidics using bulk acoustic waves

The aim of this work was to develop a droplet unit operation to switch the direction of encapsulated particles into different pathways, and thereby allow for the implementation of complex microfluidic circuits on-chip. The microfluidic chip was fabricated using dry-etching, and the droplet split had a new design compared to the droplet split presented in Paper I. The new design allowed for switching of particles between the centre and the side daughter droplets. At the first harmonic the encapsulated particles were directed into the centre daughter droplets (pathway 1), and by switching the frequency to the second harmonic the encapsulated particles were instead directed into the side daughter droplets (pathway 2), Figure 37(a). At the first harmonic 96% of the particles (10  $\mu\text{m}$  polystyrene microbeads) were enriched in the centre daughter droplets, and at the second harmonic 92% of the particles were enriched in the side daughter droplets, Figure 37(b). In the paper it was also shown that the system could be used to switch the direction of yeast cells (*Saccharomyces cerevisiae*) encapsulated inside droplets into either the centre or the side daughter droplets. This system can be integrated in various droplet microfluidic circuits where particles need to be directed into different pathways.

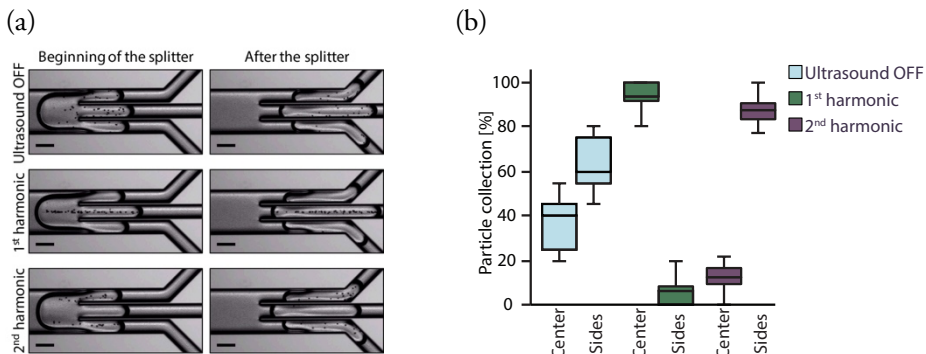


Figure 37. (a) In this paper a system to switch the direction of encapsulated particles into different daughter droplets by changing the frequency between the first and second harmonics was presented. The scale bars are 150  $\mu\text{m}$ . (b) A box plot showing the performance of the described system. Reproduced from Ref. 61 with the permission of AIP Publishing.

---

## Paper IV: Improved positioning and detectability of microparticles in droplet microfluidics using two-dimensional acoustophoresis

In droplet microfluidics encapsulated cells and microbeads are often analysed using optical read-out such as optical microscopy. To obtain accurate and reliable results it is crucial to detect all the encapsulated particles. However, this can be a challenge as the height of the microfluidic channel is often larger than the depth-of-field of the objective, meaning that all particles are not located at the same focus plane and are not detected. In this paper a method where two-dimensional acoustophoresis is used to improve particle positioning inside droplets is proposed. Creating resonance in both the lateral and vertical direction before the droplet generation caused the particles to be positioned at the same height in the channel as well as to be moved towards the centre of the channel, Figure 38(a). With the acoustic pre-aligning almost 100% of the encapsulated particles were detected compared with 79% in the control. It was also shown that using pre-alignment resulted in that a larger amount of the particles being positioned in the centre of the droplets compared with without the ultrasound applied, Figure 38(b). Numerical simulations of the flow fields inside the droplets were performed to explain these results. Two-dimensional acoustophoresis is not limited to only enhance optical detection, but has the possibility to be integrated with other read-out modalities to improve the sensitivity of the measurement.

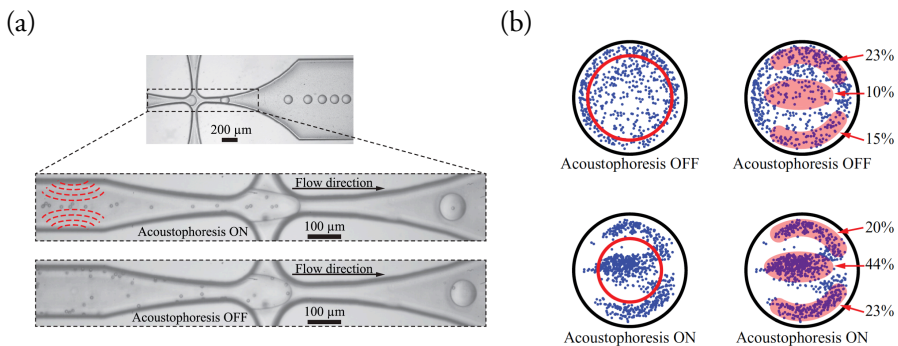


Figure 38. (a) Photographs of the droplet generation process. With the ultrasound applied the particles are aligned before the droplet generation. (b) Images showing the superposition of particles (blue dots) inside the droplets with and without the acoustic pre-alignment. The red circle shows the median particle distance from the droplet centre. Reproduced from Ref. 75 with the permission of IOP Publishing.

## Paper V: Binary particle separation in droplet microfluidics using acoustophoresis

To this point, particle manipulation methods have only been used to focus one particle species inside droplets and not for separation of different particle species. Having the possibility to separate two different particle species encapsulated in the same droplet would expand what types of assays that can be performed, and in this paper such separation method is developed. The basis for the separation is that in an acoustic standing wave-field particles with positive acoustic contrast are moved to the pressure node while particles with negative acoustic contrast are moved to the pressure anti-nodes, Figure 39(a). In the experiments, droplets containing a mixture of polystyrene microbeads (positive acoustic contrast particles) and in-house synthesised PDMS microparticles (negative acoustic contrast particles) were generated. When the ultrasound was applied the polystyrene microbeads were moved to the pressure node located along the centre-line of the droplet and the PDMS microparticles were moved to the pressure anti-nodes located along the sides of the droplet. Next, the droplet was split into three daughter droplets, and as seen in Figure 39(b) when the ultrasound was applied the polystyrene microbeads were directed into the centre daughter droplet and the PDMS microparticles were directed into the side daughter droplets. These results show proof of concept of binary particle separation in droplets, and it is expected that the presented technology can open up for more advanced assays in droplets.

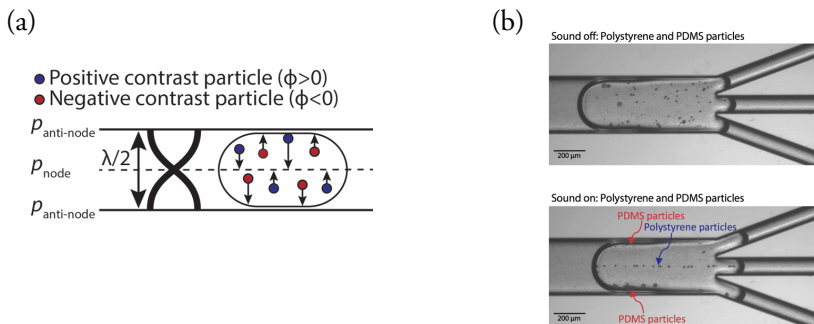


Figure 39. (a) In an acoustic standing wave-field positive acoustic contrast particles such as polystyrene microbeads are focused to the pressure node and negative acoustic contrast particles such as PDMS microparticles are focused to the pressure anti-nodes. (b) In the upper photograph the ultrasound is not applied and the polystyrene microbeads and PDMS microparticles are positioned in the entire droplet, and in the lower photograph the ultrasound is applied at the fundamental resonance and the polystyrene microbeads are directed into the centre daughter droplet and the PDMS particles are directed into the side daughter droplets. Reproduced from Ref. 102 with the permission of AIP Publishing.

## 8. Concluding remarks

In this PhD thesis proof of concept of acoustic particle focusing of encapsulated cells and microbeads in water-in-oil droplets is presented. The emphasis of this project has been on the engineering parts, but as droplet microfluidics is a highly interdisciplinary research field more aspects than the strictly engineering parts need to be considered. This chapter aims to highlight some of these aspects and discuss the prospects of the presented technology.

### 8.1 System improvements and integration

During the project several ideas how to improve the microfluidic chips and add increased functionality was discussed.

For instance, in microfluidics throughput is a key challenge and one way to increase the throughput could be to place multiple droplet generation units and acoustic particle focusing units in parallel.

To enable more advanced operations on-chip, it would be valuable to combine acoustic particle focusing with other droplet unit operations. A method to wash cells and perform buffer-exchange in droplets is very much needed, and this can be realised by combining acoustic particle enrichment with addition of fresh medium into the droplets. Furthermore, it would be valuable to integrate a droplet unit operation for analysis of the droplet content on the chip.

In addition to the microfluidic chip the rest of the experimental setup can also be improved. The current setup is complex and consists of several instruments such as amplifier, function generator, microscope, oscilloscope and several syringe pumps. All these instruments make the setup expensive and complicated to operate for a non-expert, thus work is needed to make the setup simpler and more user-friendly. Furthermore, the possibility to optimise and better integrate the external transducer on the microfluidic chip should be investigated in order to achieve a stronger acoustic force. It would also be beneficial to increase the stability of the system by adding for example temperature control and automatic frequency control.

### 8.2 Biological applications

From an application point of view, the next step is to perform a biological assay using the developed microfluidic system. The presented technology can certainly be a useful tool for miniaturising a wide range of traditional assays into droplet microfluidic systems as particle manipulation is a frequently occurring process step in biological assays. However, to fully explore the potential of droplet microfluidics the best approach might not be to miniaturise and making minor improvements of traditional assays but instead trying to find a biological question that is not even possible to solve using standard methods.<sup>103,104</sup> Finding such research question is most likely to happen by collaboration between biologists and engineers, as the biologists are the experts on what biological problems that are of interest to study and the engineers know what is technically feasible to do.

By moving towards biological applications and especially analyses of human samples one should also think about what type of biological analyses that are ethical to perform. For example, Hindson *et al.*<sup>105</sup> reported on an application where Droplet Digital polymerase chain reaction (PCR) was used to quantify circulating fetal and maternal DNA from a blood plasma sample from the mother. This may seem uncontroversial, but in the long run similar analyses can be used for more advanced prenatal diagnosis such as gender determination, detection of genetic disorders and monitoring of pregnancy-associated disorders.<sup>106</sup> Some of these analyses can be really valuable, but one should always think of what implications biological analyses might have in the long run.

### 8.3 Commercialisation

During the last years several commercial droplet microfluidic platforms have entered the market such as Droplet Digital PCR by Bio-Rad,<sup>107</sup> and a platform for single-cell RNA sequencing by 10x Genomics.<sup>108</sup> The particle focusing droplet unit operation developed in this PhD project has the potential to be commercialised as the technology opens up for more advanced biological assays in droplet microfluidic platforms.

However, going from research to a commercial product sets higher requirements on system integration and may require other chip materials and fabrication processes to decrease the cost per chip. The microfluidic chips fabricated in this PhD project were made of silicon and sealed with glass lids, and investigating the possibility to use cheaper materials such as plastics while still maintaining good acoustic focusing

---

capability would be interesting as that would open up for disposable chips.<sup>109,110</sup> Finding such technical solutions would be very valuable in all types of microfluidic systems where bulk acoustic waves are used to focus and trap cells and microbeads.

## 8.4 Conclusion

In this PhD project I present for the first time a method to focus cells and microbeads encapsulated inside water-in-oil droplets using acoustophoresis. The microfluidic chips were etched in silicon and sealed with glass lids. The channels were etched using either wet etching with KOH or dry etching using DRIE. Both etch methods resulted in functional microfluidic chips. However, etching using DRIE is preferred as it increases the design possibilities and opens up for more sophisticated channel designs.

In the first study I showed proof of concept of acoustic focusing of cells and microbeads inside water droplets using bulk acoustic standing waves. By combining acoustic particle focusing with a trident-shaped droplet split I showed that the technology can be used to enrich particles inside droplets. In the second study, numerical simulations and experiments were performed to increase the physical understanding of the system. These results showed that to obtain high quality intra-droplet acoustic particle focusing, the dispersed and continuous phase should be acoustically matched. In the third study I developed a system where particles could be switched between different fluidic pathways by using the first and second harmonic. In the fourth study it was shown that two-dimensional acoustophoresis can be used to increase the detectability of the encapsulated particles by aligning the particles before the droplet generation site. Finally, I demonstrated that acoustophoresis can be used to separate two different particle species encapsulated inside the same droplet based on the acoustic properties of the particles.

To conclude, in this PhD project I have shown that acoustophoresis is a suitable technology for focusing cells and microbeads in droplet microfluidics. It is my hope that the presented technology will open up for novel biological assays that have not been possible to perform before.



# Popular scientific summary

Millions of biological samples are analysed each day for diagnosis of various diseases as well as to investigate fundamental biological questions such as how cells communicate with each other and why cells sometimes do not function as they should. In my research I am developing microsystems to allow for faster and more sensitive studies of cells than have been possible to perform before. The vision is to miniaturise an entire laboratory with all its functions onto a small microfluidic chip, a so-called “lab-on-a-chip”, Figure 40.

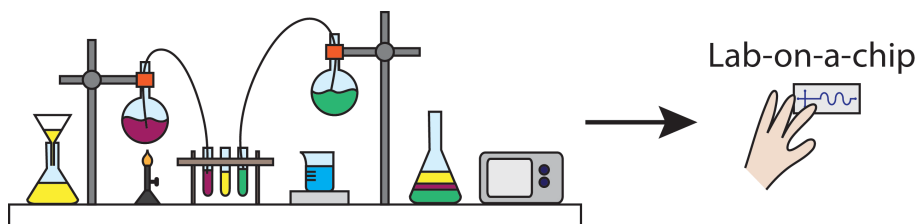


Figure 40. In my research I am developing microsystems, so-called “lab-on-a-chips” for miniaturisation of biological assays. These novel microsystems allow for faster and more sensitive analyses of cells. Moreover, the amount of sample needed for each analysis is tremendously reduced.

Microfluidics as the technology is called, is based on that cells and other particles are handled and analysed in a network of very thin fluidic channels. The width of the fluidic channels are typically only a couple of hundreds of microns. In this network of channels biological samples are mixed, reagents added and different types of analyses are performed. However, to enable more complex analyses in these microsystems new technical solutions are required.

In my PhD project I have been developing a microsystem to allow for biological analyses in small water droplets surrounded by oil. In the droplets cells or particles are encapsulated, and the idea is that each droplet can be viewed as a “mini test-tube” for biological experiments, Figure 41. The main advantage of using droplets is that the volume of each droplet is only a couple of nL-pL which is a million times less than the volume of an ordinary test-tube, and this leads to a substantial decrease in the amount of sample and reagents that are needed for each analysis. Another important advantage is that tens of thousands of droplets can be generated and analysed during a couple of minutes which increases the throughput.



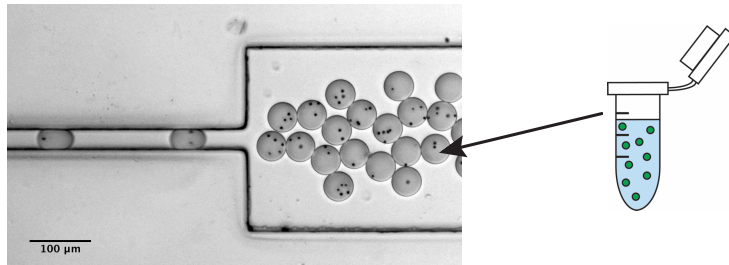


Figure 41. In microfluidic channels small water droplets containing cells or particles (black dots) can be generated. The droplets are so small that a microscope is required to see them. Each tiny water droplet function as a "mini test-tube" for biological experiments.

To allow for miniaturisation of various biological analyses into droplet-based microfluidic systems several operations need to be integrated on-chip. One unit operation that has been missing is a method to manipulate and position cells and particles inside droplets, and this is an important operation to for example enable enrichment of biological sample. The aim of this PhD project has been to study how acoustic forces can be employed to move and enrich cells and particles encapsulated inside droplets.

I fabricate the microsystems by etching a network of channels on a silicon wafer. In the channels I generate small water droplets surrounded by oil, and in the droplets cells or particles are encapsulated. To position the encapsulated cells or particles the microfluidic chip is set into vibration by using sound waves at a very high frequency so-called ultrasound, Figure 42. The applied frequency (2 MHz) is more than hundred times higher than the human ear can perceive. The vibrations in the chip create a standing sound wave in the channel with pressure nodes and anti-nodes. Cells and particles that are located in this standing sound wave are affected by the acoustic forces and are moved to the pressure nodes or anti-nodes depending on the acoustic properties they have. Most cells have such acoustic properties that they are aligned in the centre of the channel, i.e. the pressure node.

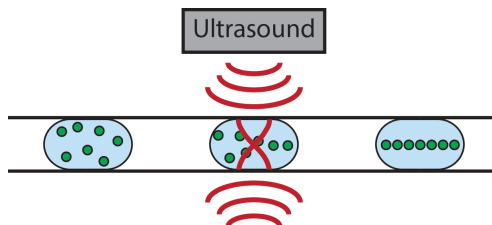
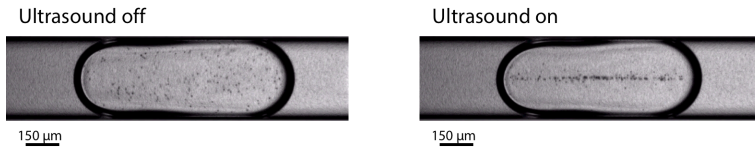


Figure 42. Ultrasound is used to create a standing sound wave in the channel, and this causes the cells or particles (green circles) to be aligned in the centre of the droplet. The droplets are flowing to the right in the channel.

---

In this PhD thesis I show for the first time that cells and particles encapsulated inside droplets can be positioned by acoustic forces, Figure 43. I have applied the technology to enrich cells and particles inside droplets. To expand the physical understanding of the system, I did investigate the acoustic field inside the droplets and which parameters that are important to optimise to obtain strong acoustic forces on the cells and particles.



*Figure 43. In this PhD thesis I have shown that by using ultrasound, yeast cells (black dots) can be aligned in the centre of a droplet.*

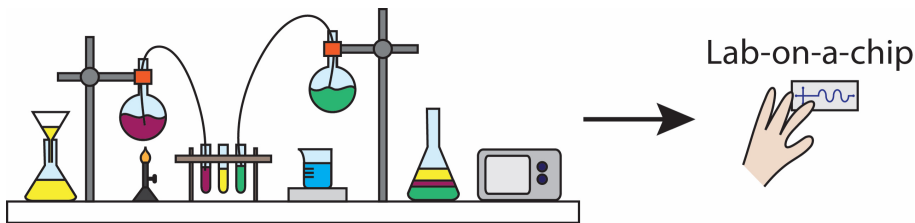
Next, I applied the technology to direct encapsulated cells and particles into different fluidic outlets by using two different ultrasound frequencies. Moreover, I have shown that acoustic forces can be used to easier detect particles inside droplets. Lastly, I have shown that it is possible to separate two different particle species inside droplets based on the acoustic properties of the particles.

My hope is that the presented technology to position and enrich cells and particles inside droplets will open up for new biological analyses that have not been possible to perform before.



# Populärvetenskaplig sammanfattning

Varje dag analyseras miljontals biologiska prover för att diagnosticera olika sjukdomar, men också för att studera grundläggande biologiska frågeställningar som till exempel hur celler kommunicerar med varandra och vad som gör att vissa celler inte fungerar som de ska. I min forskning utvecklar jag mikrosystem för att kunna studera och undersöka celler snabbare och med högre noggrannhet än tidigare. Visionen är att alla analyser som idag görs i stora laboratorier istället ska kunna göras på ett litet chip, ett så kallat "lab-on-a-chip", Figur 44.

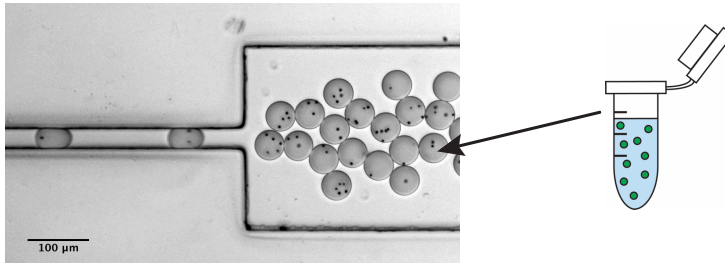


Figur 44. I min forskning utvecklar jag mikrosystem, så kallade "lab-on-a-chips" för att göra biologiska analyser av celler. I dessa nya mikrosystem kan biologiska prover analyseras snabbare och med högre noggrannhet än tidigare. Dessutom krävs det mycket mindre mängd biologiskt material för varje analys.

Mikrofluidik som tekniken kallas, bygger på att celler och andra partiklar hanteras och analyseras i nätverk av supersmala vätskekanaler på ett chip. Typiskt är vätskekanalerna på chippen bara några hundratals mikrometer breda. I dessa nätverk av kanaler kan prover blandas, reagenser tillsättas, och olika typer av analyser göras. För att kunna utföra fler och mer avancerade biologiska analyser i dessa mikrosystem krävs nya tekniska lösningar.

I mitt doktorandprojekt har jag utvecklat ett mikrosystem för att göra biologiska analyser i små vattendroppar omgivna av olja. I dropparna kapslas celler eller partiklar in och syftet är att dropparna ska fungera som "mini-provrör" för biologiska experiment, Figur 45. Fördelen med att använda droppar istället för vanliga provrör är att dropparnas volym bara är några nL-pL vilket är en miljon gånger mindre än ett vanligt provrör, vilket leder till att mindre biologiskt prov och reagenser krävs. En annan fördel med att använda droppar är att tiotusentals

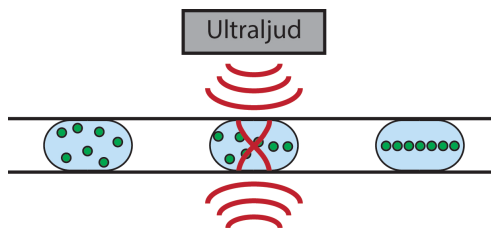
droppar kan skapas och analyseras på bara någon minut vilket leder till att många fler experiment kan utföras på kort tid.



Figur 45. I mikrokanaler kan små vattendroppar med celler eller partiklar (svarta prickar) i skapas. Dropparna är så små att ett mikroskop krävs för att se dem. Varje liten vattendroppe fungerar som ett "mini-provrör" för biologiska experiment.

För att kunna göra olika experiment i droppar krävs det komplexa mikrosystem med många integrerade funktioner. En funktion som saknats är en metod för att flytta och positionera celler och partiklar i droppar. Detta är ett viktigt steg för att till exempel kunna koncentrera prover. I mitt doktorandprojekt har jag forskat på hur akustiska krafter kan användas för att just flytta och koncentrera celler och partiklar i droppar.

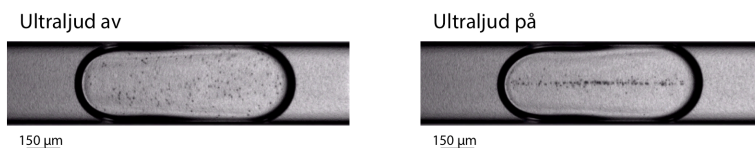
Mikrosystemen har jag tillverkat genom att etsa ett nätverk av smala kanaler på en tunn skiva av kisel. I kanalerna skapas små vattendroppar omgivna av olja, och i dropparna kapslas celler eller partiklar in. För att positionera cellerna eller partiklarna i dropparna sätts hela chipet i vibration genom att använda ljudvågor med en väldigt hög frekvens så kallat ultraljud, Figur 46. Frekvensen på ljudet (2 MHz) är mer än hundra gånger högre än vad det mänskliga örat kan uppfatta. Vibrationer leder till att en stående ljudvåg skapas i kanalen med trycknoder och tryckbukar. Celler och partiklar som befinner sig i denna stående ljudvåg kommer att påverkas av akustiska krafter och flyttas till noderna respektive bukarna beroende på cellernas och partiklarnas akustiska egenskaper. De flesta celler har sådana akustiska egenskaper att de linjeras upp i mitten av kanalen, det vill säga i trycknoden.



Figur 46. Med hjälp av ultraljud genereras en stående ljudvåg i kanalen, och detta resulterar i att cellerna eller partiklarna (gröna cirklar) linjeras upp längs mitten av droppen. Dropparna rör sig åt höger i kanalen.

---

I denna avhandling visar jag för första gången att akustiska krafter kan användas för att positionera celler och partiklar i droppar, Figur 47. För att bättre förstå systemet har jag studerat hur det akustiska fältet ser ut i droppar och vilka parametrar som är viktiga att optimera för att uppnå en stark akustisk kraft.



Figur 47. I mitt avhandlingsarbete har jag visat att genom att använda ultraljud kan celler (svarta prickar) fokuseras till mitten av droppen.

Därefter har jag använt tekniken för att kunna styra celler och partiklar i droppar mellan olika utloppskanaler genom att använda två olika frekvenser på ljudet. Jag har också visat att akustiska krafter kan användas för att lättare kunna detektera partiklar i droppar. Slutligen har jag visat att det går att separera två olika partikeltyper i droppar baserat på partiklarnas akustiska egenskaper.

Min förhoppning är att denna teknik för att flytta och anrika celler och partiklar i droppar ska öppna för nya biologiska analyser som inte har varit möjliga att göra tidigare.



# Acknowledgements

This PhD project has been an amazing journey for me, and there are many people I would like to thank. Without your help and support this PhD thesis would not have been possible to complete and the journey would not have been half as fun.

First, I would like to thank Maria Tenje for being the best supervisor one can think of. Your enthusiasm and team-spirit are amazing. I am grateful for your guidance and support throughout my PhD studies, and especially that you always have encouraged me to test my own ideas. I have really enjoyed the scientific discussions we have had during these years, and I have learned a lot by working with you. In addition to science, you have taught me the importance of good communication and leadership.

Thanks to my co-supervisor Johan Nilsson for always taking time to discuss things, especially the electronics.

I would also like to thank my second co-supervisor Håkan Jönsson for your expertise and practical tips on droplet microfluidics.

Many thanks to my co-workers in the papers for great collaborations. It has been a great learning experience to work with you.

Thanks to the whole EMBLA research group for creating such an open-minded research environment. Since I first joined, the research group has grown many hundred percent, and it has been really fun to get to know you all. Thanks for the inspiring group meetings, Blodomloppet-races, and thanks for hosting me in Uppsala during a couple of months. Especially, thanks to Axel Happstadius and Klara Björnander Rahimi for all your hard work during your MSc thesis projects.

I would like to thank my colleagues at the BME department, both for helping me with practical issues and for creating such a friendly and welcoming work environment. Marc Isaksson for being a fantastic office companion and showing how a professional lab setup should look like. Carl Johannesson for being a great office neighbor and I look forward to work with you in the next project. Maria Antfolk for the glass chips and for joining the droplet side. Mathias Ohlin for great



## Acknowledgements

---

cleanroom company and droplet chips. Thanks to all other present and former members of the Akustikgruppen: Andreas Lenshof, Thomas Laurell, Anke Urbansky, Eva Undvall, Franziska Olm, Klara Petersson, Ola Jakobsson, Cecilia Magnusson, Kevin Cushing, Fabio Garofalo, Wei Qui, Mikael Evander, Per Augustsson and Pelle Ohlsson. I would like to thank you for interesting research discussions as well as great conference company. Moreover, I would like to thank Désirée Jarebrant, Eva Everitt, Ammi Lindgren, Malgo Luczak and Ulrika Westerdahl for keeping track on everything that is not science. Anette Wolff for nice travel company to Uppsala. Martin Bengtsson for help in the cleanroom. Axel Tojo for fixing my lab computer.

Most of all, I would like to thank my family and friends for your kind words and support along this journey. Kram

# References

- <sup>1</sup> R. Hooke, *Micrographia: Or Some Physiological Descriptions of Minute Bodies, Made by Magnifying Glasses with Observations and Inquiries Thereupon* (1665).
- <sup>2</sup> A. Van Leeuwenhoek, *The Selected Works of Antony van Leeuwenhoek Containing His Microscopical Discoveries in Many of the Works of Nature* (1800).
- <sup>3</sup> R. Seemann, M. Brinkmann, T. Pfohl, and S. Herminghaus, *Rep Prog Phys* 75, 16601 (2012).
- <sup>4</sup> M.T. Guo, A. Rotem, J.A. Heyman, and D.A. Weitz, *Lab Chip* 12, 2146 (2012).
- <sup>5</sup> H.N. Joensson and H. Andersson Svahn, *Angew Chem Int Ed Engl* 51, 12176 (2012).
- <sup>6</sup> T. Schneider, J. Kreuzt, and D.T. Chiu, *Anal. Chem.* 85, 3476 (2013).
- <sup>7</sup> T.P. Lagus and J.F. Edd, *J. Phys. D. Appl. Phys.* 46, 114005 (2013).
- <sup>8</sup> D. Di Carlo and L.P. Lee, *Anal. Chem.* 78, 7918 (2006).
- <sup>9</sup> H.B. Yin and D. Marshall, *Curr. Opin. Biotechnol.* 23, 110 (2012).
- <sup>10</sup> T. Thorsen, R.W. Roberts, F.H. Arnold, and S.R. Quake, *Phys. Rev. Lett.* 86, 4163 (2001).
- <sup>11</sup> J.J. Agresti, E. Antipov, A.R. Abate, K. Ahn, A.C. Rowat, J.-C. Baret, M. Marquez, A.M. Klibanov, A.D. Griffiths, and D.A. Weitz, *Proc. Natl. Acad. Sci.* 107, 4004 (2010).
- <sup>12</sup> M. Sesen, T. Alan, and A. Neild, *Lab Chip* 17, 2372 (2017).
- <sup>13</sup> V. Chokkalingam, J. Tel, F. Wimmers, X. Liu, S. Semenov, J. Thiele, C.G. Figidor, and W.T.S. Huck, *Lab Chip* 13, 4740 (2013).
- <sup>14</sup> T.M. Squires and S.R. Quake, *Rev. Mod. Phys.* 77, 977 (2005).
- <sup>15</sup> H. Bruus, *Theoretical Microfluidics* (Oxford University Press, Oxford, 2008).
- <sup>16</sup> C.N. Baroud, F. Gallaire, and R. Dangla, *Lab Chip* 10, 2032 (2010).
- <sup>17</sup> P. Zhu and L. Wang, *Lab Chip* 17, 34 (2017).

## References

---

- <sup>18</sup> S.L. Anna, N. Bontoux, and H.A. Stone, *Appl. Phys. Lett.* 82, 364 (2003).
- <sup>19</sup> P.B. Umbanhowar, V. Prasad, and D.A. Weitz, *Langmuir* 16, 347 (2000).
- <sup>20</sup> A.R. Abate, M.B. Romanowsky, J.J. Agresti, and D.A. Weitz, 023503, 92 (2010).
- <sup>21</sup> D.J. Collins, T. Alan, K. Helmerson, and A. Neild, 3225 (2013).
- <sup>22</sup> D.R. Link, E. Grasland-Mongrain, A. Duri, F. Sarrazin, and Z. Cheng, 2556 (2006).
- <sup>23</sup> S. Hwa, B. Semin, and J.-C. Baret, 14, 1099 (2014).
- <sup>24</sup> G.F. Christopher and S.L. Anna, *J. Phys. D. Appl. Phys.* 40, (2007).
- <sup>25</sup> J.K. Nunes, S.S.H. Tsai, J. Wan, and H.A. Stone, *J. Phys. D. Appl. Phys.* 46, (2013).
- <sup>26</sup> S.-Y. Teh, R. Lin, L.-H. Hung, and A.P. Lee, *Lab Chip* 8, 198 (2008).
- <sup>27</sup> M. Hein, M. Moskopp, and R. Seemann, *Lab Chip* 15, 2879 (2015).
- <sup>28</sup> H. Kinoshita, S. Kaneda, T. Fujii, and M. Oshima, *Lab Chip* 7, 338 (2007).
- <sup>29</sup> J.D. Tice, H. Song, A.D. Lyon, and R.F. Ismagilov, *Langmuir* 19, 9127 (2003).
- <sup>30</sup> J.-C. Baret, *Lab Chip* 12, 422 (2012).
- <sup>31</sup> J. Bibette, F. Leal Calderon, and P. Poulin, *Rep. Prog. Phys.* 62, 969 (1999).
- <sup>32</sup> M. Pan, F. Lyu, and S.K.Y. Tang, *Anal. Chem.* 87, 7938 (2015).
- <sup>33</sup> B. Kintsjes, L.D. van Vliet, S.R. Devenish, and F. Hollfelder, *Curr. Opin. Chem. Biol.* 14, 548 (2010).
- <sup>34</sup> D.J. Collins, A. Neild, A. deMello, A.-Q. Liu, and Y. Ai, *Lab Chip* 3439 (2015).
- <sup>35</sup> M. Chabert and J.-L. Viovy, *Proc. Natl. Acad. Sci.* 105, 3191 (2008).
- <sup>36</sup> H.N. Joensson, M. Uhlén, and H.A. Svahn, *Lab Chip* 11, 1305 (2011).
- <sup>37</sup> J.F. Edd, D. Di Carlo, K.J. Humphry, S. Köster, D. Irimia, D.A. Weitz, and M. Toner, *Lab Chip* 8, 1262 (2008).
- <sup>38</sup> X. Niu, S. Gulati, J.B. Edel, and A.J. DeMello, *Lab Chip* 8, 1837 (2008).
- <sup>39</sup> M. Sesen, T. Alan, and A. Neild, *Lab Chip* 14, 3325 (2014).
- <sup>40</sup> K. Ahn, J. Agresti, H. Chong, M. Marquez, and D.A. Weitz, *Appl. Phys. Lett.* 88, (2006).
- <sup>41</sup> A.R. Abate, T. Hung, P. Mary, J.J. Agresti, and D.A. Weitz, *Proc Natl Acad Sci U S A* 107, 19163 (2010).

- 
- <sup>42</sup> D.R. Link, S.L. Anna, D.A. Weitz, and H.A. Stone, *Phys. Rev. Lett.* 92, 054503 (2004).
- <sup>43</sup> J.H. Jung, G. Destgeer, B. Ha, J. Park, and H.J. Sung, *Lab Chip* 16, 3235 (2016).
- <sup>44</sup> M. Tenje, A. Fornell, M. Ohlin, and J. Nilsson, *Anal. Chem.* 90, 1434 (2018).
- <sup>45</sup> H. Maenaka, M. Yamada, M. Yasuda, and M. Seki, *Langmuir* 24, 4405 (2008).
- <sup>46</sup> J.C. Baret, O.J. Miller, V. Taly, M. Ryckelynck, A. El-Harrak, L. Frenz, C. Rick, M.L. Samuels, J.B. Hutchison, J.J. Agresti, D.R. Link, D.A. Weitz, and A.D. Griffiths, *Lab Chip* 9, 1850 (2009).
- <sup>47</sup> L. Schmid, D.A. Weitz, and T. Franke, *Lab Chip* 14, 3710 (2014).
- <sup>48</sup> I. Leibacher, P. Reichert, and J. Dual, *Lab Chip* 15, 2896 (2015).
- <sup>49</sup> A. Huebner, D. Bratton, G. Whyte, M. Yang, A.J. DeMello, C. Abell, and F. Hollfelder, *Lab Chip* 9, 692 (2009).
- <sup>50</sup> E. Brouzes, M. Medkova, N. Savenelli, D. Marran, M. Twardowski, J.B. Hutchison, J.M. Rothberg, D.R. Link, N. Perrimon, and M.L. Samuels, *Proc Natl Acad Sci U S A* 106, 14195 (2009).
- <sup>51</sup> S.K. Küster, S.R. Fagerer, P.E. Verboket, K. Eyer, K. Jefimovs, R. Zenobi, and P.S. Dittrich, *Anal. Chem.* 85, 1285 (2013).
- <sup>52</sup> W. Lee, P. Tseng, and D. Di Carlo, *Microtechnology for Cell Manipulation and Sorting* (Springer International Publishing, 2017).
- <sup>53</sup> G.K. Kurup and A.S. Basu, *Biomicrofluidics* 6, 022008 (2012).
- <sup>54</sup> M. Sun, Z.S. Khan, and S.A. Vanapalli, *Lab Chip* 12, 5225 (2012).
- <sup>55</sup> D. Lombardi and P.S. Dittrich, *Anal. Bioanal. Chem.* 399, 347 (2011).
- <sup>56</sup> R. Gao, Z. Cheng, A. deMello, and J. Choo, *Lab Chip* 16, 1022 (2016).
- <sup>57</sup> K. Park, J. Park, J.H. Jung, G. Destgeer, H. Ahmed, and H.J. Sung, *Biomicrofluidics* 11, 064112 (2017).
- <sup>58</sup> S. Han, H.S. Kim, and A. Han, *Biosens. Bioelectron.* 97, 41 (2017).
- <sup>59</sup> N. Pamme, *Lab Chip* 6, 24 (2006).
- <sup>60</sup> A. Lenshof, M. Evander, T. Laurell, and J. Nilsson, *Lab Chip* 12, 684 (2012).
- <sup>61</sup> A. Fornell, M. Ohlin, F. Garofalo, J. Nilsson, and M. Tenje, *Biomicrofluidics* 11, 031101 (2017).
- <sup>62</sup> J. Voldman, *Annu. Rev. Biomed. Eng.* 8, 425 (2006).
- <sup>63</sup> A. Kundt, *Ann. Phys.* 127, 497 (1866).

## References

---

- <sup>64</sup> F. Petersson, A. Nilsson, C. Holm, H. Jonsson, and T. Laurell, *Lab Chip* 5, 20 (2005).
- <sup>65</sup> O. Manneberg, B. Vanherberghen, B. Önfelt, and M. Wiklund, *Lab Chip* 9, 833 (2009).
- <sup>66</sup> M. Nordin and T. Laurell, *Lab Chip* 12, 4610 (2012).
- <sup>67</sup> P. Li, Z. Mao, Z. Peng, L. Zhou, Y. Chen, P.-H. Huang, C.I. Truica, J.J. Drabick, W.S. El-Deiry, M. Dao, S. Suresh, and T.J. Huang, *Proc Natl Acad Sci U S A* 112, 4970 (2015).
- <sup>68</sup> P. Hoskins, K. Martin, and A. Thrush, *Diagnostic Ultrasound: Physics and Equipment*, 2nd ed. (Cambridge University Press, Cambridge, 2010).
- <sup>69</sup> J.F. Tressler, S. Alkoy, and R.E. Newnham, *J. Electroceramics* 2, 257 (1998).
- <sup>70</sup> X. Ding, P. Li, S.-C.S. Lin, Z.S. Stratton, N. Nama, F. Guo, D. Slotcavage, X. Mao, J. Shi, F. Costanzo, and T.J. Huang, *Lab Chip* 13, 3626 (2013).
- <sup>71</sup> H. Bruus, *Lab Chip* 12, 1014 (2012).
- <sup>72</sup> C. Grenvall, P. Augustsson, J.R. Folkenberg, and T. Laurell, *Anal. Chem.* 81, 6195 (2009).
- <sup>73</sup> K.W. Cushing, M.E. Piyasena, N.J. Carroll, G.C. Maestas, B.A. López, B.S. Edwards, S.W. Graves, and G.P. López, *Anal. Chem.* 85, 2208 (2013).
- <sup>74</sup> K. Cushing, E. Undvall, Y. Ceder, H. Lilja, and T. Laurell, *Anal. Chim. Acta* 1000, 256 (2018).
- <sup>75</sup> M. Ohlin, A. Fornell, H. Bruus, and M. Tenje, *J. Micromechanics Microengineering* 27, 084002 (2017).
- <sup>76</sup> M.W.H. Ley and H. Bruus, *Lab Chip* 16, 1178 (2016).
- <sup>77</sup> M. Wiklund, R. Green, and M. Ohlin, *Lab Chip* 12, 2438 (2012).
- <sup>78</sup> R. Barnkob, P. Augustsson, T. Laurell, and H. Bruus, *Phys. Rev. E* 86, (2012).
- <sup>79</sup> G. Hertz and H. Mende, *Zeitschrift Für Phys.* 114, 354 (1939).
- <sup>80</sup> L. Schmid and T. Franke, *Lab Chip* 13, 1691 (2013).
- <sup>81</sup> M.A. Burguillos, C. Magnusson, M. Nordin, A. Lenshof, P. Augustsson, M.J. Hansson, E. Elmér, H. Lilja, P. Brundin, T. Laurell, and T. Deierborg, *PLoS One* 8, 1 (2013).
- <sup>82</sup> M. Wiklund, *Lab Chip* 12, 2018 (2012).
- <sup>83</sup> P. Augustsson, R. Barnkob, S.T. Wereley, H. Bruus, and T. Laurell, *Lab Chip* 11, 4152 (2011).
- <sup>84</sup> M. Ohlin, I. Iranmanesh, A.E. Christakou, and M. Wiklund, *Lab Chip* 15,

---

3341 (2015).

- <sup>85</sup> K. Ren, J. Zhou, and H. Wu, *Acc. Chem. Res.* 46, 2396 (2013).
- <sup>86</sup> Y. Xia and G.M. Whitesides, *Annu. Rev. Mater. Sci.* 28, 152 (1998).
- <sup>87</sup> G.M. Whitesides, *Nature* 442, 368 (2006).
- <sup>88</sup> D.R. Reyes, D. Iossifidis, P.A. Auroux, and A. Manz, *Anal. Chem.* 74, 2623 (2002).
- <sup>89</sup> C. Iliescu, H. Taylor, M. Avram, J. Miao, and S. Franssila, *Biomicrofluidics* 6, 16505 (2012).
- <sup>90</sup> S.M. Sze, *Semiconductor Devices, Physics and Technology*, 2nd ed. (John Wiley & Sons, Hoboken, 2002).
- <sup>91</sup> H. Seidel, L. Csepregi, A. Hueberger, and H. Baumgärtel, *J. Electrochem. Soc.* 137, 3612 (1990).
- <sup>92</sup> F. Laermer and A. Schilp, German Pat. DE 4241045 (1994).
- <sup>93</sup> G. Wallis and D.I. Pomerantz, *J. Appl. Phys.* 40, 3946 (1969).
- <sup>94</sup> J.R. Rumble, *CRC Handbook of Chemistry and Physics*, 98th ed. (CRC Press/Taylor & Francis, Boca Raton, 2017).
- <sup>95</sup> K.W. Cushing, F. Garofalo, C. Magnusson, L. Ekblad, H. Bruus, and T. Laurell, *Anal. Chem.* 89, 8917 (2017).
- <sup>96</sup> O. Carrier, F.G. Ergin, H.-Z. Li, B.B. Watz, and D. Funfschilling, *J. Micromechanics Microengineering* 25, 084014 (2015).
- <sup>97</sup> W. Mahmood Mat Yunus, Y.W. Fen, and L.M. Yee, *Am. J. Appl. Sci.* 6, 328 (2009).
- <sup>98</sup> S.K.Y. Tang, Z. Li, A.R. Abate, J.J. Agresti, D.A. Weitz, D. Psaltis, and G.M. Whitesides, *Lab Chip* 9, 2767 (2009).
- <sup>99</sup> M. Musterd, V. Van Steijn, C.R. Kleijn, and M.T. Kreutzer, *RSC Adv.* 5, 16042 (2015).
- <sup>100</sup> W.H. Coulter, in *Proc Natl Electron Conf* (1956).
- <sup>101</sup> A. Fornell, J. Nilsson, L. Jonsson, P.K. Periyannan Rajeswari, H.N. Joensson, and M. Tenje, *Anal. Chem.* 87, 10521 (2015).
- <sup>102</sup> A. Fornell, K. Cushing, J. Nilsson, and M. Tenje, *Appl. Phys. Lett.* 112, 063701 (2018).
- <sup>103</sup> L.R. Volpatti and A.K. Yetisen, *Trends Biotechnol.* 32, 347 (2014).
- <sup>104</sup> E.K. Sackmann, A.L. Fulton, and D.J. Beebe, *Nature* 507, 181 (2014).

## References

---

- <sup>105</sup> B.J. Hindson, K.D. Ness, D.A. Masquelier, P. Belgrader, N.J. Heredia, A.J. Makarewicz, I.J. Bright, M.Y. Lucero, A.L. Hiddessen, T.C. Legler, T.K. Kitano, M.R. Hodel, J.F. Petersen, P.W. Wyatt, E.R. Steenblock, P.H. Shah, L.J. Bousse, C.B. Troup, J.C. Mellen, D.K. Wittmann, N.G. Erndt, T.H. Cauley, R.T. Koehler, A.P. So, S. Dube, K.A. Rose, L. Montesclaros, S. Wang, D.P. Stumbo, S.P. Hodges, S. Romine, F.P. Milanovich, H.E. White, J.F. Regan, G.A. Karlin-Neumann, C.M. Hindson, S. Saxonov, and B.W. Colston, *Anal. Chem.* 83, 8604 (2011).
- <sup>106</sup> Y.M. Dennis Lo and R.W.K. Chiu, *Nat. Rev. Genet.* 8, 71 (2007).
- <sup>107</sup> <http://www.bio-rad.com>, (2018).
- <sup>108</sup> <https://www.10xgenomics.com>, (2018).
- <sup>109</sup> I. González, M. Tijero, A. Martin, V. Acosta, J. Berganzo, A. Castillejo, M.M. Bouali, and J.L. Soto, *Micromachines* 6, 574 (2015).
- <sup>110</sup> P. Dow, K. Kotz, S. Gruszka, J. Holder, and J. Fiering, *Lab Chip* 1629 (2017).

# Paper I

## **Controlled Lateral Positioning of Microparticles Inside Droplets Using Acoustophoresis**

A. Fornell, J. Nilsson, L. Jonsson, P. K. Periyannan  
Rajeswari, H. N. Joensson, and M. Tenje

Reprinted with permission from A. Fornell, J. Nilsson,  
L. Jonsson, P. K. Periyannan Rajeswari, H. N. Joensson,  
and M. Tenje. Controlled Lateral Positioning of  
Microparticles Inside Droplets Using Acoustophoresis.  
*Analytical Chemistry*, 87(20), 10521-10526 (2015).  
©2015 American Chemical Society.





## Controlled Lateral Positioning of Microparticles Inside Droplets Using Acoustophoresis

Anna Fornell,<sup>\*,†</sup> Johan Nilsson,<sup>†</sup> Linus Jonsson,<sup>†</sup> Prem Kumar Periyannan Rajeswari,<sup>‡</sup> Haakan N. Joensson,<sup>‡</sup> and Maria Tenje<sup>†,§</sup>

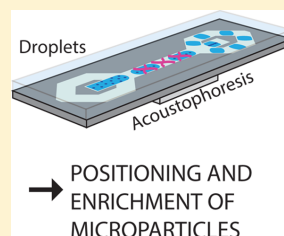
<sup>†</sup>Dept. Biomedical Engineering, Lund University, Box 118, S-221 00, Lund, Sweden

<sup>‡</sup>Div. of Proteomics and Nanobiotechnology, Science for Life Laboratory, KTH Royal Institute of Technology, Box 1031, S-171 21 Solna, Sweden

<sup>§</sup>Dept. Engineering Sciences, Science for Life Laboratory, Uppsala University, Box 534, S-751 21 Uppsala, Sweden

**W** Web-Enhanced Feature

**ABSTRACT:** In this paper, we utilize bulk acoustic waves to control the position of microparticles inside droplets in two-phase microfluidic systems and demonstrate a method to enrich the microparticles. In droplet microfluidics, different unit operations are combined and integrated on-chip to miniaturize complex biochemical assays. We present a droplet unit operation capable of controlling the position of microparticles during a trident shaped droplet split. An acoustic standing wave field is generated in the microchannel, and the acoustic forces direct the encapsulated microparticles to the center of the droplets. The method is generic, requires no labeling of the microparticles, and is operated in a noncontact fashion. It was possible to achieve 2+-fold enrichment of polystyrene beads (5  $\mu\text{m}$  in diameter) in the center daughter droplet with an average recovery of 89% of the beads. Red blood cells were also successfully manipulated inside droplets. These results show the possibility to use acoustophoresis in two-phase systems to enrich microparticles and open up the possibility for new droplet-based assays that are not performed today.



Droplet microfluidics has been the focus of intensive research within recent years.<sup>1,2</sup> The principle of this technology is to use two immiscible phases to create a two-phase system where each droplet, or plug, can be viewed as an independent reservoir for biological or chemical reactions. The applications and motivation for such a system is to provide miniaturization and increased throughput of different biological and chemical assays as well as a tool for material synthesis.<sup>3–5</sup> In this work, we present a method to reduce the droplet volume while maintaining the majority of the microparticles in a predetermined daughter droplet, by first positioning the microparticles to the center of the droplet using bulk acoustic waves and then splitting the droplet into three daughter droplets.

To miniaturize complex assays on chip, several droplet “unit operations” have been developed that can be combined into highly advanced microsystems designed for specific applications. Examples of such unit operations include encapsulation of single cells inside droplets, injection of reagents into droplets, droplet splitting, and droplet sorting.<sup>6–9</sup> However, there is still a need for a flexible unit operation to laterally position microparticles or cells in a label-free manner inside droplets. This is useful for the development of droplet washing procedures, or for microparticle enrichment inside droplets, where the final destination of the microparticles after a splitting step must be possible to control. Today, droplets are typically split using T-crosses without any positioning of the encapsulated microparticles; thus, the microparticles are

randomly distributed between the outlets, leading to no controlled enrichment in the daughter droplets.<sup>8,10</sup> Some researchers have addressed this and similar topics by controlling the position of microparticles inside droplets using magnetic forces, but this technique cannot easily be transferred to label-free cell-based assays since it requires magnetic properties of the microparticles.<sup>11,12</sup> A recent report also shows how hydrodynamics can be used to position microparticles inside droplets.<sup>13</sup> However, that technique relies upon particle sedimentation and requires slow flows to successfully handle biologically relevant microparticles, thus limiting its use for high-throughput screening applications. In addition, it cannot be externally regulated on-demand.

Acoustic forces have proven a suitable miniaturized method to manipulate small particles or objects in microfluidic channels (i.e., acoustophoresis) in a noncontact fashion.<sup>14,15</sup> The forces exerted to achieve the particle positioning are gentle, resulting in no negative side effects when handling, e.g., cells.<sup>16</sup> As opposed to other manipulation methods such as dielectrophoresis and magnetophoresis, it is unaffected by particle charge, pH, and ionic strength of the solutions.<sup>14</sup>

In earlier work, acoustics have been applied to droplets in order to move microparticles inside sessile droplets surrounded

Received: July 22, 2015

Accepted: September 30, 2015

Published: September 30, 2015

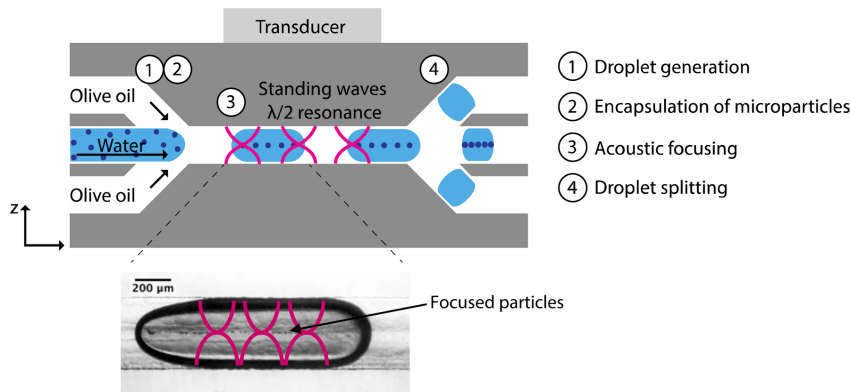


**Figure 1.** Acoustic positioning and enrichment of microparticles inside droplets. Aqueous droplets with encapsulated microparticles are generated. A standing wave field is created in the channel, and the microparticles are positioned to the center of the droplets. Each droplet is split into three daughter droplets with the center droplet containing the largest amount of the microparticles. The volume of the droplet before splitting is approximately 80 nL.

by air,<sup>17,18</sup> manipulate entire droplets,<sup>19,20</sup> control droplet size,<sup>21</sup> steer and split plugs,<sup>22</sup> control merging,<sup>23</sup> and align cells before single cell printing with a drop dispenser.<sup>24</sup> However, this is the first time acoustic forces are used to position and enrich microparticles and cells inside moving droplets.

A comprehensive overview of the theory of acoustic manipulation of particles in microfluidic channels can be found in the literature, and only the main concepts are described here.<sup>25</sup> Acoustophoresis utilizes ultrasonic standing waves to generate forces that can be used to position particles inside microsystems. By matching the frequency of the sound to the width of the microchannel, a standing wave field will be created across the channel with pressure minima and maxima at specific locations.

For a 1D planar standing  $\lambda/2$ -wave, the primary acoustic radiation force,  $F_z^{\text{rad}}$ , is described by eq 1,

$$F_z^{\text{rad}} = 4\pi\phi(\bar{\kappa}, \bar{\rho})ka^3E_{\text{ac}}\sin(2kz) \quad (1)$$

where  $\phi$  is the acoustic contrast factor,  $k$  is the wavenumber ( $k = 2\pi/\lambda$ ),  $a$  is the particle radius,  $E_{\text{ac}}$  is the acoustic energy density, and  $z$  is the distance from the wall. Depending on the sign of the acoustic contrast factor, particles will be moved either toward the pressure nodes or antinodes. The acoustic contrast factor relates the compressibility ( $\kappa$ ) and the density ( $\rho$ ) of the suspended particles ( $\kappa_p, \rho_p$ ) to the surrounding fluid ( $\kappa_0, \rho_0$ ) and is described by eqs 2a–2c.

$$\phi(\bar{\kappa}, \bar{\rho}) = \frac{1}{3} \left( \frac{5\bar{\rho} - 2}{2\bar{\rho} + 1} - \bar{\kappa} \right) \quad (2a)$$

$$\bar{\kappa} = \frac{\kappa_p}{\kappa_0} \quad (2b)$$

$$\bar{\rho} = \frac{\rho_p}{\rho_0} \quad (2c)$$

Our system is operated by creating resonance between the channel walls since the two phases (in our case water and olive oil) have similar acoustic impedance, meaning that the channel

is the resonance chamber. Since the channel height is  $< \lambda/2$ , no vertical particle manipulation is expected. In earlier work with acoustic manipulation of particles inside sessile water droplets surrounded by air,<sup>17</sup> the droplet itself is the resonance chamber due to the large difference in acoustic impedance between water and air. To be able to manipulate microparticles inside droplets in a two-phase system with similar acoustic impedance, essentially two requirements must be fulfilled. First, as in single-phase systems, resonance must be generated in the microchannel. The frequency to create a standing  $\lambda/2$ -wave depends on the channel dimensions and the sound velocity in the fluid. In a two-phase system, the dispersed phase is surrounded by the continuous phase; thus, the frequency of the standing wave is dependent on the combination of sound velocities in both phases. Even if the droplets apparently fill the width of the channel, there is still a thin lubricating film of the continuous phase present between the droplet and the channel wall.<sup>26</sup> Second, a high degree of coupling of the sound into the droplets must be achieved. If there is a mismatch in acoustic impedance between the two phases, this will reflect and refract the sound at the dispersed/continuous phase interface.<sup>27</sup> This indicates the importance of acoustic impedance matching between the two phases to achieve strong acoustic forces inside the droplets.

Here, as illustrated in Figure 1, we show how acoustophoresis can be combined with droplet microfluidics to create a droplet microfluidics unit operation capable of controlling the position of microparticles during a droplet splitting step. We have operated our system at  $\lambda/2$ -resonance that positions the microparticles to the center of the droplets, and by combining it with a trident shaped droplet split, the microparticles are directed to the center daughter droplet during the split, here named *controlled splitting*. We quantify the success of this operation by reporting on microparticle recovery and microparticle enrichment factor in the center daughter droplet. We show that acoustic focusing of microparticles in droplets can be applied both to polystyrene beads and red blood cells.

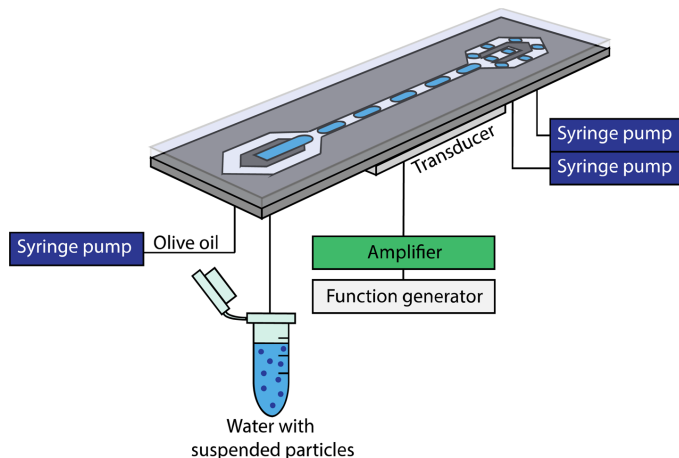


**Figure 2.** Experimental setup for acoustic positioning of microparticles inside droplets. Aqueous droplets with encapsulated microparticles are generated on-chip, and the microparticles are positioned by the acoustic forces to the center of the droplets. The droplets are split in a trifurcation point to obtain enrichment of microparticles in the center daughter droplets.

## EXPERIMENTAL SECTION

**Microchip Design.** All required steps for enrichment (i.e., droplet generation, encapsulation of microparticles, positioning of microparticles, and droplet splitting) are integrated on a single microfluidic chip and performed in a continuous mode. Monodisperse aqueous droplets were generated in oil using a flow focusing geometry, where the dispersed phase entered from the center channel and the continuous phase entered from the two side channels. The inlets and outlets had a symmetric design, and the center and side channels were oriented  $45^\circ$  in relation to each other. To minimize flow fluctuations, the two side channels had a common fluid inlet and outlet, respectively.

**Microchip Fabrication.** The microfluidic channels were fabricated by photolithography and anisotropic wet etching with KOH (40 g/100 mL  $\text{H}_2\text{O}$ ,  $80^\circ\text{C}$ ) of a (100) silicon wafer. The main channel structures were oriented  $45^\circ$  in relation to the primary flat of the wafer resulting in main channels with a rectangular cross-section with a depth of  $165\ \mu\text{m}$  and width of  $400\ \mu\text{m}$ . Holes for fluid inlets and outlets were wet etched through the wafer, and the chip was sealed by anodic bonding of a 1.1 mm thick glass lid. A piezoelectric element (Pz26, Ferroperm Piezoceramics A/S) was glued using cyanoacrylate glue (Loctite 420, Henkel AG & Co.) on the silicon side of the chip to ensure good acoustic coupling into the chip. The channels were treated with a surface coating agent (Repel-Silane ES, Pharmacia Biotech) to render the channels hydrophobic.

**Experimental Setup.** An illustration of the experimental setup is shown in Figure 2. The piezoelectric element was actuated with a function generator (33220A, Agilent Technologies Inc.) connected via an amplifier (75A250, Amplifier Research). The frequency was matched to create  $\lambda/2$ -resonance in the channel ( $1.80\ \text{MHz}$  at  $25\ \text{V}_{\text{peak-peak}}$ ).

The fluid flows were controlled by syringe pumps (NEMESYS, Cetoni GmbH) connected to the chip via Teflon tubings. The flow in the side inlets and all the outlets were directly controlled by the syringe pumps, and the dispersed

phase was introduced to the system via a submerged Teflon tubing in an Eppendorf tube to ensure no pressure difference buildup in the system. The flow rates were optimized to achieve stable droplet generation and splitting. In the experiments with polystyrene beads, the volumetric flow rate of the continuous phase was set at  $6\ \mu\text{L}/\text{min}$ , and the flow rates in the center and side outlets were set at 6 and  $12\ \mu\text{L}/\text{min}$ , respectively. In the cell experiment, the volumetric flow rate of the continuous phase was set at  $5\ \mu\text{L}/\text{min}$ , and the flow rates in the center and side outlets were set at 4 and  $6\ \mu\text{L}/\text{min}$ , respectively. Images of the droplets were acquired with a camera (XM10, Olympus) mounted on a microscope (BX51W1, Olympus) with a  $4\times$  or  $10\times$  objective.

Olive oil ( $v_{\text{olive oil}} = 1450\ \text{m/s}$ ,  $\rho_{\text{olive oil}} = 0.91\ \text{kg}/\text{dm}^3$ ) was chosen as the continuous phase since olive oil and water ( $v_{\text{water}} = 1481\ \text{m/s}$ ,  $\rho_{\text{water}} = 1.00\ \text{kg}/\text{dm}^3$ ) have similar acoustic properties. The specific acoustic impedances ( $z = \rho v$ ) of olive oil and water are 1.32 and 1.48 MRayl, respectively. Our experimental results show that the use of fluorinated oil (HFE Novec 7500,  $z_{\text{HFE Novec 7500}} = 1.07\ \text{MRayl}$ ) as the continuous phase does not result in a sufficiently strong acoustic resonance in our system.

**Experimental Procedure.** Water droplets were generated in olive oil and polystyrene beads ( $5\ \mu\text{m}$ , Fluka) were encapsulated ( $6 \times 10^9$  beads/mL, resulting in  $\sim 475$  beads in each droplet). This concentration was chosen for easy visualization of the experiments and since it is a typical concentration found in bead-based assays. Downstream of the channel, the droplets were split into three daughter droplets at a trifurcation, resulting in a splitting ratio of approximately  $1/3$  in each channel with slightly less in the sides. This splitting step was performed with both ultrasound on and off, and there was no difference noted in the volumes of the daughter droplets.

To perform quantitative analysis of recovery and enrichment, the droplets were collected in reservoir Teflon tubings with a volume of  $300\ \mu\text{L}$ . The droplets were transferred to new individual Eppendorf tubes and allowed to coalesce. In the

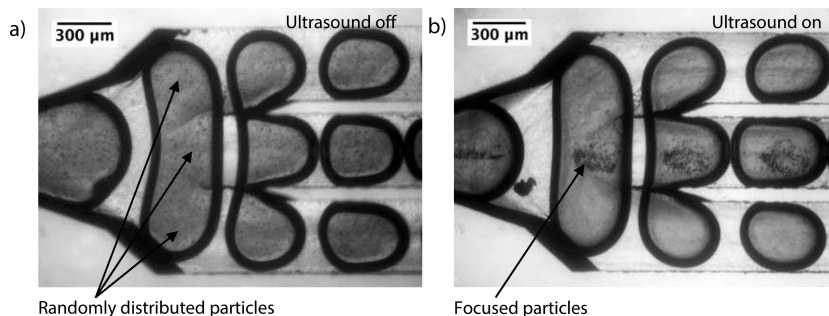


**Figure 3.** Acoustic positioning and enrichment of microparticles during a trident shaped droplet split. (a) Without ultrasound. The microparticles are distributed in the entire main droplet, resulting in no considerable enrichment of the microparticles. (b) With ultrasound. The microparticles are positioned to the center of the droplets by the acoustic forces, directing the microparticles to the center daughter droplet after splitting, leading to a 2+-fold enrichment of microparticles.

Eppendorf tubes, the oil and water phases form a heterogeneous solution and the oil could be removed by pipetting. The concentration of polystyrene beads in the aqueous phase collected at the center and side outlets was counted using a microparticle counter (Multisizer 3, Beckman Coulter, Inc.).

To demonstrate the possibility to manipulate cells inside droplets, red blood cells were encapsulated in droplets. Blood samples were obtained from healthy volunteers under informed consent. Before droplet generation, the red blood cells were transferred from whole blood to phosphate-buffered saline (PBS) via centrifugation 5 times with repeated removals and additions of 1 mL of PBS and then diluted 200 times in PBS to obtain a suitable concentration of cells for visualization, followed by droplets generation and acoustic manipulation of the encapsulated cells.

**Analysis.** The volume of the droplets was determined by measuring the cross-sectional area of the droplets using ImageJ software making the assumption that the droplets have the height of the channel. This yields a small and consistent overestimation of the volume due to the lubricating film between the channel and the droplets and the fact that the droplets are rounded at the front and back end.

Recovery is determined by measuring the concentrations and volume of the daughter droplets as previously described and calculated according to eq 3,

$$\begin{aligned} \text{recovery} &= \frac{n_{\text{center droplet}}}{n_{\text{center droplet}} + 2n_{\text{side droplet}}} \\ &\rightarrow \frac{C_{\text{center droplets}} V_{\text{center droplet}}}{C_{\text{center droplets}} V_{\text{center droplet}} + 2(C_{\text{side droplets}} V_{\text{side droplet}})} \\ &= \frac{C_{\text{center droplets}}}{C_{\text{center droplets}} + \frac{2V_{\text{side droplet}}}{V_{\text{center droplet}}} C_{\text{side droplets}}} \end{aligned} \quad (3)$$

where  $n$  is the number of microparticles in each center droplet ( $n_{\text{center droplet}}$ ) and side droplet ( $n_{\text{side droplet}}$ ),  $C$  is the concentration of microparticles in the center droplets ( $C_{\text{center droplets}}$ ) and the side droplets ( $C_{\text{side droplets}}$ ),  $V$  is the volume of a daughter droplet in the center outlet ( $V_{\text{center droplet}}$ ) and side outlet ( $V_{\text{side droplet}}$ ), respectively.

The enrichment factor after droplet splitting is defined as eq 4.

$$\text{enrichment factor} = \frac{C_{\text{center droplets}}}{C_{\text{initial}}} \quad (4)$$

To avoid measurement errors caused by sedimentation of the microparticles in the Eppendorf tube, the initial concentration was calculated from the measured microparticle concentrations in the center and the side droplets combined.

## RESULTS AND DISCUSSION

Aqueous droplets containing polystyrene beads were generated; ultrasound was applied to the system, and the frequency was optimized to create resonance. Polystyrene beads in water have positive acoustic contrast factor and are expected to be moved to the center of the droplets, i.e., the pressure nodes, by the acoustic forces, which was also observed when ultrasound was activated (see the photograph in Figure 1). At the trifurcation point downstream of the channel, every droplet was split into three daughter droplets. The volumes of the daughter droplets in the center and side channels were 28 and 25 nL, respectively. When the acoustic forces were applied during the droplet splitting step, it was possible to direct the majority of the microparticles in the original droplet into the center daughter droplet, while significantly fewer microparticles were collected in the side daughter droplets; see Figure 3 and the video.

When droplets are transported through microfluidic channels, a complex pattern of flow fields arises due to the presence of the immiscible interface between the continuous and dispersed phase.<sup>26,28</sup> These flow fields were also observed in the system and imply that there is a competition between the acoustic forces acting to position the microparticles to the center of the droplets and the drag forces on the microparticles from the circulating flows inside the moving droplets. Hein et al. recently showed how microparticles accumulate at the sides of the droplets depending on the relation between capillary number of the system and particle sedimentation rate.<sup>13</sup> As we operate with microparticles of lower sedimentation rate (0.68  $\mu\text{m/s}$ ) and higher capillary number (0.009), this effect does not play a dominant role in our system.

The concentration of microparticles in the center and side daughter droplets was measured with and without ultrasound,

and the results are presented in Table 1. The experiments were performed three times ( $n = 3$ ), with data acquisition in

**Table 1. Concentration of Polystyrene Beads in the Center and Side Daughter Droplets<sup>a</sup>**

|                |         | $C_{\text{center droplets}}$<br>(beads/mL) | $C_{\text{side droplets}}$<br>(beads/mL) |
|----------------|---------|--|--|
| ultrasound on  | run 1   | $11.0 \times 10^6$                         | $1.1 \times 10^6$                        |
|                | run 2   | $13.7 \times 10^6$                         | $0.7 \times 10^6$                        |
|                | run 3   | $13.2 \times 10^6$                         | $1.0 \times 10^6$                        |
|                | average | $12.6 \pm 1.4 \times 10^6$                 | $0.9 \pm 0.2 \times 10^6$                |
| ultrasound off | run 1   | $6.2 \times 10^6$                          | $4.8 \times 10^6$                        |
|                | run 2   | $7.2 \times 10^6$                          | $5.1 \times 10^6$                        |
|                | run 3   | $5.5 \times 10^6$                          | $4.5 \times 10^6$                        |
|                | average | $6.3 \pm 0.8 \times 10^6$                  | $4.8 \pm 0.3 \times 10^6$                |

<sup>a</sup>Errors are reported as one standard deviation of the measurements.

triplicates. Errors are reported as one standard deviation of the measurements. A recovery of microparticles of  $89 \pm 4\%$  was achieved when ultrasound was applied, compared with only  $43 \pm 2\%$  in the negative control. This means that close to 90% of the microparticles in the original droplet were found in the center daughter droplet after the split. Achieving a high recovery is especially important when handling scarce samples and if several consecutive controlled splitting steps would be performed.

When ultrasound was applied,  $2.45 \pm 0.10$ -fold enrichment was achieved in the center droplets. Even in the negative control with no ultrasound applied, a small enrichment was found in the center droplets. We measured  $1.17 \pm 0.05$ , indicating that the complex pattern of internal motions and aggregation of the microparticles in the droplet may play a role here. The enrichment factor is interesting to study because it also takes into account the amount of liquid removed from the original droplet, which is a critical parameter for the development of on-chip droplet washing unit operation.

The experiments were also performed with 8 times lower microparticle concentration ( $7.5 \times 10^5$  beads/mL) resulting in a similar recovery and enrichment factor. Thus, the initial microparticle concentration is not critical for successful system performance.

To increase enrichment further, the design of the splitting trifurcation and the flow ratio between the center and side channels may be optimized to remove more liquid to the sides while microparticles still are retained in the center daughter droplets. In addition, it would be beneficial to achieve stronger

acoustic field by, e.g., increasing the voltage to attain stronger acoustic focusing. However, when handling biological material or other heat sensitive reactions, this must be balanced by the need to avoid excessive heating.

To evaluate the suitability of the described technique for droplet-based cell assays, red blood cells were used to show the possibility to manipulate cells inside droplets. Red blood cells have been used extensively in acoustofluidics systems and have positive acoustic contrast factor in PBS.<sup>14</sup> The cells were encapsulated in PBS droplets, and at the activation of ultrasound, the cells were positioned to the center of the droplets, as shown in Figure 4. This shows the possibility to use the presented method for biological applications.

## CONCLUSIONS

We have successfully demonstrated that acoustophoresis can be used to laterally position microparticles inside droplets and combined it with a trident shaped droplet split to achieve enrichment of microparticles inside droplets. We have also shown that it is possible to manipulate red blood cells inside droplets. Particle enrichment and removal of medium are key parts in many standard biological assays, and we believe that the described technique will prove a useful tool that can be integrated in droplet microfluidic circuitry to be able to perform cell-based assays that are not possible to perform today.

## ASSOCIATED CONTENT

### Web-Enhanced Feature

A video of the acoustic focusing and splitting of the droplets in AVI format is available in the online version of the paper.

## AUTHOR INFORMATION

### Corresponding Author

\*E-mail: [anna.fornell@bme.lth.se](mailto:anna.fornell@bme.lth.se).

### Notes

The authors declare no competing financial interest.

## ACKNOWLEDGMENTS

This work was funded by the Swedish Research Council, the Crafoord Foundation, Foundation Maja and Erik Lindqvist, and Foundation Olle Engkvist Byggmästare through grants received by M.T. H.N.J. acknowledges financial support by the Swedish Research Council Formas "Strong research Environments" project No. 2011-1692, BioBridges.

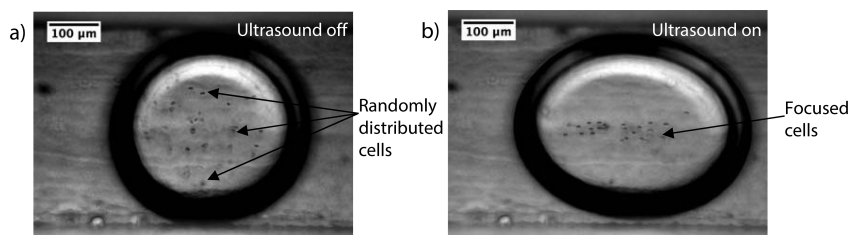


**Figure 4.** Acoustic focusing of red blood cells inside a droplet. (a) Without ultrasound. The cells are distributed in the entire droplet. (b) With ultrasound. The cells are positioned to the center of the droplet by the acoustic forces. Note that the droplet interface is deformed by the applied ultrasound due to the difference in acoustic properties of the two fluids.

## ■ REFERENCES

- (1) Seemann, R.; Brinkmann, M.; Pfohl, T.; Herminghaus, S. *Rep. Prog. Phys.* **2012**, *75* (1), 016601.
- (2) Teh, S. Y.; Lin, R.; Hung, L. H.; Lee, A. P. *Lab Chip* **2008**, *8* (2), 198–220.
- (3) Guo, M. T.; Rotem, A.; Heyman, J. A.; Weitz, D. A. *Lab Chip* **2012**, *12* (12), 2146–2155.
- (4) Joensson, H. N.; Andersson Svahn, H. *Angew. Chem., Int. Ed.* **2012**, *51* (49), 12176–12192.
- (5) Song, H.; Chen, D. L.; Ismagilov, R. F. *Angew. Chem., Int. Ed.* **2006**, *45* (44), 7336–7356.
- (6) Clausell-Tormos, J.; Lieber, D.; Baret, J. C.; El-Harrak, A.; Miller, O. J.; Frenz, L.; Blouwolf, J.; Humphry, K. J.; Koster, S.; Duan, H.; Holtze, C.; Weitz, D. A.; Griffiths, A. D.; Merten, C. A. *Chem. Biol.* **2008**, *15* (5), 427–437.
- (7) Abate, A. R.; Hung, T.; Mary, P.; Agresti, J. J.; Weitz, D. A. *Proc. Natl. Acad. Sci. U. S. A.* **2010**, *107* (45), 19163–19166.
- (8) Link, D. R.; Anna, S. L.; Weitz, D. A.; Stone, H. A. *Phys. Rev. Lett.* **2004**, *92* (5), 054503.
- (9) Schmid, L.; Weitz, D. A.; Franke, T. *Lab Chip* **2014**, *14* (19), 3710–3718.
- (10) Lagus, T. P.; Edd, J. F. *J. Phys. D: Appl. Phys.* **2013**, *46* (11), 114005.
- (11) Brouzes, E.; Kruse, T.; Kimmerling, R.; Strey, H. H. *Lab Chip* **2015**, *15*, 908–919.
- (12) Lombardi, D.; Ditttrich, P. S. *Anal. Bioanal. Chem.* **2011**, *399* (1), 347–352.
- (13) Hein, M.; Moskopp, M.; Seemann, R. *Lab Chip* **2015**, *15*, 2879–2886.
- (14) Lenshof, A.; Magnusson, C.; Laurell, T. *Lab Chip* **2012**, *12* (7), 1210–1223.
- (15) Ding, X.; Li, P.; Lin, S.-C. S.; Stratton, Z. S.; Nama, N.; Guo, F.; Slotcavage, D.; Mao, X.; Shi, J.; Costanzo, F.; Huang, T. J. *Lab Chip* **2013**, *13* (18), 3626–3649.
- (16) Wiklund, M. *Lab Chip* **2012**, *12* (11), 2018–2028.
- (17) Oberti, S.; Neild, A.; Quach, R.; Dual, J. *Ultrasonics* **2009**, *49* (1), 47–52.
- (18) Rogers, P. R.; Friend, J. R.; Yeo, L. Y. *Lab Chip* **2010**, *10* (21), 2979–2985.
- (19) Li, S.; Ding, X.; Guo, F.; Chen, Y.; Lapsley, M. I.; Lin, S. C. S.; Wang, L.; McCoy, J. P.; Cameron, C. E.; Huang, T. J. *Anal. Chem.* **2013**, *85* (11), 5468–5474.
- (20) Leibacher, I.; Reichert, P.; Dual, J. *Lab Chip* **2015**, *15*, 2896–2905.
- (21) Schmid, L.; Franke, T. *Lab Chip* **2013**, *13* (9), 1691–1694.
- (22) Sesen, M.; Alan, T.; Neild, A. *Lab Chip* **2015**, *15*, 3030–3038.
- (23) Sesen, M.; Alan, T.; Neild, A. *Lab Chip* **2014**, *14* (17), 3325–3333.
- (24) Leibacher, I.; Schoendube, J.; Dual, J.; Zengerle, R.; Koltay, P. *Biomicrofluidics* **2015**, *9* (2), 024109.
- (25) Laurell, T.; Lenshof, A., Eds. *Microscale Acoustofluidics*; The Royal Society of Chemistry: Cambridge, 2015.
- (26) Baroud, C. N.; Gallaire, F.; Dangling, R. *Lab Chip* **2010**, *10*, 2032–2045.
- (27) Kinsler, L. E.; Frey, A. R.; Coppens, A. B.; Sanders, J. V. *Fundamentals of Acoustics*, 4th ed.; John Wiley & Sons: New York, 2000.
- (28) Kurup, G. K.; Basu, A. S. *Biomicrofluidics* **2012**, *6* (2), 022008.

# Paper II

**Intra-droplet acoustic particle focusing:  
simulations and experimental observations**

A. Fornell, F. Garofalo, J. Nilsson, H. Bruus,  
and M. Tenje

*Submitted*





# Intra-droplet acoustic particle focusing: simulations and experimental observations

A. Fornell,<sup>1\*</sup> F. Garofalo,<sup>1</sup> J. Nilsson,<sup>1</sup> H. Bruus,<sup>2</sup> and M. Tenje<sup>1,3</sup>

<sup>1</sup> Department Biomedical Engineering, Lund University, Lund, Sweden

<sup>2</sup> Department of Physics, Technical University of Denmark, Kongens Lyngby, Denmark

<sup>3</sup> Department Engineering Sciences, Science for Life Laboratory, Uppsala University, Uppsala, Sweden

\*Corresponding author: [anna.fornell@bme.lth.se](mailto:anna.fornell@bme.lth.se)

## Abstract

The aim of this paper is to study resonance conditions for acoustic particle focusing inside droplets in two-phase microfluidic systems. A bulk acoustic wave microfluidic chip was designed and fabricated for focusing microparticles inside aqueous droplets (plugs) surrounded by a continuous oil phase in a 380-micrometer wide channel. The quality of the acoustic particle focusing was investigated by considering the influence of the acoustic properties of the continuous phase in relation to the dispersed phase. To simulate the system and study the acoustic radiation force on the particles inside droplets, a simplified 3D model was used. The resonance conditions and focusing quality were studied for two different cases: (i) the dispersed and continuous phase were acoustically mismatched (water droplets in fluorinated oil) and (ii) the dispersed and continuous phase were acoustically matched (water droplets in olive oil). Experimentally, we observed poor acoustic particle focusing inside droplets surrounded by fluorinated oil while good focusing was observed in droplets surrounded by olive oil. The experimental results are supported qualitatively by our simulations. These show that the acoustic properties (density and compressibility) of the dispersed and continuous phases must be matched to generate a strong and homogeneous acoustic field inside the droplet that is suitable for high quality intra-droplet acoustic particle focusing.

## Acknowledgements

Financial support was provided by the Swedish Research Council, the Crafoord Foundation, Knut and Alice Wallenberg Foundation (Grant No. KAW 2012.0023), Längmanska Kulturfonden, the Royal Physiographic Society of Lund, and Foundation Olle Engkvist Byggmästare.

## 1. Introduction

Manipulation of particles in microfluidic channels using acoustic forces, acoustophoresis, has shown to be a useful tool in a number of lab-on-a-chip applications including the separation of rare cells (Nordin and Laurell 2012; Li et al. 2015), concentration of bacteria (Carugo et al. 2014) and cell trapping (Hammarström et al. 2010; Christakou et al. 2015; Collins et al. 2015). Recently, acoustic particle manipulation has also been implemented in droplet-based microfluidic systems for manipulation of whole droplets (Schmid et al. 2014; Leibacher et al. 2015; Sesen et al. 2015) and focusing of particles and cells inside droplets (Fornell et al. 2015, 2017; Park et al. 2017).

The interest in droplet microfluidics has emerged because droplets are perfectly suited as miniaturized reaction chambers for encapsulation and investigation of cells at the single cell level (Schneider et al. 2013; Shembekar et al. 2016), and the technology allows for improved genome engineering and screening of cells (Agresti et al. 2010; Sjoström et al. 2014). In most of these applications, having the possibility to precisely handle the particles inside the droplets expands the complexity of the assays that can be performed on-chip. Particle manipulation allows, for example, intra-droplet particle enrichment and buffer-exchange which are often required in multistep assays (Tenje et al. 2017).

To control the position of particles inside droplets both active and passive methods have been implemented including magnetophoresis (Lombardi and Dittrich 2011; Lee et al. 2014; Brouzes et al. 2015), dielectrophoresis (Han et al. 2017), acoustophoresis (Fornell et al. 2015, 2017; Park et al. 2017) and hydrodynamic methods (Kurup and Basu 2012; Sun et al. 2012; Hein et al. 2015). Of these, acoustophoresis has the advantages of being label-free, gentle, and operated in non-contact mode. However, in our previous work there have been experimental indications that the acoustic particle focusing inside droplets is impaired by a difference in acoustic properties between the droplet and the continuous phase (Fornell et al. 2015). Typically, water-based solutions are used as the dispersed phase as living cells are often encapsulated inside the droplets, and fluorinated oils like Novec HFE-7500 or FC-40 with the addition of fluorosurfactants are used as the continuous phase (also known as the carrier oil). These oils are preferred in droplet-based applications as they allow for the generation of stable water droplets and low cross-contamination between individual droplets, as well as having high gas solubility which is essential for cell viability and proliferation (Baret 2012). However, these oils have very different acoustic properties compared with water, and that is thought to have a negative impact on intra-droplet acoustic particle focusing in two-phase microfluidic systems.

The interaction of sound waves and liquid interfaces has been studied for a long time in both micro- and macrosystems. Almost 80 years ago the deformation of the interface between two immiscible liquids with different acoustic properties caused by a directed ultrasonic beam was studied (Hertz and Mende 1939). Additionally, the acoustic forces can also act on liquid interfaces in miscible systems, and it has been shown that laminated liquids with different acoustic properties exposed to a standing wavefield can be relocated or stabilized within a microfluidic channel (Deshmukh et al. 2014).

Motivated by these observations and studies, this paper investigates acoustic particle focusing in two-phase systems and in particular how the acoustic properties of the continuous phase influence the acoustic radiation force on particles encapsulated inside droplets. The study is restricted to two cases: water droplets (plugs) generated in fluorinated oil and vegetable olive oil, respectively. Fluorinated oil is chosen since this oil type is commonly used in droplet microfluidic systems, and olive oil is chosen since it has similar acoustic properties as water. First, a simplified 3D model is set up and the acoustic pressure field and the acoustic radiation force on the encapsulated particles is calculated. Second, acoustic particle focusing is analyzed experimentally. This study provides a wider understanding of the fundamental physical principles of intra-droplet acoustic particle focusing, which is essential for the development of optimal system design for acoustic particle manipulation in two-phase microfluidic systems.

## 2. Theory and numerical simulations

### 2.1. Acoustophoresis

Ultrasonic standing waves can be used to position particles in microfluidic channels. For particles larger than 2  $\mu\text{m}$  suspended in water, the acoustic boundary layer and viscosity in the MHz-range can be neglected. In this case, the acoustic velocity field  $\mathbf{v}_1$  is given by the gradient of the acoustic pressure field  $p_1$  as  $\mathbf{v}_1 = \frac{-i}{\omega \rho_{\text{WA}}} \nabla p_1$ , and the acoustic radiation force  $\mathbf{F}^{\text{rad}}$  acting on the microparticle is a gradient force given by, (Bruus 2012)

$$\mathbf{F}^{\text{rad}} = -\nabla U^{\text{rad}}, \quad \text{with} \quad U^{\text{rad}} = \pi a_{\text{p}}^3 \left( \frac{f_0}{3} \kappa_{\text{WA}} |p_1|^2 - \frac{f_1}{2} \rho_{\text{WA}} |\mathbf{v}_1|^2 \right), \quad (1)$$

$$f_0 = 1 - \frac{\kappa_{\text{p}}}{\kappa_{\text{WA}}}, \quad \text{and} \quad f_1 = \frac{2(\rho_{\text{p}} - \rho_{\text{WA}})}{2\rho_{\text{p}} + \rho_{\text{WA}}}.$$

Here,  $\omega$  is the angular frequency,  $f_0$  and  $f_1$  are the monopole and dipole coefficients,  $a_{\text{p}}$ ,  $\rho_{\text{p}}$ , and  $\kappa_{\text{p}}$  are the radius, density and compressibility of the microparticle, and  $\rho_{\text{WA}}$  and  $\kappa_{\text{WA}}$  are the density and compressibility of water. As seen in Equation (1), the acoustic properties of the particle relative to the surrounding water determine the direction of the radiation force on the particle: a particle with high density and low compressibility is focused to the pressure node whereas a particle with low density and high compressibility is focused to the pressure anti-node. Both plastic particles and cells in water have such acoustic properties that they are focused to the pressure node in an acoustic standing wavefield. The focusing time  $t_{\text{foc}}$ , defined as the time it takes a particle to move from  $y = -\frac{7}{16}W$  to  $y = -\frac{1}{16}W$  or  $\sim 40\%$  of the half channel width  $W$ , is given in terms of the particle radius  $a_{\text{p}}$ , viscosity  $\eta$ , and the acoustic energy density  $E_{\text{ac}}$  as (Bruus 2012),

$$t_{\text{foc}} = \frac{9}{(4f_0 + 6f_1)\pi^2} \frac{W^2}{a_{\text{p}}^2} \frac{\eta}{E_{\text{ac}}} \ln \left[ \frac{\tan\left(\frac{7}{16}\pi\right)}{\tan\left(\frac{1}{16}\pi\right)} \right]. \quad (2)$$

## 2.2. Model system used in the numerical simulations

The system is modelled by considering a water-in-oil droplet confined in a rectangular channel of height  $H = 100 \mu\text{m}$  and width  $W = 380 \mu\text{m}$  in an acoustically-hard silicon-pyrex chip to which the ultrasound is supplied by oscillating the bottom plane with a frequency near 2 MHz, see Fig. 1.

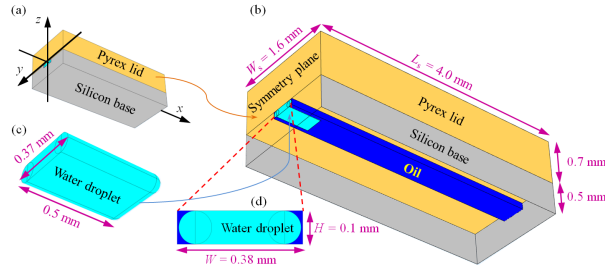


**Fig. 1** 3D model of the microfluidic device used in the numerical simulations. (a) A sketch of the chip with its  $\langle 100 \rangle$ -oriented single-crystal silicon base (gray) and pyrex lid (beige). The device is assumed to be symmetric around the  $y$ - $z$  plane, such that only half of the system ( $x > 0$ ) needs to be simulated. (b) The detailed geometry of the device is shown with the silicon layer opened up to make the water droplet (cyan) visible in the long, straight, rectangular oil-filled channel (blue). (c) The detailed geometry of the flattened water droplet. (d) End view in the symmetry plane of the water droplet (cyan) and surrounding oil (blue). The bottom plane is actuated vertically as  $\mathbf{u}_1 = d_1(1/2 + y/W) e^{-i\omega t} \mathbf{e}_z$  with a frequency near 2 MHz.

While the width  $W$  and height  $H$  of the channel as well as the height of the silicon and pyrex layers equal the experimental values, the width  $W_s$  of the solid chip and the length  $L_s$  of the system has been reduced to enable the demanding 3D simulation on the available 128 GB RAM computer. A further reduction is achieved by limiting the study to systems with rectangular channels that are symmetric around the vertical  $x$ - $z$  plane, such that only half of the system needs to be simulated. Moreover, we neglect the thin film of the continuous phase between the droplet and the channel walls (Baroud et al. 2010). The material and geometrical parameters used in the simulations are listed in Table 1.

**Table 1.** Material and geometrical parameters used in the modelling of the droplet systems.

| Parameters for the solids                                |                         | Parameters for the fluids   |                                |
|--|-------------------------|---|--------------------------------|
| Chip base height, $H_b$                                  | 0.5 mm                  | Water density <sup>a</sup> , $\rho_{WA}$  | 997 kg m <sup>-3</sup>         |
| Chip lid height, $H_l$                                   | 0.7 mm                  | Water sound speed <sup>c</sup> , $c_{WA}$   | 1497 m s <sup>-1</sup>         |
| Chip width, $W_c$  | 1.6 mm                  | Water viscosity <sup>a</sup> , $\eta_{WA}$  | 0.89 mPa s                     |
| Chip length, $L_s$                                       | 8.0 mm                  | Fluorinated oil density <sup>c</sup> , $\rho_{HFE}$                                   | 1621 kg m <sup>-3</sup>        |
| Channel height, $H$                                      | 0.1 mm                  | Fluorinated oil sound speed <sup>c</sup> , $c_{HFE}$                                  | 659 m s <sup>-1</sup>          |
| Channel width, $W$                                       | 0.38 mm                 | Fluorinated oil viscosity <sup>d</sup> , $\eta_{HFE}$                                 | 1.24 mPa s                     |
| Pyrex density <sup>a</sup> , $\rho_{py}$                 | 2230 kg m <sup>-3</sup> | Olive oil density <sup>c</sup> , $\rho_{OLV}$   | 910 kg m <sup>-3</sup>         |
| Pyrex longitudinal sound speed <sup>d</sup> , $c_{L,py}$ | 5592 m s <sup>-1</sup>  | Olive oil sound speed <sup>c</sup> , $c_{OLV}$  | 1450 m s <sup>-1</sup>         |
| Pyrex transverse sound speed <sup>d</sup> , $c_{T,py}$   | 3424 m s <sup>-1</sup>  | Olive oil viscosity <sup>e</sup> , $\eta_{OLV}$                                       | 60.8 mPa s                     |
| Silicon density <sup>b</sup> , $\rho_{si}$               | 2329 kg m <sup>-3</sup> | Damping coefficient for all fluids <sup>f</sup> , $I_f$                               | 0.004                          |
| Silicon elastic constant <sup>b</sup> , $C_{11}$         | 165.7 GPa               | Droplet height, $H_d$   | 0.1 mm                         |
| Silicon elastic constant <sup>b</sup> , $C_{12}$         | 63.9 GPa                | Droplet width, $W_d$  | 0.37 mm                        |
| Silicon elastic constant <sup>b</sup> , $C_{44}$         | 79.6 GPa                | Droplet length, $L_d$   | 1.0 mm                         |
| Damping coefficient all solids <sup>f</sup> , $I_s$      | 0.001                   | <b>Parameters for 10-<math>\mu\text{m}</math>-diameter polystyrene test particles</b> |                                |
|  |                         | Acoustophoretic mobility, $\mu_{ac}$  | 12 ( $\mu\text{m s}^{-1}$ )/pN |
|  |                         | Buoyancy-corrected gravity force, $F_{grav}^r$  | 0.26 pN                        |
|  |                         | Sedimenting time $H = 100 \mu\text{m}$ , $t_{sed}$                                    | 32 s                           |

<sup>a</sup>Values from Ley and Bruus (Ley and Bruus 2017)

<sup>b</sup>Values from Hopcroft (Hopcroft et al. 2010)

<sup>c</sup>Measured with a Density and Sound Velocity Meter (DSA 5000M, Anton Paar)

<sup>d</sup>Data sheet from the manufacturer (3M)

<sup>e</sup>Measured with falling ball microviscometer (Minivis II, Grabner Instruments)

### 2.3. Numerical simulations: method

Simulations of the systems are performed using the finite-element solver COMSOL Multiphysics (version 5.2) using the method of Ley and Bruus (Ley and Bruus 2017) for pyrex-water systems, extended to include the single-crystal silicon base using the method of Dual and Schwarz (Dual and Schwarz 2012). The acoustic field is calculated numerically using the linear elastic equations for the displacement field  $\mathbf{u}_1$  in the solid wall with density  $\rho_s$  and stress tensor  $\boldsymbol{\sigma}_1$  coupled to the pressure field  $p_1$  governed by the Helmholtz wave equation in the two fluids (a) and (b),

$$-\rho_s \omega^2 (1 + i\Gamma_s) \mathbf{u}_1 = \nabla \cdot \boldsymbol{\sigma}_1, \quad \nabla^2 p_1^{(a)} = -(1 + i\Gamma_a) \frac{\omega^2}{c_a^2} p_1^{(a)}, \quad \nabla^2 p_1^{(b)} = -(1 + i\Gamma_b) \frac{\omega^2}{c_b^2} p_1^{(b)}. \quad (3)$$

To mimic the non-symmetric actuation of the experiment on the bottom of the silicon base, a harmonically oscillating vertical displacement of the form  $\mathbf{u}_1 = d_1 \left( \frac{1}{2} + \frac{y}{W} \right) e^{-i\omega t} \mathbf{e}_z$  for  $-\frac{1}{2}W < y < \frac{1}{2}W$  is imposed, with  $d_1 = 0.4$  nm and using complex-time notation. Here,  $\omega = 2\pi f$  where  $\omega$  and  $f$  are the angular frequency and frequency, respectively. On the vertical  $yz$  planes at  $x = 0$  and  $x = L$ , we use symmetry boundary conditions (hard wall conditions), and all other outer boundaries have the no-stress condition. On the internal solid-liquid and liquid-liquid interfaces the boundary conditions are continuity of the normal component of the stress and of the displacement velocities. The corresponding tangential stresses are set to zero. In summary,

$$\text{Solid-fluid interface: } \boldsymbol{\sigma}_1 \cdot \mathbf{n} = -p_1 \mathbf{n} \text{ (stress) and } \omega \mathbf{n} \cdot \mathbf{u}_1 = \frac{1}{\omega \rho_f} \mathbf{n} \cdot \nabla p_1 \text{ (velocity),} \quad (4a)$$

$$\text{Fluid}^{(a)}\text{-Fluid}^{(b)}: p_1^{(a)} = p_1^{(b)} \text{ (pressure) and } \frac{1}{\omega \rho_f^{(a)}} \mathbf{n} \cdot \nabla p_1^{(a)} = \frac{1}{\omega \rho_f^{(b)}} \mathbf{n} \cdot \nabla p_1^{(b)} \text{ (velocity),} \quad (4b)$$

$$\text{Solid-air boundary: } \boldsymbol{\sigma}_1 \cdot \mathbf{n} = \mathbf{0}, \quad \text{Actuation boundary: } \mathbf{u}_1 = d_1 \left( \frac{1}{2} + \frac{y}{W} \right) e^{-i\omega t} \mathbf{e}_z, \quad (4c)$$

where  $\mathbf{n}$  is the interface normal vector. We performed a standard numerical convergence study (Ley and Bruus 2017) and found the fields to have converged within a relative deviation of 1%.

Because the size of the chip in the numerical model is smaller than the actual chip, we first characterize the system with air in the channel to locate the resonances determined solely by the geometry of the solid. In the range from 1.5 to 2.1 MHz we find only two resonances, namely at 1.60 MHz and at 2.01 MHz, as shown in Fig. 2, where the black line shows the average acoustic energy density  $\langle E_{ac}^{\text{solid}} \rangle$  versus frequency  $f$ . In the subsequent analysis with liquid in the channel, we then make sure to avoid these resonances by working in the range from 1.64 to 1.96 MHz. Our numerical results are thus independent of the specific smaller chip geometry of the model and can be applied to the larger actual chip geometry. The optimal frequency for acoustophoresis inside the droplet is found by locating resonance peaks in plots of the acoustic radiation force  $\langle \mathbf{F}^{\text{rad}} \rangle$  versus frequency  $f$  for a 10- $\mu\text{m}$ -diameter polystyrene test particle averaged over its position in the water droplet, see Equation (1). Ideally, the vertical component should vanish,  $\langle F_z^{\text{rad}} \rangle = 0$ , while the horizontal component should be anti-symmetric and pointing towards the  $x$ - $z$  plane with as big as magnitude as possible,  $\langle \text{sign}(y) F_y^{\text{rad}} \rangle < 0$ , where the sign of the  $y$  coordinate,  $\text{sign}(y)$ , is inserted to pick up the anti-symmetry of the radiation force component in the spatial average.

#### 2.4. Numerical simulations: results and discussion

The resonance curves for a water droplet surrounded by fluorinated oil (marked as HFE) and olive oil (marked as OLV) are shown in Fig. 2. Strong resonances are found at  $f = 1.718$  MHz with  $\langle \text{sign}(y) F_y^{\text{rad}} \rangle = -1.9$  pN for a water droplet in fluorinated oil, and at  $f = 1.865$  MHz with  $\langle \text{sign}(y) F_y^{\text{rad}} \rangle = -5.4$  pN for a water droplet in olive oil. The vertical components are negligible in the entire frequency range.

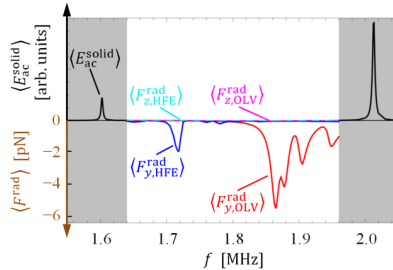


**Fig. 2** Resonance curves: averaged acoustic energy density  $\langle E_{\text{ac}}^{\text{solid}} \rangle$  vs.  $f$  in the solid walls for the empty chip (black line), and the averaged  $y$  and  $z$  components  $\langle F_{y,z}^{\text{rad}} \rangle$  of the acoustic radiation force on a 10- $\mu\text{m}$ -diameter polystyrene test particle in the water droplet in fluorinated oil ( $\langle F_{y,\text{HFE}}^{\text{rad}} \rangle$  blue and  $\langle F_{z,\text{HFE}}^{\text{rad}} \rangle$  cyan), and olive oil ( $\langle F_{y,\text{OLV}}^{\text{rad}} \rangle$  red and  $\langle F_{z,\text{OLV}}^{\text{rad}} \rangle$  magenta). The resonances are found to be at  $f = 1.718$  MHz for fluorinated oil, and at  $f = 1.865$ , 1.878, 1.905, and 1.950 MHz for olive oil. The latter resonance series corresponds to the number of axial nodes being 0, 1, 2, and 3.

A physical interpretation of the resonances and their ability to facilitate acoustophoresis is obtained by studying the acoustic pressure  $p$  in the fluids and the displacement  $u$  in the solids as well as the acoustic radiation force  $\langle F^{\text{rad}} \rangle$  in the water droplet for the main resonances at  $f = 1.718$  MHz (fluorinated oil) and at  $f = 1.865$  MHz (olive oil) shown in Fig. 3 (a) and (b), respectively.

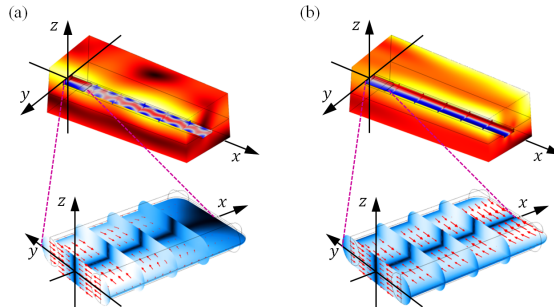


**Fig. 3** (a) The chip with a water droplet in fluorinated oil at resonance  $f = 1.718$  MHz: The acoustic pressure  $p$  from -156 kPa (blue) to 156 kPa (red) and the magnitude of the acoustic displacement  $u$  from 0 nm (black) to 0.35 nm (white) in the solids. The inset shows the acoustic radiation force  $\langle F^{\text{rad}} \rangle$  inside the water droplet with a magnitude from 0 pN (black) to 4.5 pN (white). (b) The same but for olive oil at resonance  $f = 1.865$  MHz and with amplitudes for  $p$  from -448 kPa (blue) to 447 kPa (red), for  $u$  from 0 nm (black) to 0.35 nm (white), and for  $\langle F^{\text{rad}} \rangle$  from 0 pN (black) to 10.7 pN (white).

We first note that for an ideal hard-walled system of width  $W = 380$   $\mu\text{m}$ , a standing one-half wavelength resonance should occur at  $f_{\text{WA}} = c_{\text{WA}}/(2W) = 1.970$  MHz in water and at  $f_{\text{OLV}} = c_{\text{OLV}}/(2W) = 1.907$  MHz in olive oil where  $c$  is the sound speed, while a standing two-half wavelength resonance should occur at  $f_{\text{HFE}} = c_{\text{HFE}}/W = 1.734$  MHz in fluorinated oil. We have tested this simple prediction with simulations on the system without a water droplet but filled uniformly with either water, fluorinated oil, or olive oil and found the following resonance

frequencies numerically:  $f_{WA}^{num} = 1.918$  MHz,  $f_{HFE}^{num} = 1.722$  MHz, and  $f_{OLV}^{num} = 1.864$  MHz. For a water droplet in fluorinated oil, Fig. 3 (a), we first of all note that the numerically obtained resonance frequency  $f = 1.718$  MHz is close to the pure fluorinated oil two-half wavelength resonance of  $f_{HFE}^{num} = 1.722$  MHz. However, we also observe a clear mismatch between the approximate one-half and two-half standing pressure wavelengths in the water droplet and in the fluorinated oil, respectively. This mismatch leads to a zero pressure and a zero radiation force near the front end of the droplet. Not only is the average magnitude of the radiation force lowered by the acoustic mismatch between the water and the surrounding oil, but the suppression of the radiation force near the front end implies that the the radiation force cannot counter balance the drag forces from the internal circulation flow roll that occurs as the droplet moves inside that channel, forcing the particles away from the center plane (Ohlin et al. 2017). In conclusion, the simulation predicts low-quality acoustophoresis in water droplet surrounded by fluorinated oil. In contrast, the acoustic mismatch between water and olive oil is minute, and we see in Fig. 3 (b) a near perfect standing one-half wavelength resonance throughout the fluid domain at  $f = 1.865$  MHz, close to the pure olive oil one-half wave resonance  $f_{OLV}^{num} = 1.864$  MHz, when the water droplet is surrounded by olive oil. As a consequence, there is no suppression of the radiation force near the droplet front end, and the internal flow rolls cannot disperse the particles away from the center axis. In conclusion, the simulation predicts high-quality of acoustophoresis in a water droplet surrounded by olive oil.

### 3. Experiments

#### 3.1. Fabrication of the device

A silicon-glass microfluidic chip for droplet generation, particle encapsulation, and intra-droplet acoustic particle focusing is fabricated, and in Fig 4. (a) the chip design is shown schematically.

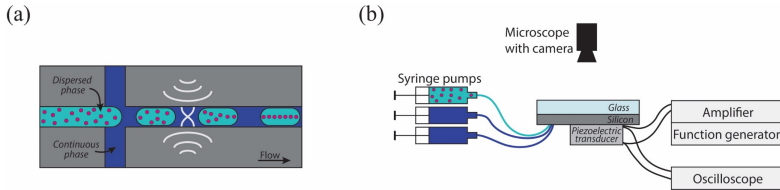


**Fig. 4** (a) Schematic of the microfluidic chip design and (b) the experimental setup.

The microchannels are fabricated using standard photolithography and deep reactive-ion etching on a silicon wafer (500  $\mu\text{m}$  thick,  $\langle 100 \rangle$ -orientation). Deep reactive-ion etching is a highly anisotropic etching method that yields channels with rectangular cross-sections. The width of the channels are 380  $\mu\text{m}$  and the height is 100  $\mu\text{m}$ . Holes for fluid inlets and outlets are drilled through the silicon wafer. The channels are sealed by anodic bonding of a glass wafer (700  $\mu\text{m}$  thick, Borofloat-33), and the silicon-glass wafer is diced into individual chips. Short pieces of silicone tubings are glued to the chip as fluid connectors. The channels are silanized by flushing the channels with Repel-Silane (Pharmacia Biotech) to make the channels hydrophobic, which is a requirement for generating water-in-oil droplets. To supply the ultrasound a 12 mm x 12 mm piezoelectric transducer (1 mm thick yielding 2 MHz fundamental resonance frequency, Pz26, Ferroperm Piezoceramics A/S) is glued on the silicon side of the chip using cyanoacrylate glue (Loctite 420, Henkel AG & Co.), and electrical wires are soldered on the piezoelectric transducer.



### 3.2. Experimental method

The experimental setup is shown in Fig. 4 (b). The piezoelectric transducer is actuated by a sinusoidal signal from a function generator (33220A, Agilent Technologies Inc.) after amplification of the signal (75A250, Amplifier Research). The output voltage from the function generator is kept constant in the experiments and the voltage over the transducer is monitored using a digital oscilloscope (TDS 1002, Tektronix). The voltage in the experiments over the transducer is between 10-25 V<sub>peak-peak</sub> depending on the exact frequency of the ultrasound. The frequency is manually swept between 1.50 MHz and 2.50 MHz in steps of 0.05 MHz to find the strongest particle focusing at the fundamental resonance for each system. The focusing strength is determined by the operator by visually inspecting the system and identifying when the particles are focusing using an optical microscope (BX51W1, Olympus) equipped with a 4x objective. Images are acquired with a camera (XM10, Olympus) mounted on the microscope.

The fluid flows are controlled by three syringe pumps (NEMESYS, Cetoni GmbH) mounted with plastic syringes and connected to the inlet channels via Teflon tubing whereas the outlet channel is kept open. In the experiments the dispersed phase is Milli-Q water. In the acoustically mismatched system fluorinated oil (Novec HFE-7500, 3M) containing 2% surfactant (Krytox FSH-157, Dupont) is used as the continuous phase, and in the acoustically matched droplet system vegetable olive oil (Di Luca & Di Luca) is used as the continuous phase. Microparticles (10 µm polystyrene particles, Sigma-Aldrich) are suspended in the water phase, and in the droplet generation process the particles are encapsulated inside the droplets. The total flow rate is kept constant in the experiments (5 µL/min) to ensure the residence time of the droplet in the channel is the same. However, the length of the droplets is known to be influenced by the material properties of the fluid phases (Utada et al. 2007; Chen et al. 2014), and in the experiment this effect is partly adjusted for by changing the water:oil flow ratio. For generation of water droplets in olive oil the flow ratio is set to 2:3 compared with 1:4 for generation of water droplets in fluorinated oil.

### 3.3. Experimental results and discussion

In the experiments water droplets were generated in fluorinated oil and olive oil, respectively, and polystyrene particles were encapsulated inside the droplets. Without actuation of the ultrasound the particles were positioned in the entire droplet, see Fig. 5 (a) and Fig. 5 (c). To focus the encapsulated particles ultrasound at the fundamental resonance frequency was applied. For each system the frequency was tuned manually to find the strongest particle focusing frequency. To minimize the influence of variations in the acoustic field arising from external factors such as the gluing of the transducer and differences from the microfabrication process, the same microfluidic chip and the same part of the channel was studied throughout the experimental series.

For water droplets in fluorinated oil no strong focusing was observed when the ultrasound was applied, however, it was noted that at  $f = 1.70 - 1.75$  MHz the particles were weakly affected by the ultrasound, see Fig. 5 (b). In contrast, when the water droplets were surrounded by olive oil, it was observed that the encapsulated particles were strongly affected by the ultrasound and focused on a very straight line along the center line of the droplets, see Fig. 5 (d). The strongest particle focusing was seen at  $f = 1.70 - 1.90$  MHz for water droplets in olive oil, but some focusing could be observed at higher frequencies, see Table 2. The fact that the observed frequency range for particle focusing in water droplets surrounded by olive oil was wide indicates that this system is robust and

not particular sensitive to small fabrication and temperature variations, and thus easy and stable to operate.

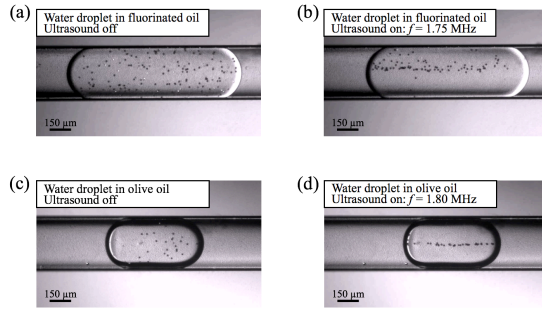


**Fig. 5** Photographs of acoustic focusing of microparticles inside water droplets in fluorinated oil and olive oil, respectively. At actuation of the ultrasound at the fundamental resonance a standing wavefield is created between the channel walls, and the particles are affected by the radiation force. The particles are most strongly focused in the water droplet surrounded by olive oil. The droplets are flowing towards the right in the photographs.

**Table 2** Measured and simulated resonance frequencies for intra-droplet acoustic particle focusing.

| System                            | Simulation<br>strong focusing | Experimental<br>strong focusing | Simulation<br>weak focusing | Experimental<br>weak focusing |
|-----------------------------------|-------------------------------|---------------------------------|-----------------------------|-------------------------------|
| Water droplets in fluorinated oil | Not observed                  | Not observed                    | 1.72 MHz                    | 1.70-1.75 MHz                 |
| Water droplets in olive oil       | 1.86-1.90 MHz                 | 1.70-1.90 MHz                   | above 1.90 MHz              | 1.95-2.05 MHz                 |

#### 4. Concluding discussion

The numerical simulations and experiments show the importance of matching the acoustic properties of the dispersed and the continuous phase to achieve good quality intra-droplet acoustic particle focusing. Experimentally good particle focusing was only observed for water droplets in olive oil whereas for water droplets in fluorinated oil the significant difference in the acoustic properties between the two phases resulted in weak particle focusing. This can be explained qualitatively from the simulations, which clearly show that strong and uniform focusing occurs in systems with good acoustic matching between the droplet and the continuous phase (olive oil), while focusing is only maintained near the center of droplets having a poor acoustic matching with the continuous phase (fluorinated oil). The lack of focusing forces near the droplet ends is crucial in explaining the poor overall acoustophoretic behavior: as droplets move in microfluidic channels flow rolls are induced inside them (Kinoshita et al. 2007; Ma et al. 2014), and these flow rolls counteract the acoustic focusing force in the front of the droplet (Ohlin et al. 2017). Consequently, in acoustically mismatched droplets the acoustic focusing is too weak to balance the defocusing Stokes drag force from the flow rolls, and such droplets are unlikely to exhibit good acoustic particle focusing. Furthermore, in actual experiments, the acoustic fields are never completely perfect and homogeneous, but instead there are areas in the channel with a higher or lower acoustic energy (“hot spots” and “weak spots”) due to periodical variations along the length of the channel (Barnkob et al. 2010) as well as bad acoustic coupling, and here the internal flow rolls can have a larger impact and spread the particles more.

To quantify the influence from the flow rolls, we note that the fluid flow rolls affect the particles through the Stokes drag force  $\mathbf{F}^{\text{drag}} = 6\pi\eta a (\mathbf{v}_d - \mathbf{v}_p)$ , where  $\mathbf{v}_d$  is the fluid velocity in the droplet and  $\mathbf{v}_p$  is the particle velocity. In our experiments, the flow rate was 5  $\mu\text{L}/\text{min}$ , which corresponds to an average fluid

velocity of 2 mm/s. In rectangular channels, the velocity  $\mathbf{v}_d$  of the droplets is a factor 0.1 – 0.4 slower than the fluid velocity, and the relative velocity  $\mathbf{v}_d - \mathbf{v}_p$  is typically another order of magnitude lower (Baroud et al. 2010). We therefore estimate the drag force on the particles in our experiment to be of the order  $F^{\text{drag}} \approx 2 - 20$  pN. Following Barnkob et al. (2010), the magnitude of the radiation force in our experiments is determined by measuring the typical focusing time  $t_{\text{foc}} = 1$  s, which by Eq. (2) gives a typical energy density  $E_{\text{ac}} = 6$  Pa. In the simulations, this value of the energy density is obtained by choosing the actuation amplitude to be  $d_1 = 0.4$  nm, a value for which the resulting radiation force becomes  $F^{\text{rad}} \approx 11$  pN, or somewhat smaller, as shown in Figs. 2 and 3. Thus, it is within the experimental control of the drag force through the flow rate and of the radiation force through the actuation voltage on the piezo crystal to cross over from a radiation force dominated to drag force dominated behavior. However, for a given setting of the control parameters, the focusing ability of the acoustically matched olive oil system is better than for the mismatched fluorinated oil system. Because the typical time scales for the acoustic focusing of the particles, for the passage of the droplets through the channel, and for the sedimentation of the particles in our experiments is 1 s, 5 s, and 32 s, respectively, it follows that the influence of gravity is negligible.

The purpose of this study was to investigate how the acoustic properties of the continuous phase affect particle focusing in acoustofluidic two-phase systems, however, from the application viewpoint in addition to suitable acoustic properties, care must also be taken to find fluid phases that provide monodisperse droplet generation, high droplet stability, no cross-contamination and are biocompatible.

## 5. Conclusion

In this work, acoustic focusing of microparticles encapsulated in water-in-oil droplets was studied. Two different systems were considered: one where there was a significant difference in the acoustic properties of the dispersed and continuous phase (water droplets in fluorinated oil) and one where the phases had similar acoustic properties (water droplets in olive oil). The simulations and experimental results show that to obtain high quality acoustic focusing inside the droplets the acoustic properties of the dispersed and continuous phase should be matched. We believe that these findings will provide important information in designing experiments regarding acoustofluidics in two-phase systems.

## References

- Agresti JJ, Antipov E, Abate AR, et al (2010) Ultrahigh-throughput screening in drop-based microfluidics for directed evolution. *Proc Natl Acad Sci* 107:4004–4009. doi: 10.1073/pnas.0910781107
- Baret J-C (2012) Surfactants in droplet-based microfluidics. *Lab Chip* 12:422–433. doi: 10.1039/C1LC20582J
- Barnkob R, Augustsson P, Laurell T, Bruus H (2010) Measuring the local pressure amplitude in microchannel acoustophoresis. *Lab Chip* 10:563–570. doi: 10.1039/b920376a
- Baroud CN, Gallaire F, Dangla R (2010) Dynamics of microfluidic droplets. *Lab Chip* 10:2032–2045.
- Brouzes E, Kruse T, Kimmerling R, Strey HH (2015) Rapid and continuous magnetic separation in droplet microfluidic devices. *Lab Chip* 15:908–919. doi: 10.1039/C4LC01327A
- Bruus H (2012) Acoustofluidics 7: The acoustic radiation force on small particles. *Lab Chip* 12:1014–21. doi: 10.1039/c2lc21068a
- Carugo D, Octon T, Messaoudi W, et al (2014) A thin-reflector microfluidic resonator for continuous-flow concentration of microorganisms: a new approach to water quality analysis using acoustofluidics. *Lab Chip* 14:3830. doi: 10.1039/C4LC00577E
- Chen X, Glawdel T, Cui N, Ren CL (2014) Model of droplet generation in flow focusing generators operating in the squeezing regime. *Microfluid Nanofluidics* 1341–1353. doi: 10.1007/s10404-014-1533-5
- Christakou AE, Ohlin M, Onfelt B, Wiklund M (2015) Ultrasonic three-dimensional on-chip cell culture for dynamic studies of tumor immune surveillance by natural killer cells. *Lab Chip* 15:3222–3231. doi: 10.1039/C5LC00436E
- Collins DJ, Morahan B, Garcia-Bustos J, et al (2015) Two-dimensional single-cell patterning with one cell per well driven by surface acoustic waves. *Nat Commun* 6:8686. doi: 10.1038/ncomms9686
- Deshmukh S, Brzozka Z, Laurell T, Augustsson P (2014) Acoustic radiation forces at liquid interfaces impact the performance of acoustophoresis. *Lab Chip* 14:3394. doi: 10.1039/C4LC00572D
- Dual J, Schwarz T (2012) Acoustofluidics 3: Continuum mechanics for ultrasonic particle manipulation. *Lab Chip* 12:244–252. doi: 10.1039/C1LC20837C
- Fornell A, Nilsson J, Jonsson L, et al (2015) Controlled Lateral Positioning of Microparticles Inside Droplets Using Acoustophoresis. *Anal Chem* 87:10521–10526. doi: 10.1021/acs.analchem.5b02746
- Fornell A, Ohlin M, Garofalo F, et al (2017) An intra-droplet particle switch for droplet microfluidics using bulk acoustic waves. *Biomicrofluidics* 11:31101. doi: 10.1063/1.4984131
- Hammarström B, Evander M, Barbeau H, et al (2010) Non-contact acoustic cell trapping in disposable glass capillaries. *Lab Chip* 10:2251–2257. doi: 10.1039/c004504g
- Han S, Kim HS, Han A (2017) In-droplet cell concentration using dielectrophoresis. *Biosens Bioelectron* 97:41–45. doi: 10.1016/j.bios.2017.05.036
- Hein M, Moskopp M, Seemann R (2015) Flow field induced particle accumulation inside droplets in rectangular channels. *Lab Chip* 15:2879–2886. doi: 10.1039/C5LC00420A
- Hertz G, Mende H (1939) Der Schallstrahlungsdruck in Flüssigkeiten. *Zeitschrift für Phys* 114:354–367. doi: 10.1007/BF01337001
- Hopcroft MA, Nix WD, Kenny TW (2010) What is the Young 's Modulus of Silicon? *J Microelectromechanical Syst* 19:229–238. doi: 10.1109/JMEMS.2009.2039697
- Kinoshita H, Kaneda S, Fujii T, Oshima M (2007) Three-dimensional measurement and visualization of internal flow of a moving droplet using confocal micro-PIV. *Lab Chip* 7:338–46. doi: 10.1039/b617391h

- Kurup GK, Basu AS (2012) Field-free particle focusing in microfluidic plugs. *Biomicrofluidics* 6:22008. doi: 10.1063/1.3700120
- Lee H, Xu L, Oh KW (2014) Droplet-based microfluidic washing module for magnetic particle-based assays. *Biomicrofluidics* 8:44113. doi: 10.1063/1.4892495
- Leibacher I, Reichert P, Dual J (2015) Microfluidic droplet handling by bulk acoustic wave (BAW) acoustophoresis. *Lab Chip* 15:2896–2905. doi: 10.1039/C5LC00083A
- Ley MWH, Bruus H (2017) Three-dimensional numerical modeling of acoustic trapping in glass capillaries. *Phys Rev Appl* 8:1–15. doi: 10.1103/PhysRevApplied.8.024020
- Li P, Mao Z, Peng Z, et al (2015) Acoustic separation of circulating tumor cells. *Proc Natl Acad Sci U S A* 112:4970–4975. doi: 10.1073/pnas.1504484112
- Lombardi D, Dittrich PS (2011) Droplet microfluidics with magnetic beads: a new tool to investigate drug-protein interactions. *Anal Bioanal Chem* 399:347–352. doi: 10.1007/s00216-010-4302-7
- Ma S, Sherwood JM, Huck WTS, Balabani S (2014) On the flow topology inside droplets moving in rectangular microchannels. *Lab Chip* 14:3611. doi: 10.1039/C4LC00671B
- Nordin M, Laurell T (2012) Two-hundredfold volume concentration of dilute cell and particle suspensions using chip integrated multistage acoustophoresis. *Lab Chip* 12:4610. doi: 10.1039/c2lc40629b
- Ohlin M, Fornell A, Bruus H, Tenje M (2017) Improved positioning and detectability of microparticles in droplet microfluidics using two-dimensional acoustophoresis. *J Micromechanics Microengineering* 27:84002. doi: 10.1088/1361-6439/aa7967
- Park K, Park J, Jung JH, et al (2017) In-droplet microparticle separation using travelling surface acoustic wave. *Biomicrofluidics* 11:64112. doi: 10.1063/1.5010219
- Schmid L, Weitz DA, Franke T (2014) Sorting drops and cells with acoustics: acoustic microfluidic fluorescence-activated cell sorter. *Lab Chip* 14:3710–8. doi: 10.1039/c4lc00588k
- Schneider T, Kreutz J, Chiu DT (2013) The potential impact of droplet microfluidics in biology. *Anal Chem* 85:3476–3482. doi: 10.1021/ac400257c
- Sesen M, Alan T, Neild A (2015) Microfluidic plug steering using surface acoustic waves. *Lab Chip* 15:3030–3038. doi: 10.1039/C5LC00468C
- Shembekar N, Chaipan C, Utharala R, Merten CA (2016) Droplet-based microfluidics in drug discovery, transcriptomics and high-throughput molecular genetics. *Lab Chip* 16:1314–1331. doi: 10.1039/C6LC00249H
- Sjostrom SL, Bai Y, Huang M, et al (2014) High-throughput screening for industrial enzyme production hosts by droplet microfluidics. *Lab Chip* 14:806–813. doi: 10.1039/C3LC51202A
- Sun M, Khan ZS, Vanapalli SA (2012) Blood plasma separation in a long two-phase plug flowing through disposable tubing. *Lab Chip* 12:5225–5230. doi: 10.1039/c2lc40544j
- Tenje M, Fornell A, Ohlin M, Nilsson J (2017) Particle manipulation methods in droplet microfluidics. *Anal Chem*. doi: 10.1021/acs.analchem.7b01333
- Utada AS, Fernandez-Nieves A, Stone HA, Weitz DA (2007) Dripping to jetting transitions in coflowing liquid streams. *Phys Rev Lett* 99:1–4. doi: 10.1103/PhysRevLett.99.094502
- 3M Data sheet [https://multimedia.3m.com/mws/media/65496O/3mtm-novectm-7500-engineered-fluid.pdf&fn=prodinfo\\_nvc7500.pdf](https://multimedia.3m.com/mws/media/65496O/3mtm-novectm-7500-engineered-fluid.pdf&fn=prodinfo_nvc7500.pdf) Accessed: 2018-05-21

## Paper III

### **An intra-droplet particle switch for droplet microfluidics using bulk acoustic waves**

A. Fornell, M. Ohlin, F. Garofalo, J. Nilsson, and M. Tenje

Reproduced from A. Fornell, M. Ohlin, F. Garofalo, J. Nilsson, and M. Tenje. An intra-droplet particle switch for droplet microfluidics using bulk acoustic waves. *Biomicrofluidics*, 11(3), 031101 (2017). With the permission of AIP Publishing.



## An intra-droplet particle switch for droplet microfluidics using bulk acoustic waves

Anna Fornell,<sup>1,a)</sup> Mathias Ohlin,<sup>2</sup> Fabio Garofalo,<sup>1</sup> Johan Nilsson,<sup>1</sup> and Maria Tenje<sup>1,2,3</sup>

<sup>1</sup>Department Biomedical Engineering, Lund University, Lund, Sweden

<sup>2</sup>Department Engineering Sciences, Uppsala University, Uppsala, Sweden

<sup>3</sup>Science for Life Laboratory, Uppsala University, Uppsala, Sweden

(Received 24 April 2017; accepted 13 May 2017; published online 26 May 2017)

To transfer cell- and bead-assays into droplet-based platforms typically requires the use of complex microfluidic circuits, which calls for methods to switch the direction of the encapsulated particles. We present a microfluidic chip where the combination of acoustic manipulation at two different harmonics and a trident-shaped droplet-splitter enables direction-switching of microbeads and yeast cells in droplet microfluidic circuits. At the first harmonic, the encapsulated particles exit the splitter in the center daughter droplets, while at the second harmonic, the particles exit in the side daughter droplets. This method holds promises for droplet-based assays where particle-positioning needs to be selectively controlled. © 2017 Author(s). All article content, except where otherwise noted, is licensed under a Creative Commons Attribution (CC BY) license (<http://creativecommons.org/licenses/by/4.0/>). [<http://dx.doi.org/10.1063/1.4984131>]

### INTRODUCTION

Compartmentalization of biological assays in small droplets allows for improved analytical analysis.<sup>1–3</sup> The small volumes make droplet-based platforms particularly useful for assays where reaction reagents are expensive, the sample is scarce, or there is an interest to probe large numbers of single cells.<sup>4–8</sup> The miniaturization of biological assays does however require the integration of several unit operators capable of encapsulating particles,<sup>9</sup> adding reagents,<sup>10</sup> and analyzing the droplet content.<sup>11,12</sup> Although the microfluidic platform allows for these to be integrated with a compact foot-print, further advantages could be obtained by increasing the complexity of each circuit in analogy to the design of electronic or optical circuits. This calls for the need of microfluidic switches that can be included to direct the encapsulated particles into desired pathways. Consequently, methods to handle the content inside the droplets with high recovery are also needed.

In the previous work, acoustic,<sup>13,14</sup> magnetic,<sup>15–17</sup> and hydrodynamic forces<sup>18–20</sup> have been used for intra-droplet particle manipulation. Of these, acoustic forces are particularly interesting, since acoustic methods allow for on-demand control and have the possibility to manipulate a variety of particles and cells. Acoustic forces have, since long, been reported to focus particles in one-phase systems,<sup>21–24</sup> but it is first recently that acoustics have been applied for manipulation in two-phase systems.<sup>25–27</sup> Previously, we reported on acoustic particle enrichment inside droplets using the first harmonic.<sup>13</sup> However, using only the first harmonic may limit the applications of the technique since particles can only be aligned at the center-line of the droplets. In this paper, we present a device that combining an improved droplet-splitter and using the first and second harmonics enable direction-switching of encapsulated particles into either the center (following pathway 1) or the side daughter droplets (following pathway 2). This opens for on-demand direction of particles into different daughter droplets, further increasing the capability of droplet-based platforms.

<sup>a)</sup> Author to whom correspondence should be addressed: [anna.fornell@bme.lth.se](mailto:anna.fornell@bme.lth.se)



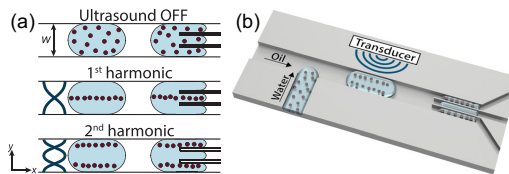


FIG. 1. (a) Acoustic manipulation of particles inside droplets. (b) Acoustic-controlled positioning of particles (here shown for the second harmonic).

## METHOD

The operating principle is shown in Fig. 1. First, water-in-oil droplets containing particles are generated. Transducer activation generates vibrations in the device, and a standing wave is set between the channel walls at resonance. The standing wave induces the acoustic radiation force on the encapsulated particles that migrate towards the pressure nodal-lines.<sup>28</sup> At the first harmonic, a single pressure nodal-line is generated at the center of the channel, and at the second harmonic, two pressure nodal-lines are generated at  $y = w/4$  and  $y = 3w/4$ , where  $w$  is the channel width [Fig. 1(a)]. By changing the frequency between the first and second harmonics, the particles can be directed to either the center or the side daughter droplets in a trident-shaped droplet-splitter.

The microfluidic channels were dry-etched in silicon and anodic bonded to a glass lid.<sup>29</sup> The main channel is  $370 \times 100 \mu\text{m}^2$ . The droplet-splitter consists of two vertical side walls  $10 \mu\text{m}$  thick dividing the main channel into three equally large outlets. A piezoelectric transducer (0.7 mm thick, 2.9 MHz resonance frequency, Pz26, Ferroperm Piezoceramics) was glued on the chip and actuated by a function generator (33220A, Agilent Technologies) after amplification (75A250, Amplifier Research), and the voltage was  $30 V_{pp}$ . The dispersed phase was deionized water, and the continuous phase was olive oil. Polystyrene microbeads ( $10 \mu\text{m}$  diameter, Sigma-Aldrich) or yeast cells (Kronjäst, Jästbolaget) were suspended in the aqueous phase. The flows were controlled by syringe pumps (NEMESYS, Cetoni). All experimental results were captured by a camera (XM10, Olympus) mounted on a microscope (BX51W1, Olympus). The system performance was evaluated by manually counting the beads from the videos.

## RESULTS AND DISCUSSION

A microfluidic chip for intra-droplet particle switching has been evaluated. In the first experiment, droplets containing polystyrene beads were generated, and each droplet was split into three daughter droplets. The fluid flows were adjusted to give daughter droplets of approximately the same volume (6 nl). Figure 2(a) shows the effect of applying ultrasound. At the first harmonic (1.83 MHz), the beads were moved towards the center-line of the droplets, and this resulted in the enrichment of particles in the center daughter droplets. To allow for particle switching, the actuation frequency was increased to the second harmonic (3.67 MHz) and the beads were moved into two pressure nodal-lines instead, causing the beads to be enriched in the side daughter droplets.

The number of beads in the daughter droplets was counted, and the results are presented in Figs. 2(b) and 2(c). Without ultrasound, the beads were distributed in all daughter droplets. It is however noted that the distribution is not completely equal, i.e.,  $1/3$  in the center and  $2/3$  in the sides, and this might be attributed to small variation in volume between the center and side daughter droplets, and internal fluid advection in the droplets.<sup>19,20,30</sup> However, at acoustic actuation, a pronounced difference between the center and side daughter droplets was observed. At the first harmonic, the system showed  $96 \pm 5\%$  collection of beads in the center daughter droplets, whereas at the second harmonic,  $92 \pm 7\%$  of the beads were collected in the side daughter droplets. The system showed high performance regardless of the initial bead concentration [Fig. 2(c)]. In the [supplementary material](#), a video shows the direct effect of switching the frequency as the beads are immediately moved into opposite daughter droplets.

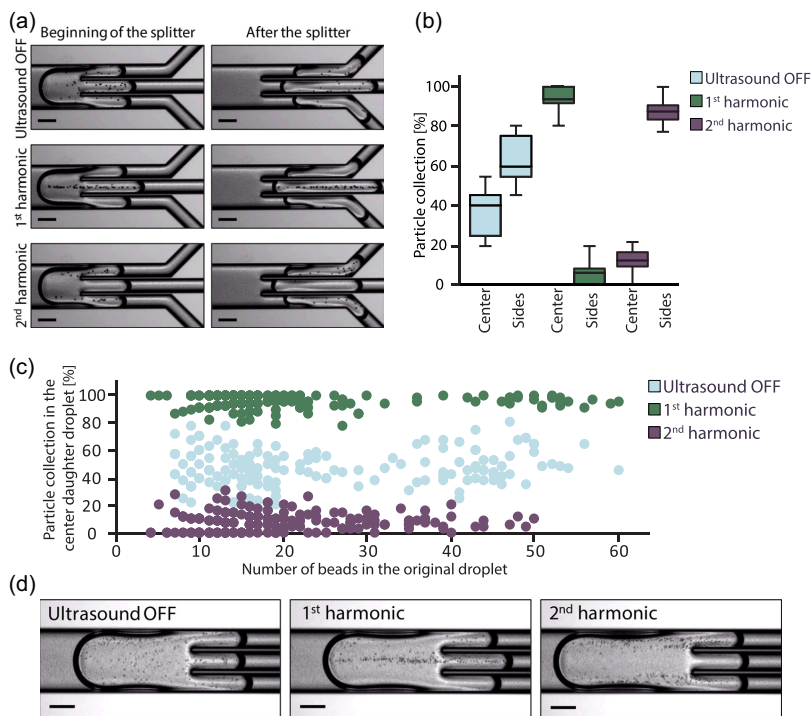


FIG. 2. (a) Acoustic-controlled positioning of encapsulated polystyrene beads. Total flow rate is  $9 \mu\text{l}/\text{min}$ . (b) Box plot showing the system performance. The data are presented as the ratio of beads in the center or side daughter droplets compared with the total number of beads in the center and side daughter droplets. (c) Particle collection in the center daughter droplets compared with the total number of beads as a function of the bead concentration in the original droplet. Note that the “banding effect” visible at low bead counts occurs since the quantization step per bead is relatively large there. In both (b) and (c),  $N = 180$  droplets in each experiment. (d) Acoustic-controlled positioning of yeast cells. Total flow rate is  $3 \mu\text{l}/\text{min}$ . All scale bars:  $150 \mu\text{m}$ .

There are mainly three effects affecting the particle-positioning within the droplets: acoustic forces, internal fluid advection, and particle sedimentation. Sedimentation is mostly relevant in slow-moving droplets, while the internal advection increases with the flow rate.<sup>30</sup> Consequently, there is an upper limit when the acoustic force is not strong enough to compete with the rapid mixing. The acoustic radiation force is proportional to the applied voltage squared,<sup>28</sup> and depending on the set-up and the intended application, the voltage may need to be constrained to avoid excessive heating. The presented system has been evaluated with good acoustic focusing at  $3\text{--}18 \mu\text{l}/\text{min}$  (see [supplementary material](#)). In addition to direct effects on the acoustic particle-positioning, the total flow rate also affects the droplet length,<sup>31</sup> which in turn influences the droplet splitting. This effect seems to have a more pronounced impact on the enrichment performance than the increased advection at higher flows.

The presented method can also be applied to direct yeast cells into different daughter droplets [Fig. 2(d)]. The fact that the method can handle cells without labelling makes the technology favorable for biological applications and is advantageous compared to magnetic manipulation.<sup>15–17</sup> The proposed system shows better performance compared with hydrodynamic methods as these require large and heavy particles and/or very low flows to achieve acceptable particle accumulation.<sup>18–20</sup> However, the most striking difference is that no other method as of today can switch particles on-demand into different daughter droplets in a continuous operation. These aspects make acoustic particle manipulation using the first and second harmonics an essential tool for the development of novel droplet-based assays.

## CONCLUSION

We have demonstrated an acoustic method to direct particles into different daughter droplets. Using the first harmonic, the encapsulated particles exit the droplet splitter in the center daughter droplets, while using the second harmonic, the particles exit in the side daughter droplets instead. We show that polymer microparticles as well as yeast cells can be manipulated. The presented method expands the droplet microfluidic tool-box since the acoustic manipulation is the only available method that continuously can switch particles on-demand into different daughter droplets.

## SUPPLEMENTARY MATERIAL

See [supplementary material](#) for the video showing intra-droplet particle-switching (S1), and photographs of acoustic-controlled positioning at different total flow rates (S2).

## ACKNOWLEDGMENTS

The authors would like to thank Klara Björnander Rahimi, Fredrik Ekström, Anders Holmberg, and Karolina Svensson (Uppsala University) for the fabrication of the microfluidic chips. This work was funded by the Swedish Research Council, the Crafoord Foundation, Uppsala University, Knut and Alice Wallenberg Foundation (KAW Grant No. 2012.0023), and Foundation Olle Engkvist Byggmästare.

- <sup>1</sup>R. Seemann, M. Brinkmann, T. Pfohl, and S. Herminghaus, *Rep. Prog. Phys.* **75**, 16601 (2012).
- <sup>2</sup>S. L. Anna, *Annu. Rev. Fluid Mech.* **48**, 285 (2016).
- <sup>3</sup>S.-Y. Teh, R. Lin, L.-H. Hung, and A. P. Lee, *Lab Chip* **8**, 198 (2008).
- <sup>4</sup>T. P. Lagus and J. F. Edd, *J. Phys. D: Appl. Phys.* **46**, 114005 (2013).
- <sup>5</sup>L. S. Casadevall and A. DeMello, *Chem. Commun.* **47**, 1936 (2011).
- <sup>6</sup>T. Schneider, J. Kreutz, and D. T. Chiu, *Anal. Chem.* **85**, 3476 (2013).
- <sup>7</sup>D. J. Eastburn, A. Sciambi, and A. R. Abate, *Anal. Chem.* **85**, 8016 (2013).
- <sup>8</sup>J. J. Agresti, E. Antipov, A. R. Abate, K. Ahn, A. C. Rowat, J. C. Baret, M. Marquez, A. M. Klibanov, A. D. Griffiths, and D. Weitz, *Proc. Natl. Acad. Sci. U. S. A.* **107**, 4004 (2010).
- <sup>9</sup>J. F. Edd, D. Di Carlo, K. J. Humphry, S. Köster, D. Irimia, D. A. Weitz, and M. Toner, *Lab Chip* **8**, 1262 (2008).
- <sup>10</sup>A. R. Abate, T. Hung, P. Mary, J. J. Agresti, and D. A. Weitz, *Proc. Natl. Acad. Sci. U. S. A.* **107**, 19163 (2010).
- <sup>11</sup>J. C. Baret, O. J. Miller, V. Taly, M. Ryckelynck, A. El-Harrak, L. Frenz, C. Rick, M. L. Samuels, J. B. Hutchison, J. J. Agresti, D. R. Link, D. A. Weitz, and A. D. Griffiths, *Lab Chip* **9**, 1850 (2009).
- <sup>12</sup>E. Brouzes, M. Medkova, N. Savenelli, D. Marran, M. Twardowski, J. B. Hutchison, J. M. Rothberg, D. R. Link, N. Perrimon, and M. L. Samuels, *Proc. Natl. Acad. Sci. U. S. A.* **106**, 14195 (2009).
- <sup>13</sup>A. Fornell, J. Nilsson, L. Jonsson, P. K. Periyannan Rajeswari, H. N. Joensson, and M. Tenje, *Anal. Chem.* **87**, 10521 (2015).
- <sup>14</sup>J. H. Jung, G. Destgeer, B. Ha, J. Park, and H. J. Sung, *Lab Chip* **16**, 3235 (2016).
- <sup>15</sup>D. Lombardi and P. S. Dittrich, *Anal. Bioanal. Chem.* **399**, 347 (2011).
- <sup>16</sup>E. Brouzes, T. Kruse, R. Kimmerling, and H. H. Strey, *Lab Chip* **15**, 908 (2015).
- <sup>17</sup>R. Gao, Z. Cheng, A. deMello, and J. Choo, *Lab Chip* **16**, 1022 (2016).
- <sup>18</sup>M. Sun, Z. S. Khan, and S. A. Vanapalli, *Lab Chip* **12**, 5225 (2012).
- <sup>19</sup>G. K. Kurup and A. S. Basu, *Biomicrofluidics* **6**, 22008 (2012).
- <sup>20</sup>M. Hein, M. Moskopp, and R. Seemann, *Lab Chip* **15**, 2879 (2015).
- <sup>21</sup>H. Bruus, *Lab Chip* **12**, 1014 (2012).
- <sup>22</sup>A. Lenshof, C. Magnusson, and T. Laurell, *Lab Chip* **12**, 1210 (2012).
- <sup>23</sup>X. Ding, P. Li, S.-C. S. Lin, Z. S. Stratton, N. Nama, F. Guo, D. Slotcavage, X. Mao, J. Shi, F. Costanzo, and T. J. Huang, *Lab Chip* **13**, 3626 (2013).
- <sup>24</sup>D. J. Collins, B. Morahan, J. Garcia-Bustos, C. Doerig, M. Plebanski, and A. Neild, *Nat. Commun.* **6**, 8686 (2015).
- <sup>25</sup>L. Schmid, D. A. Weitz, and T. Franke, *Lab Chip* **14**, 3710 (2014).
- <sup>26</sup>I. Leibacher, P. Reichert, and J. Dual, *Lab Chip* **15**, 2896 (2015).
- <sup>27</sup>M. Sesen, T. Alan, and A. Neild, *Lab Chip* **15**, 3030 (2015).
- <sup>28</sup>T. Laurell and A. Lenshof, *Microscale Acoustofluidics* (Royal Society of Chemistry, 2015).
- <sup>29</sup>M. Ohlin, A. Fornell, and M. Tenje, in *Micromechanics Microsystems Europe Workshop* (2016).
- <sup>30</sup>C. N. Baroud, F. Gallaire, and R. Dangla, *Lab Chip* **10**, 2032 (2010).
- <sup>31</sup>H. Liu and Y. Zhang, *J. Appl. Phys.* **106**, 034906 (2009).

## Paper IV

### **Improved positioning and detectability of microparticles in droplet microfluidics using two-dimensional acoustophoresis**

M. Ohlin, A. Fornell, H. Bruus, and M. Tenje

Reproduced from M. Ohlin, A. Fornell, H. Bruus, and M. Tenje. Improved positioning and detectability of microparticles in droplet microfluidics using two-dimensional acoustophoresis. *Journal of Micromechanics and Microengineering*, 27(8), 084002 (2017). With the permission of IOP Publishing.



# Improved positioning and detectability of microparticles in droplet microfluidics using two-dimensional acoustophoresis

M. Ohlin<sup>1</sup>, A. Fornell<sup>2</sup>, H. Bruus<sup>3</sup> and M. Tenje<sup>1,2,4</sup>

<sup>1</sup> Department of Engineering Sciences, Uppsala University, Uppsala, Sweden

<sup>2</sup> Department of Biomedical Engineering, Lund University, Lund, Sweden

<sup>3</sup> Department of Physics, Technical University of Denmark, Kgs. Lyngby, Denmark

<sup>4</sup> Science for Life Laboratory, Uppsala University, Uppsala, Sweden

E-mail: mathias.ohlin@angstrom.uu.se

## Abstract

We have fabricated a silicon-glass two-phase droplet microfluidic system capable of generating sub 100- $\mu\text{m}$ -sized,  $\varnothing = (74 \pm 2) \mu\text{m}$ , spherical droplets at rates up to hundreds of hertz. By implementing a two-dimensional acoustophoresis particle-positioning method, we show a fourfold improvement in both vertical and lateral particle positioning inside the droplets compared to unactuated operation. The efficiency of the system has been optimized by incorporating aluminum matching layers in the transducer design permitting biocompatible operational temperatures ( $<37^\circ\text{C}$ ). Furthermore, by using acoustic actuation,  $(99.8 \pm 0.4)\%$  of all encapsulated microparticles can be detected compared to only  $(79.0 \pm 5.1)\%$  for unactuated operation. In our experiments we observed a strong ordering of the microparticles in distinct patterns within the droplet when using two-dimensional acoustophoresis; to explain the origin of these patterns we simulated numerically the fluid flow inside the droplets and compared with the experimental findings.

## Acknowledgments

Financial support is provided by Uppsala University, The Swedish Research Council, and The Crafoord Foundation.

## 1. Introduction

Droplet microfluidics which has emerged from microfluidics, a well-established research field [1] almost three decades old, has of recent years expanded rapidly and offers now solutions to a vast amount of biotechnological problems [2, 3]. Two-phase droplet microfluidic systems are typically used to compartmentalize assays in nanoliter or less aqueous droplets surrounded by an immiscible carrier fluid. These, often water-in-oil, self-contained and dispersed microreactors provide increased throughputs, reduced consumption and costs of reagents and samples due to the very small droplet volumes, which facilitates, e.g., single-cell analysis [2, 4, 5]. Moreover, droplet microfluidics has the ability to be automated and parallelized, drastically decreasing the experiment time compared to assays in normally much larger reaction volumes. Droplet microfluidics provide a broad spectrum of complex assays and reactions, for example, droplet microfluidics has been used for high-throughput biological assays such as detection and analysis of cell-surface protein biomarkers, directed evolution of yeast cells, and encapsulation and screening of single-cells [6-9]. Importantly, all of these assays require encapsulation of microparticles such as cells or microbeads, and they all utilize optical detection methods.

Optical read-out is commonly used in combination with droplet microfluidics as a direct read-out method or internal trigger for consecutive steps in a microfluidic circuit [10-12]. To be able to easily detect the encapsulated microparticles optically, it is crucial that they are in focus, i.e. within the depth-of-field (DOF) of the optical imaging system. This is especially true for high numerical aperture (NA) objectives with their short DOF [13], often much shorter than the microfluidic channel depth. Although optical detection is one of the most versatile read-out methods [14], there are still many challenges as a result of sedimentation and unpredictable positioning of the encapsulated microparticles inside the droplets.

In this paper, we present a method to position microparticles at optically ideal positions inside the droplets both laterally and vertically using acoustic standing waves. Acoustic standing wave manipulation techniques in continuous flow microfluidics termed acoustophoresis offers a gentle non-contact, label-free, charge independent, and in-chip particle and cell handling method [15]. There are two main types of acoustophoresis both defined by how the sound is propagated through the system, bulk acoustic waves (BAW) acoustophoresis where the sound is propagated through the bulk of the material and surface acoustic waves (SAW) acoustophoresis where the sound propagates along the surface of the material. Both types of acoustophoresis have been used to manipulate suspended microparticles [16, 17] and droplets [18, 19]. Rather than using channel geometries to restrict the droplet movement confining the droplet into the DOF [6] we have instead focused on contact-less acoustophoretic manipulation of the suspended microparticles prior to droplet encapsulation, leaving the droplet undisturbed. We have previously reported on lateral positioning of microparticles inside large droplets (“plugs”) by one-dimensional (1D) BAW acoustophoresis [20], and in this paper we expand the droplet microfluidic toolbox with two-dimensional (2D) BAW acoustophoresis [21-23] prior to droplet encapsulation in a purpose build silicon-glass droplet microfluidic system optimized for BAW to obtain improved microparticle positioning and detectability within the droplets.

## 2. Theory

Acoustophoresis is a non-contact method to manipulate microparticles in microfluidic channels using ultrasonic standing waves. The primary acoustic radiation force focuses microparticles to either the pressure nodal lines or anti-nodal lines depending on the acoustic properties of the microparticles in relation to that of the surrounding fluid [24]. Polystyrene microparticles and cells in water have a positive acoustic contrast factor and are therefore focused to the pressure nodal lines. Acoustophoresis can be applied in either one or two dimensions [21, 23]. Acoustic microparticle manipulation in a water-filled rectangular microfluidic channel of height  $H$  and width  $W$  at the half-wave resonances is shown schematically in Figure 1. In Figure 1(a) an acoustic vertical standing half-wave with frequency  $f_1$  is created in the channel by setting  $f_1 = 2 c_0/H$ , where  $c_0$  is the speed of sound in water. This wave causes microparticles with a positive acoustic contrast factor to be focused in the horizontal  $xy$ -plane located in the middle of the channel, and further it counteracts sedimentation. As shown in Figure 1(b), microparticles can also be focused in the vertical  $xz$ -plane by applying an acoustic horizontal standing half-wave at frequency  $f_2 = 2 c_0/W$ . This wave causes microparticles with a positive acoustic contrast factor to be focused in the vertical  $xz$ -plane in the middle of the channel. Figure 1(c) shows that when frequency  $f_1$  and  $f_2$  are applied simultaneously, a two-dimensional acoustic standing wave results. This wave causes microparticles with a positive acoustic contrast factor to be focused at the intersection of the horizontal and vertical plane in the middle of the channel, a situation termed 2D acoustophoresis. When a Poiseuille flow is set up along the channel  $x$ -axis, focusing by 2D acoustophoresis ensures that all microparticles experience the same velocity in the flow profile (cf. the red region in Figure 1).

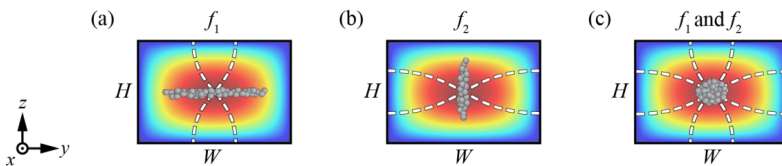


**Figure 1.** Schematic cross-section of a water-filled rectangular channel showing the working principle of 1D and 2D acoustophoresis, as microparticles experience the half-wave frequencies (a)  $f_1$  (1D vertical acoustophoresis), (b)  $f_2$  (1D horizontal acoustophoresis), and (c)  $f_1$  and  $f_2$  combined (2D acoustophoresis). The color plot represents the Poiseuille flow velocity profile from zero velocity (blue) to maximum velocity (red).

For two-phase flow, where a water droplet is submerged in oil flowing through a rectangular channel, intra-droplet flow rolls develop driven by the viscous forces between the water and oil phases at the droplet surface [25]. In a narrow channel, the flow field is toroidal with a significant horizontal component, while in a wide channel mainly vertically oriented flow rolls appear as shown in Section 4. This flow pattern governs the intra-droplet microparticle dynamics after the formation of the droplets.

## 3. Experimental

### 3.1 Fabrication of the silicon-glass chip

An overview of the system implementing dual transducer technology for 2D acoustophoresis is shown in Figure 2, a photograph showing the system during operation can be seen in the supplementary material (Figure S1). The system consists of a silicon-glass chip fabricated in-house using photolithography and dry-etching technology. The channels and droplet generator structures are dry-etched in a  $\langle 100 \rangle$  oriented, 500  $\mu\text{m}$  thick silicon wafer using deep reactive ion etching (DRIE) producing approximately 100  $\mu\text{m}$  deep



channels with vertical side walls. The smallest features of the flow-focusing droplet generator are the 50  $\mu\text{m}$  wide inlets and outlets which were analyzed by scanning-electron-microscope (SEM). Inlets and outlet were manually drilled through the silicon wafer using a micro diamond-drill bit (400  $\mu\text{m}$  in diameter) attached to a Dremel rotary power tool. To seal the system, anodic bonding of a 700  $\mu\text{m}$  thick borofloat-33 glass wafer to the silicon wafer was performed (cf. “Glass” in Figure 2(b)). The bonded silicon and glass wafers were diced into individual chips using a diamond dicing saw. Connectors made of 10 mm long silicone tubing (228-0700, VWR, Sweden) with an inner diameter of 1 mm were glued (Wacker RTV-1 A07, Wacker Chemie AG, Germany) on the silicon backside to the drilled inlets and outlet. Prior to usage the channels were treated with a surface coating agent (Repel-silane ES, GE Healthcare, USA) to render the channels hydrophobic for increased droplet formation stability.

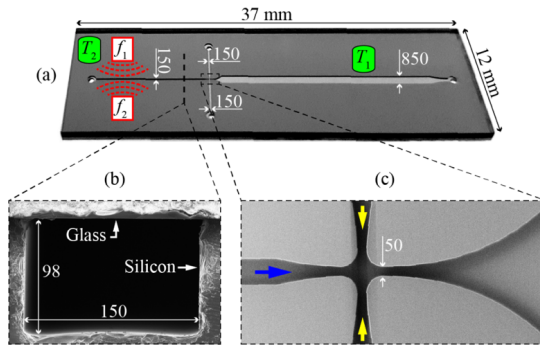


**Figure 2.** (a) A photograph of the silicon-glass chip with overlaid schematics. The unit is  $\mu\text{m}$  if not indicated otherwise. Here  $f_1, f_2$  and  $T_1, T_2$  are the locations of the transducers and thermocouples attached to the silicon backside, respectively. (b) SEM image showing the cross-section of the inlet channel carrying the dispersed water phase. (c) SEM image of the flow-focusing droplet generator. Here, the fluid flow directions are indicated for the continuous oil phase (yellow arrows) and dispersed water phase (blue arrow).

### 3.2 Transducer design

In the acoustic active region of our system, the channel has height  $H = 98 \mu\text{m}$  and width  $W = 150 \mu\text{m}$ . For water, this results in the respective half-wave resonance frequencies  $f_1 = 7.7 \text{ MHz}$  and  $f_2 = 5.0 \text{ MHz}$ . To obtain 2D acoustophoresis at these frequencies, a dual transducer technology was implemented by the use of two piezoelectric elements with thicknesses of 0.25 mm (APC-840, APC International, Ltd., USA) having a resonance frequency of 8 MHz and 0.4 mm (APC-841, APC International, Ltd., USA) having a resonance frequency of 5 MHz. Both piezoelectric elements were fitted with optimized matching and backing layers. The matching layers were made of Aluminum-7075, since with its given density  $\rho$  and sound speed  $c$ , it has an acoustic impedance  $Z = \rho c$ , which is a close match to the theoretical optimum value  $Z_{opt}$  given as the geometric mean of the acoustic impedances of the piezoelectric material (pz) and of silicon (si),  $Z_{opt} = \sqrt{Z_{pz}Z_{si}}$  [26]. Furthermore, the layer thicknesses are chosen to ensure maximum transmission for plane waves. Using the expressions in Ref. [18], we find the optimal matching layer thicknesses for Aluminum-7075 to be 2.57 mm at 8 MHz and 2.84 mm at 5 MHz, resulting in theoretical transmission coefficients around 94%. The aluminum matching layers were attached with a thin layer of cyanoacrylate adhesive (Loctite 420, Henkel Norden AB, Sweden) to the piezoelectric elements. Electrical connectors were attached using solder and small 26 AWG enameled copper wires to minimize mass loading effect such as resonance frequency shifts. A high bond strength epoxy adhesive (Loctite 3450, Henkel Norden AB, Sweden) was dispensed on the backside of the piezoelectric elements working as backing layers. As a result

of adding backing and matching layer, the electrical resonance frequency of the transducers broadens, enabling efficient frequency-modulation (FM) actuation of the transducer and resulting in a more robust 2D acoustophoresis [27, 28]. Additionally, using FM it is possible to compensate for the small variations in channel geometry caused by the dry-etching technique: a FM with 100 kHz span and a rate of 1 kHz results in a depth-compensation ability of approximately  $\pm 3 \mu\text{m}$ . Additionally, using FM actuation the system becomes less sensitive to resonance drifts due to temperature changes. Finally, the use of aluminum as a matching layers material ensures good heat transporting capabilities [29].

### ***3.3 Materials and instrumentation***

The flow-focusing droplet generator is designed to suspend microparticles in water droplets surrounded by immiscible oil. In this system the continuous oil phase consisted of fluorinated oil Novec HFE-7500 (Kemi-Intressen AB, Sweden) with 2% Krytox (The Chemours Company, USA) surfactant. The dispersed water phase consisted of Milli-Q water with 0.1% Triton-X (X100, DuPont, USA) surfactant, containing suspended 9.9- $\mu\text{m}$ -diameter polystyrene microparticles (Fluoro-Max G1000, Thermo Scientific, USA) at a concentration of  $2.3 \times 10^6$  particles/mL. Both the surfactants Triton-X and Krytox were used to stabilize the interface and prevent coalescence of the water-in-oil droplets [30]. Moreover, Triton-X in the dispersed water phase helps to prevent particle agglomeration by increasing the hydrophilicity of the polystyrene microparticles facilitating single-particle encapsulation. The two piezoelectric transducers were driven by a two-channel function generator (AFG3022C, Tektronix, USA) generating frequency modulated, sinusoidal 10 Vpp (peak-to-peak voltage) signals enabling 2D acoustophoresis. The chip was connected to a syringe pump (Nemesys, Cetoni GmbH, Germany) equipped with plastic syringes using polyethylene tubing (427406, Becton Dickinson and Company, USA) with an outer diameter of 1.09 mm resulting in a tight fit with the glued inlet and outlet silicone connectors. The continuous oil phase was pushed into the two inlets (cf. the yellow arrows in Figure 2(c)) at a flow rate of 40  $\mu\text{L}/\text{min}$  per inlet, whereas the dispersed water phase was pulled, to minimize microparticle sedimentation in the syringe, with a flow rate of 5  $\mu\text{L}/\text{min}$ . A high-speed camera (Miro M310, Vision Research Inc., USA) mounted to an inverted microscope (TE2000-U, Nikon, Japan) was used with a 10X/0.30 Plan Fluor objective (Nikon, Japan) with a DOF < 15  $\mu\text{m}$  to record high-speed videos with a frame rate of 2,000 frames per second. Using the internal microscope magnification of 1.5X the total magnification was 15X. To ensure adequate lighting an 80 W LED (pE-300 white, CoolLED Ltd., UK) was used in full white intensity mode. To minimize heating due to electrical losses in the piezoelectric material of the two transducers, a 12 Vdc blower (GB1205PKV1-8AY, Sunonwealth Electric Machine Industry Co., Ltd., Taiwan) was implemented and used continuously during the experiments. The temperature on the chip (cf.  $T_1$  and  $T_2$  in Figure 2(a)) was monitored using two K-type isolated junction surface temperature thermocouple probes (433-4313, RS Components Ltd., UK) attached with heat conducting adhesive (WLK 10, Fischer Elektronik GmbH & Co. KG, Germany), and the room temperature was measured using a single K-type exposed junction thermocouple probe (363-0250, RS Components Ltd., UK); all three connected to a four channel data logger (TM-947SD, Lutron Electronic Enterprise CO., Ltd., Taiwan).

### ***3.4 Image analysis***

The acquired high-speed videos were converted into still frames using the camera software. The still frames were manually analyzed in ImageJ [31] to estimate droplet size, droplet generation frequency as well as quantity and detectability of the encapsulated microparticles. MATLAB (R2015b, The MathWorks Inc.,

USA) was used to manually determine positions of individual single encapsulated microparticles within each droplet by marking positions and calculating distances from droplet center.

### 3.5 Theoretical simulations

Numerical simulations were carried out using COMSOL Multiphysics 5.2 (COMSOL AB, Sweden). We studied segments of the rectangular channel of length  $L = 360 \mu\text{m}$ , height  $H = 98 \mu\text{m}$ , and varying width  $W$ . First, we studied the acoustophoretic force  $F_{\text{ac}}$  on 10- $\mu\text{m}$ -diameter spherical polystyrene microparticles in a water-filled channel of width  $W = 150 \mu\text{m}$  and having acoustically hard walls. Using the methods of Ref. [32] extended from 2D to 3D, we found that oscillating the top-bottom walls at 7.7 MHz and the side walls at 5.0 MHz with an amplitude of 0.1 nm, the expected half-wave resonances were found, and  $F_{\text{ac}}$  was calculated to be around 0.1 nN ensuring good 2D acoustophoretic focusing. Then, keeping the two frequencies and the channel geometry fixed, but changing the liquid to HFE-7500 oil and embedding a 74- $\mu\text{m}$ -diameter water droplet at the center of the channel segment, we found that the acoustic resonances disappeared and  $F_{\text{ac}}$  dropped three orders of magnitude to around 1 pN, thus rendering acoustophoresis negligible. Similar results for water droplets in oil were obtained in subsequent simulations for a more narrow channel with  $W = 85 \mu\text{m}$  and a wider channel with  $W = 200 \mu\text{m}$ .

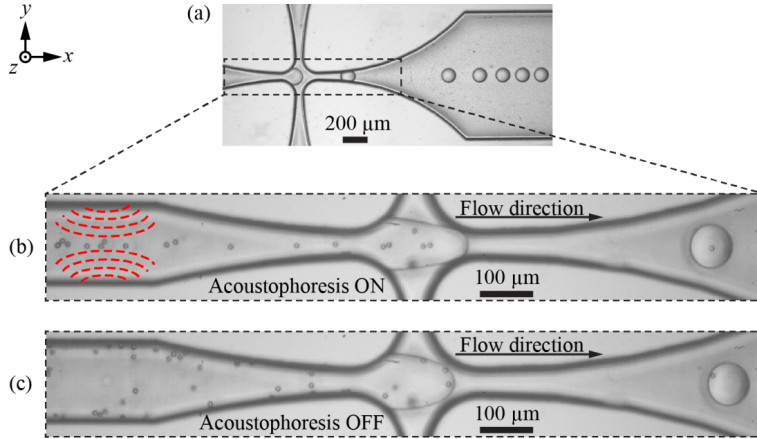
We then moved on to simulate the velocity field as an incompressible Stokes flow inside a spherical 74- $\mu\text{m}$ -diameter water droplet submerged in HFE-7500 oil that flows through the channel. We studied this both for a narrow width  $W = 85 \mu\text{m}$  and for a wide one  $W = 200 \mu\text{m}$ . Since a relative flow velocity as low as  $v = 20 \text{ mm/s}$  around a sphere of diameter  $d = 74 \mu\text{m}$  leads to a Stokes drag force of  $F_{\text{drag}} = 3\pi\eta d v \approx 1 \text{ nN}$ , the minute 1-pN-acoustophoretic force is neglected. We imposed the Poiseuille flow profile at the rectangular inlet and outlet [33], we used the no slip condition at the channel walls, and on the droplet surface in its rest frame, we applied zero normal velocity and continuous tangential stress. By iteration, we adjusted the amplitude of the Poiseuille flow such that the droplet center speed was 110 mm/s relative to the fixed walls as in the experiments, while the surface integral of the stress on the droplet surface was zero (the stationary situation).

Finally, using the COMSOL particle trajectory module, we studied the motion of spherical 10- $\mu\text{m}$ -diameter polystyrene tracer particles inside the droplet for the obtained velocity fields [32]. While acoustophoresis is negligible for the particle dynamics in the droplet, it enters through the initial position of the tracer particles: with acoustic actuation, the tracer particles start out near the intersection of the two focal planes, while without the acoustic actuation, they start out randomly distributed throughout the droplet volume.

## 4. Results and discussion

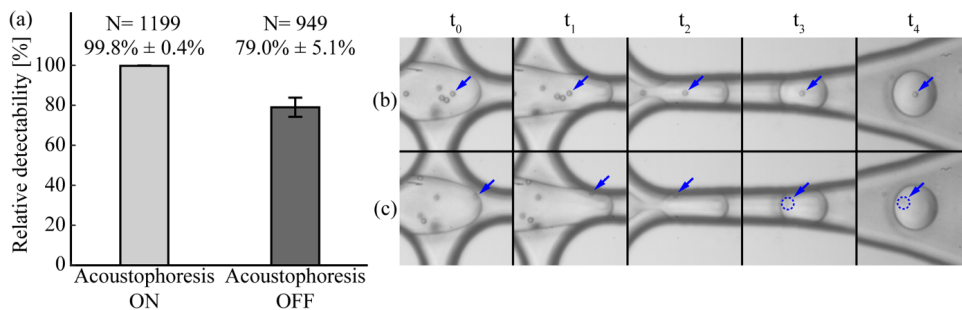
The temperature of the system with blower assisted cooling measured with the thermocouples  $T_1$  and  $T_2$  were  $(28.6 \pm 0.5)^\circ\text{C}$  and  $(29.2 \pm 0.5)^\circ\text{C}$ , respectively, at a room temperature of  $(24.2 \pm 0.5)^\circ\text{C}$  and actuation voltages of 10  $V_{\text{pp}}$  for each transducer. Owing to relatively high thermal conductivity of silicon, the temperature gradient across the system is negligible. The sub-30  $^\circ\text{C}$  operational temperatures, which is beneficial for biological samples such as cells [34], can partly be attributed to the aluminum matching layers which physically elevate the heat generating piezoelectric elements away from the chip surface and at the same time functions as heat sinks.

Figure 3 shows the formation of water droplets in the oil phase, and the effect of 2D acoustophoresis in the inlet channel. The system can produce droplets as small as  $(74 \pm 2) \mu\text{m}$  in diameter resulting in droplet volumes in the order of hundreds of picoliter. With the acoustic actuation on, the suspended microparticles are focused by 2D acoustophoresis along the channel center axis in the water phase, before entering the droplet formation region. The system can be driven with a droplet generation frequency of  $(298 \pm 85) \text{ Hz}$  with retained 2D acoustophoretic function, see Figure 3(b). For the unactuated control experiments, microparticles enter the flow-focusing junction randomly, see Figure 3(c).



**Figure 3.** (a) Photograph showing the droplet formation process. Inserts are zoomed still frames from the high-speed video showing how the microparticles are aligned during the droplet formation processes when the 2D acoustophoresis is (b) on, and (c) off.

A comparison of the relative particle detectability between the acoustic-actuated and the unactuated operation of the system can be seen in Figure 4 using data from four sets of experiments. The recorded 40,000 still images were manually analyzed, and among these a total of 2,148 droplets containing microparticles were identified, while empty droplets were excluded. For each particle-containing droplet the relative detectability was determined. The distinction between a detected and an undetected microparticle is shown in examples in Figure 4(b)-(c). The effect of 2D acoustophoresis is two-fold; it prevents sedimentation, and it moves particles towards the channel center thus minimizing particle-wall interactions. These acoustophoretic effects combined lead to a nearly 100% relative detectability of the encapsulated microparticles, as opposed to only 79% without acoustophoresis.



**Figure 4.** (a) Relative particle detectability with and without 2D acoustic actuation of the microparticles in the inlet channel. (b)-(c): Zoomed still frames from the high-speed video showing encapsulation of a microparticle when the 2D acoustophoresis is (b) on and (c) off. The encapsulated microparticle in (b) can easily be detected optically whereas the encapsulated microparticle in (c) is out of focus.

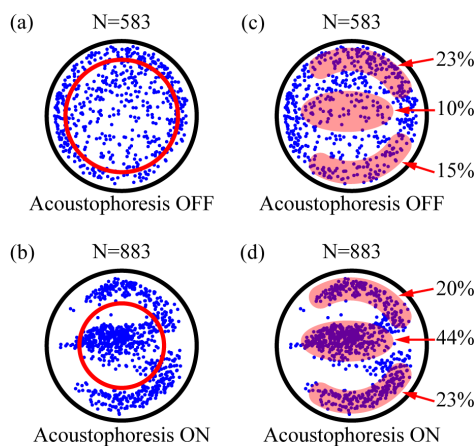


**Figure 5.** The positions (blue dots) of a total of 1,466 single encapsulated microparticles are superimposed within a single droplet moving to the right. (a) and (b) The red circle indicates the median particle distance from the droplet center. (c) and (d) Three regions with high particle concentration are marked.

Figure 5 shows particle positions for the two operational modes of the system: 2D acoustophoresis on and off. The positions are acquired approximately  $500\ \mu\text{m}$  after the flow-focusing junction inside the droplets which travel with a speed of  $(110 \pm 13)\ \text{mm/s}$ . For each droplet containing a single microparticle, the position was manually determined and superimposed. The result of 2D acoustophoresis on particle position (blue dots) is depicted in two ways: Figure 5(a) and (b) show the median distance (red circle) from the droplet center, while (c) and (d) show the positions divided into three regions. It is clearly seen that 2D acoustophoresis positions microparticles closer to the droplet center and that the majority of the encapsulated microparticles ends up in the central region compared to the unacted operation of the system. Using 2D acoustophoresis, 86% of the microparticles are focused to one of the three regions within the droplet, in contrast to only 48% for the unactuated control. In particular, with 2D acoustophoresis the central region holds 44% of all microparticles compared to only 10% for the unactuated control. This fourfold increase of microparticles located in the center part of the droplet using 2D acoustophoresis is favorable for all biological droplet assays where single-particle analysis with minimal optical aberration is of importance. Interestingly, with 2D acoustophoresis the particle positions are distributed in three distinct regions as seen in Figure 5(d).

The experimental findings can be explained qualitatively by numerical studies of the flow field inside a given droplet. Immediately following the droplet formation, the droplet moves along a narrow channel segment with a height of  $98\ \mu\text{m}$  and a width of only  $50\ \mu\text{m}$ . The droplet center moves with the speed  $v_{\text{drop}} = 110\ \text{mm/s}$  relative to the fixed confining walls, and this results in a toroidal flow field inside the droplet due to the viscous shear forces, as shown numerically in Figure 6(a). In the simulations, where the channel width has been increased to  $85\ \mu\text{m}$  to avoid deformation of the droplet, the toroidal flow field shows up as distinct pairs of counter-rotating vortices in both the horizontal and vertical center planes. The significant  $y$ -component of the flow field in the horizontal center plane is emphasized in the color plot (dark blue and dark red colors). Then,  $200\ \mu\text{m}$  downstream, the channel begins to widen, and ultimately it reaches a width of  $850\ \mu\text{m}$ . This situation we simulated using a width of only  $200\ \mu\text{m}$  to reduce the very demanding computer-memory requirements of the 3D simulations. However, already at this width, the vertical walls are so far from the droplet that the much nearer horizontal walls completely dominates the flow field inside the droplet. This is seen in Figure 6(b) by the strong flow rolls that remain in the vertical center plane, while the  $y$ -component of the flow field nearly vanishes in the  $xy$ -plane (grayish color).

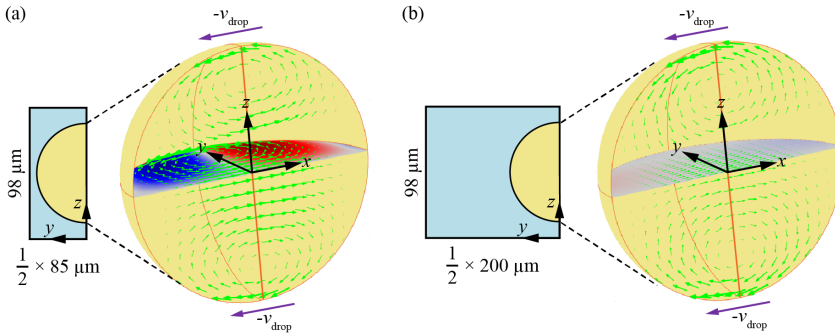


**Figure 6.** Numerical simulations of the velocity field in the rest frame of a spherical  $74\text{-}\mu\text{m}$ -diameter water droplet submerged in HFE-7500 oil that flows through a rectangular channel of height  $H = 98\ \mu\text{m}$  and width  $W$ . The droplet center moves along the  $x$ -axis with the speed  $v_{\text{drop}} = 110\ \text{mm/s}$  (purple arrows) relative to the fixed walls. Due to mirror symmetry around the vertical  $xz$  center plane only one half of the droplet is shown. The velocity (green arrows) relative to the droplet center are shown in the vertical  $xz$  center plane and in the horizontal  $xy$  center plane for (a) a narrow channel  $W = 85\ \mu\text{m}$ , and (b) a wide channel  $W = 200\ \mu\text{m}$ . The color plot in the  $xy$ -plane represents the  $y$ -component of the velocity field from  $-25\ \text{mm/s}$  (blue), through  $0\ \text{mm/s}$  (gray), to  $25\ \text{mm/s}$  (red). The insets show the vertical cross section of the channel with oil (light blue) at the center position of the droplet (beige).

These flow fields combined with the initial position of the particles at the location of the droplet formation can explain the observations. Clearly, using 2D acoustophoresis the suspended microparticles in the water phase are focused both horizontally and vertically in the middle of the inlet channel, see Figures 3(b), 4(b), and 7(a). This effect is partially preserved at the location of the droplet formation as shown in Figure 7(a), where a projection onto the  $xy$ -plane of approximately 5000 still frames is displayed. In the corresponding simulation we therefore take the initial particle positions to be distributed close to the center axis, and then let it propagate in time using the flow field of Figure 6(a). Due to the particle-wall interactions in the  $98\text{-}\mu\text{m}$ -high channel, the Stokes drag coefficient of the  $10\text{-}\mu\text{m}$ -diameter particles is enhanced by a factor of 1.11 according to the Faxén-Brenner expression given in Ref. [35]. The result after  $1.5\ \text{ms}$ , shown in Figure 7(b), indicates that particles encapsulated close to the droplet center will be moved by the horizontal part of the toroidal flow field and therefore be spread out along the  $x$ -axis and the droplet periphery much like the experimental results in Figure 5(d). Without the acoustic actuation, we observe that the microparticles arrive to the droplet formation location at random positions, and then they are advected by the toroidal flow field

to end up anywhere in the entire droplet volume (cf. Figure 7(c)). In the corresponding simulation we therefore take the initial particle positions to be distributed evenly throughout the droplet volume. We then again simulate the propagation for 1.5 ms using the flow field of Figure 6(a), and the resulting distribution, shown in Figure 7(d), indicates that now the particles end up with randomly distributed positions in agreement with the observations in Figure 5(a). For a deeper analysis of the internal fluid flows inside moving droplets of various sizes and channel geometries the authors refer to the work [36-38], where micro-particle image velocimetry was used for fluid flow analysis within droplets. However, the patterns shown in Figure 5 are dependent on the time scale of the system, i.e., the time it takes for a droplet to move from the droplet formation location to the imaging point, here approximately 5 ms, as well as on the channel geometry, since both these parameters influence the particle transport and hence the location of the encapsulated microparticles. Furthermore, a lower bound for the particle size used in our acoustophoretic system is the general value of  $2\ \mu\text{m}$ , below which acoustic streaming begins to dominate over the acoustic radiation force [32]. An upper bound would be the channel height  $H$ , where particle-wall interactions and clogging effects begin to dominate.

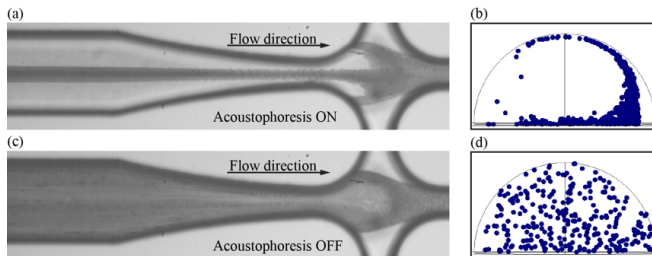


**Figure 7.** (a) Minimum intensity  $z$ -projection to the  $xy$ -plane of the particle distribution with 2D acoustophoresis during the formation of 865 droplets. (b) Numerical simulation of 800 particles inside a droplet advected by the internal fluid flow of Figure 6(a), and with initial particle positions taken to be near the horizontal center axis of the droplet due to 2D acoustophoresis. (c) Minimum intensity  $z$ -projection to the  $xy$ -plane showing particle distribution for the formation of 521 droplets without 2D acoustophoresis. (d) Same as panel (b), but with the initial particle positions taken to be evenly distributed throughout the droplet.

## 5. Conclusion

In this work, we have presented a silicon-glass two-phase droplet microfluidic system capable of producing sub 100-micrometer-sized spherical water droplets in oil at a rate of hundreds of droplets per second. We have implemented dual transducer technology for 2D acoustophoresis to avoid particle sedimentation and particle-wall interactions and for improved lateral and vertical particle positioning inside the droplets. To understand the effect 2D acoustophoresis has on the encapsulated microparticles we simulated numerically the fluid flow inside the droplets for various scenarios concluding that the initial particle position at the location of droplet formation is decisive. By equipping the two ultrasonic transducers with optimized aluminum matching layers the system showed biological compatible operation temperatures. As a result of 2D acoustophoresis, the system showed a fourfold increase in the amount of particles located in the central region of the droplet compared to unactuated operation. Moreover, using 2D acoustophoresis close to 100% of all encapsulated microparticles were detected compared to only 79% for unactuated operation of the system. This makes 2D acoustophoresis suitable in droplet-based biological assays in which the encapsulated particles are scarce and a high detectability is paramount such as in single-cell analysis.

## References

1. Sackmann, E.K., A.L. Fulton, and D.J. Beebe, *The present and future role of microfluidics in biomedical research*. Nature, 2014. 507(7491): p. 181-189.
2. Teh, S.Y., R. Lin, L.H. Hung, and A.P. Lee, *Droplet microfluidics*. Lab on a Chip, 2008. 8(2): p. 198-220.
3. Schneider, T., J. Kreutz, and D.T. Chiu, *The Potential Impact of Droplet Microfluidics in Biology*. Analytical Chemistry, 2013. 85(7): p. 3476-3482.
4. Whitesides, G.M., *The origins and the future of microfluidics*. Nature, 2006. 442(7101): p. 368-373.
5. Seemann, R., M. Brinkmann, T. Pfohl, and S. Herminghaus, *Droplet based microfluidics*. Reports on Progress in Physics, 2012. 75(1): p. 016601 1-41.
6. Brouzes, E., et al., *Droplet microfluidic technology for single-cell high-throughput screening*. Proceedings of the National Academy of Sciences of the United States of America, 2009. 106(34): p. 14195-14200.
7. Clausell-Tormos, J., et al., *Droplet-based microfluidic platforms for the encapsulation and screening of Mammalian cells and multicellular organisms*. Chem Biol, 2008. 15(5): p. 427-37.
8. Koster, S., et al., *Drop-based microfluidic devices for encapsulation of single cells*. Lab Chip, 2008. 8(7): p. 1110-5.
9. Joensson, H.N., et al., *Detection and analysis of low-abundance cell-surface biomarkers using enzymatic amplification in microfluidic droplets*. Angew Chem Int Ed Engl, 2009. 48(14): p. 2518-21.
10. Guo, M.T., A. Rotem, J.A. Heyman, and D.A. Weitz, *Droplet microfluidics for high-throughput biological assays*. Lab Chip, 2012. 12(12): p. 2146-55.
11. Baret, J.C., et al., *Fluorescence-activated droplet sorting (FADS): efficient microfluidic cell sorting based on enzymatic activity*. Lab Chip, 2009. 9(13): p. 1850-8.
12. Joensson, H.N. and H. Andersson Svahn, *Droplet microfluidics--a tool for single-cell analysis*. Angew Chem Int Ed Engl, 2012. 51(49): p. 12176-92.
13. Wiklund, M., H. Brismar, and B. Onfelt, *Acoustofluidics 18: Microscopy for acoustofluidic micro-devices*. Lab Chip, 2012. 12(18): p. 3221-34.
14. Zhu, Y. and Q. Fang, *Analytical detection techniques for droplet microfluidics-A review*. Analytica Chimica Acta, 2013. 787: p. 24-35.
15. Lenshof, A., C. Magnusson, and T. Laurell, *Acoustofluidics 8: Applications of acoustophoresis in continuous flow microsystems*. Lab on a Chip, 2012. 12(7): p. 1210-1223.
16. Ding, X.Y., et al., *Standing surface acoustic wave (SSAW) based multichannel cell sorting*. Lab on a Chip, 2012. 12(21): p. 4228-4231.
17. Petersson, F., L. Aberg, A.M. Sward-Nilsson, and T. Laurell, *Free flow acoustophoresis: Microfluidic-based mode of particle and cell separation*. Analytical Chemistry, 2007. 79(14): p. 5117-5123.
18. Leibacher, I., P. Reichert, and J. Dual, *Microfluidic droplet handling by bulk acoustic wave (BAW) acoustophoresis*. Lab on a Chip, 2015. 15(13): p. 2896-2905.
19. Li, S.X., et al., *An On-Chip, Multichannel Droplet Sorter Using Standing Surface Acoustic Waves*. Analytical Chemistry, 2013. 85(11): p. 5468-5474.
20. Fornell, A., et al., *Controlled Lateral Positioning of Microparticles Inside Droplets Using Acoustophoresis*. Analytical Chemistry, 2015. 87(20): p. 10521-10526.
21. Grenvall, C., C. Antfolk, C.Z. Bisgaard, and T. Laurell, *Two-dimensional acoustic particle focusing enables sheathless chip Coulter counter with planar electrode configuration*. Lab on a Chip, 2014. 14(24): p. 4629-4637.
22. Manneberg, O., J. Svennebring, H.M. Hertz, and M. Wiklund, *Wedge transducer design for two-dimensional ultrasonic manipulation in a microfluidic chip*. Journal of Micromechanics and Microengineering, 2008. 18(9): p. 095025 1-9.
23. Nordin, M. and T. Laurell, *Two-hundredfold volume concentration of dilute cell and particle suspensions using chip integrated multistage acoustophoresis*. Lab on a Chip, 2012. 12(22): p. 4610-4616.



24. Settnes, M. and H. Bruus, *Forces acting on a small particle in an acoustical field in a viscous fluid*. Physical Review E, 2012. 85(1): p. 016327 1-12.
25. Baroud, C.N., F. Gallaire, and R. Dangla, *Dynamics of microfluidic droplets*. Lab on a Chip, 2010. 10(16): p. 2032-2045.
26. Kinsler, L.E., *Fundamentals of acoustics*. 4. ed. 2000, New York: Wiley. 548 s.
27. Manneberg, O., B. Vanherberghen, B. Onfelt, and M. Wiklund, *Flow-free transport of cells in microchannels by frequency-modulated ultrasound*. Lab on a Chip, 2009. 9(6): p. 833-837.
28. Iranmanesh, I., R. Barnkob, H. Bruus, and M. Wiklund, *Tunable-angle wedge transducer for improved acoustophoretic control in a microfluidic chip*. Journal of Micromechanics and Microengineering, 2013. 23(10): p. 105002 1-10.
29. Lenshof, A., M. Evander, T. Laurell, and J. Nilsson, *Acoustofluidics 5: Building microfluidic acoustic resonators*. Lab Chip, 2012. 12(4): p. 684-95.
30. Baret, J.C., *Surfactants in droplet-based microfluidics*. Lab on a Chip, 2012. 12(3): p. 422-433.
31. Schneider, C.A., W.S. Rasband, and K.W. Eliceiri, *NIH Image to ImageJ: 25 years of image analysis*. Nature Methods, 2012. 9(7): p. 671-675.
32. Muller, P.B., R. Barnkob, M.J.H. Jensen, and H. Bruus, *A numerical study of microparticle acoustophoresis driven by acoustic radiation forces and streaming-induced drag forces*. Lab on a Chip, 2012. 12(22): p. 4617-4627.
33. Bruus, H., *Theoretical microfluidics*. Oxford master series in physics. 2008, Oxford ; New York: Oxford University Press. 346 p.
34. Wiklund, M., *Acoustofluidics 12: biocompatibility and cell viability in microfluidic acoustic resonators (vol 12, pg 2018, 2012)*. Lab on a Chip, 2012. 12(24): p. 5283-5283.
35. Barnkob, R., P. Augustsson, T. Laurell, and H. Bruus, *Acoustic radiation- and streaming-induced microparticle velocities determined by microparticle image velocimetry in an ultrasound symmetry plane*. Physical Review E, 2012. 86(5): p. 056307 1-11.
36. Kinoshita, H., S. Kaneda, T. Fujii, and M. Oshima, *Three-dimensional measurement and visualization of internal flow of a moving droplet using confocal micro-PIV*. Lab on a Chip, 2007. 7(3): p. 338-346.
37. Ma, S.H., J.M. Sherwood, W.T.S. Huck, and S. Balabani, *On the flow topology inside droplets moving in rectangular microchannels*. Lab on a Chip, 2014. 14(18): p. 3611-3620.
38. Hein, M., M. Moskopp, and R. Seemann, *Flow field induced particle accumulation inside droplets in rectangular channels*. Lab on a Chip, 2015. 15(13): p. 2879-2886.

# Paper V

## **Binary particle separation in droplet microfluidics using acoustophoresis**

A. Fornell, K. Cushing, J. Nilsson, and M. Tenje

Reproduced from A. Fornell, K. Cushing, J. Nilsson, and M. Tenje. Binary particle separation in droplet microfluidics using acoustophoresis. *Applied Physics Letters*, 112(6), 063701 (2018). With the permission of AIP Publishing.



## Binary particle separation in droplet microfluidics using acoustophoresis

Anna Fornell,<sup>1,a)</sup> Kevin Cushing,<sup>1</sup> Johan Nilsson,<sup>1</sup> and Maria Tenje<sup>1,2</sup>

<sup>1</sup>Department Biomedical Engineering, Lund University, Lund, Sweden

<sup>2</sup>Department Engineering Sciences, Science for Life Laboratory, Uppsala University, Uppsala, Sweden

(Received 22 December 2017; accepted 25 January 2018; published online 6 February 2018)

We show a method for separation of two particle species with different acoustic contrasts originally encapsulated in the same droplet in a continuous two-phase system. This was realized by using bulk acoustic standing waves in a 380  $\mu\text{m}$  wide silicon-glass microfluidic channel. Polystyrene particles (positive acoustic contrast particles) and in-house synthesized polydimethylsiloxane (PDMS) particles (negative acoustic contrast particles) were encapsulated inside water-in-oil droplets either individually or in a mixture. At acoustic actuation of the system at the fundamental resonance frequency, the polystyrene particles were moved to the center of the droplet (pressure node), while the PDMS particles were moved to the sides of the droplet (pressure anti-nodes). The acoustic particle manipulation step was combined in series with a trifurcation droplet splitter, and as the original droplet passed through the splitter and was divided into three daughter droplets, the polystyrene particles were directed into the center daughter droplet, while the PDMS particles were directed into the two side daughter droplets. The presented method expands the droplet microfluidics tool-box and offers new possibilities to perform binary particle separation in droplet microfluidic systems. *Published by AIP Publishing.*

<https://doi.org/10.1063/1.5020356>

Droplet microfluidics has emerged as a powerful technology for fast and sensitive analytical analysis on-chip. Typically, water-in-oil droplets are generated where one major application of the technology is to use the droplets as individual reaction chambers for bead- and cell-based assays.<sup>1,2</sup> Monodisperse droplets can be generated at high frequency, and the technology has several other advantages such as fast and controlled reaction times and reduced cost due to the small amount of samples and reagents required for each analysis compared with standard methods. Examples of applications include single-cell analysis,<sup>3,4</sup> droplet PCR (polymerase chain reaction),<sup>5,6</sup> and high throughput assays.<sup>7,8</sup>

In many applications, the precise control of the individual droplets and the content inside the droplets is required.<sup>9</sup> For this purpose, unit-operators to sort,<sup>10,11</sup> trap,<sup>12,13</sup> and manipulate particles inside droplets<sup>14–20</sup> have been developed. Manipulation of particles encapsulated inside droplets is of high interest since it can be used for numerous applications such as particle enrichment and washing. Recently, several methods to control the position of particles inside droplets have been reported including acoustophoresis,<sup>14,15</sup> dielectrophoresis,<sup>16</sup> magnetophoresis,<sup>17,18</sup> and methods relying on sedimentation and the hydrodynamic flow patterns inside the droplets.<sup>19,20</sup> However, methods to separate one particle species from another encapsulated in the same droplet are still missing. Here, we have developed such a technology by combining an acoustic particle manipulation step with a droplet splitter to separate particles based on the material properties (the acoustic contrast factor).

During the last few years, acoustic particle manipulation (acoustophoresis) has been used to focus, concentrate, and separate particles in various one-phase microfluidic systems,<sup>21–23</sup> and recently, acoustics has also been implemented

in two-phase systems to sort whole droplets and to manipulate particles inside droplets.<sup>11,14,15,24,25</sup> Particles in an acoustic standing wave-field will experience an acoustic radiation force ( $F_{\text{rad}}$ ), and the force on a particle in a 1-dimensional  $\lambda/2$ -standing wave-field is described by

$$F_{\text{rad}} = 4\pi\Phi(\tilde{\kappa}, \tilde{\rho})ka^3E_{\text{ac}}\sin(2ky), \quad (1a)$$

$$\Phi(\tilde{\kappa}, \tilde{\rho}) = \frac{1}{3} \left[ \frac{5\tilde{\rho} - 2}{2\tilde{\rho} + 1} - \tilde{\kappa} \right], \quad \text{where } \tilde{\rho} = \frac{\rho_p}{\rho_0} \text{ and } \tilde{\kappa} = \frac{\kappa_p}{\kappa_0}, \quad (1b)$$

where  $\Phi$  is the acoustic contrast factor,  $k$  is the wavenumber ( $k = 2\pi/\lambda$ ),  $a$  is the radius of the particle,  $\lambda$  is the wavelength of the sound,  $E_{\text{ac}}$  is the acoustic energy density,  $y$  is the distance from the wall,  $\rho_p$  and  $\rho_0$  are the densities of the particle and the fluid, and  $\kappa_p$  and  $\kappa_0$  are the compressibilities of the particle and the fluid.<sup>26</sup> As seen in Eq. (1), the direction of the acoustic force on the particle depends on the sign of the acoustic contrast factor. A particle with positive acoustic contrast is moved to the pressure node, while a particle with negative acoustic contrast is moved to the pressure anti-nodes (Fig. 1). Cells and most common microparticles used in bead-based assays such as polystyrene, glass, and silica particles all have a positive acoustic contrast factor in water. However, there are a few natural occurring examples of negative acoustic contrast particles such as fat particles in

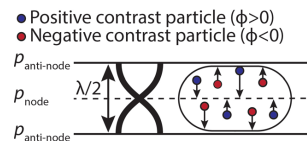


FIG. 1. In an acoustic standing wave-field, microparticles are moved to the pressure node or anti-nodes depending on the acoustic contrast factor.

<sup>a)</sup>Author to whom correspondence should be addressed: [anna.fornell@bme.lth.se](mailto:anna.fornell@bme.lth.se)

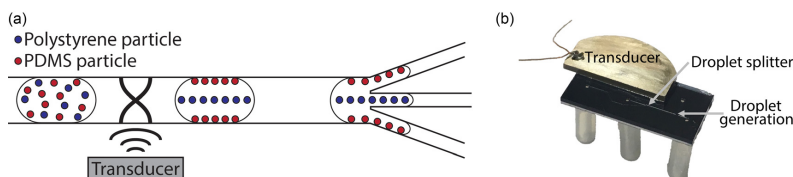


FIG. 2. (a) Schematic of the separation principle. Droplets containing two different particle species are generated, and in the acoustic standing wave-field, the two particle species are separated based on the acoustic contrast. In the droplet splitter, the polystyrene particles, focused in the center of the droplets, are directed into the center daughter droplet, while the PDMS particles, focused to the sides of the droplets, are directed into the side daughter droplets. (b) Photograph showing the fabricated microfluidic chip and the attached piezoelectric transducer. The dimensions of the chip are  $2\text{ cm} \times 1\text{ cm}$ .

milk and lipid particles in human blood.<sup>21,27</sup> In addition, researchers have synthesized particles in special materials that exhibit negative acoustic contrast in water such as polymer-shelled gas bubbles<sup>28</sup> and particles made of PDMS (polydimethylsiloxane).<sup>29</sup> For our study, standard polystyrene particles were used as positive acoustic contrast particles and PDMS particles were synthesized and used as negative acoustic contrast particles. PDMS particles were used as negative acoustic contrast particles since in future applications, these particles can be easily surface-functionalized to enable separation of bioparticles.<sup>30</sup> However, surface-functionalizing of PDMS particles is outside the scope of this paper where we show the proof-of-principle of separation of two particle species inside droplets.

The microfluidic system is shown in Figs. 2(a) and 2(b). The channels were etched on a silicon wafer using deep reactive-ion etching and sealed with a glass lid using anodic bonding. The height of all channels was  $100\ \mu\text{m}$ , and the main channel was  $380\ \mu\text{m}$  wide which gives a  $\lambda/2$ -resonance close to 2 MHz. The droplet splitter consisted of a trifurcation where the side outlet channels were angled  $20^\circ$  with respect to the main channel, and the width of these channels was  $117\ \mu\text{m}$ . The channels were hydrophobic surface-coated using silane (Repel-Silane ES, GE Healthcare). A 1 mm thick piezoelectric transducer (PZT26, Ferroperm or APC-840, APC International) having fundamental resonance at 2 MHz was glued to the chip.

The transducer was actuated by an AC-signal, and the voltage over the transducer was  $22\ V_{\text{peak-peak}}$  and the frequency was 1.83–1.85 MHz. To generate droplets, the incoming fluid phases were controlled by two syringe pumps (NEMESYS, Cetoni) operated in the continuous injection mode. The continuous phase was olive oil (Di Luca & Di Luca), and the disperse phase was water containing micro-particles (polystyrene particles and/or PDMS particles).

To control the droplet splitting, the flow rates in the side outlets were set by one common syringe pump (NEMESYS, Cetoni) operated in the withdrawal mode while the center channel outlet was connected directly to an open container. The total flow rate was  $2\text{--}3\ \mu\text{l}/\text{min}$  in all experiments except for the video in the [supplementary material](#). Images of the experiments were acquired using a camera (XM10, Olympus) mounted on an optical microscope (BX51W1, Olympus).

The key feature in this work is separation of two particle species into individual daughter droplets based on the material properties of the particles. To demonstrate this concept, polystyrene particles ( $10\ \mu\text{m}$  diameter, Sigma-Aldrich) were

used along with PDMS particles. The PDMS particles were prepared according to a similar protocol as described by Choi *et al.*<sup>31</sup> First, PDMS (Sylgard 184, Dow Corning) was mixed in a 10:1 ratio and then degassed. Two plastic syringes (5 ml, Henke Saas Wolf) with syringe needles (18 G blunt fill needle, Becton Dickinson) were connected to each other via a piece of silicone tubing (228-0701, VWR). One of the syringes was filled with 4 ml water and the other syringe was filled with 0.4 ml PDMS. The pistons were manually pushed back-and-forth 5 times to create a PDMS-water emulsion. The resulting emulsion was then ejected into a bottle with 10 ml water placed on a heating plate ( $74^\circ\text{C}$ ) under constant stirring. To ensure that all PDMS particles had cross-linked completely, the bottle was kept on the heating plate for 1 h. In Fig. 3, a photograph of the PDMS particles is shown, and as seen in the photograph, the synthesized PDMS particles are highly spherical and have a wide size distribution. In applications where a narrow particle size distribution is wanted, size-fractionation using, for example, centrifugation can be employed.<sup>30</sup> However, in this study, we wanted to evaluate the acoustophoretic manipulation of a large range of particle sizes, and thus, no size-fractionation was performed.

To characterize the system, water droplets containing polystyrene particles and/or PDMS particles were generated. In the first experiment, only polystyrene particles were encapsulated inside the droplets. Without the ultrasound, the polystyrene particles were positioned in the entire droplet [Fig. 4(a)], and when the ultrasound was applied at the fundamental resonance frequency, the polystyrene particles were focused to the center of the droplet [Fig. 4(b)]. In the second experiment, PDMS particles were encapsulated

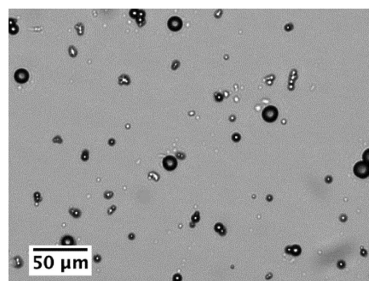


FIG. 3. Photograph of the synthesized PDMS particles.

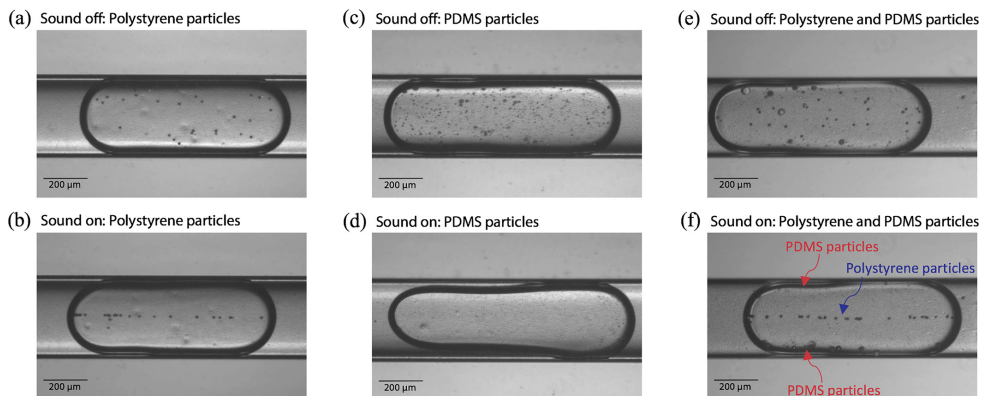


FIG. 4. Without the ultrasound applied, the polystyrene particles (a), PDMS particles (c), and a mixture of these (e) are all positioned throughout the entire droplets. With the ultrasound applied, the polystyrene particles are moved to the center (b), the PDMS particles are moved to the sides (d), and with a mixture of the two particle species, the polystyrene particles are moved to the center, while the PDMS particles are moved to the sides (f). The direction of flow is towards the right in the images.

instead. Without the ultrasound, the PDMS particles were positioned in the entire droplet [Fig. 4(c)], and when the ultrasound was applied at the fundamental resonance frequency, the PDMS particles were moved towards the sides of the droplet [Fig. 4(d)]. As seen in Fig. 4(d), both the smaller and larger PDMS particles could be moved by the ultrasound. In the [supplementary material](#), a video of the movement of the PDMS particles in response to the onset of the ultrasound is available. As seen in Fig. 4(d) and in the video, when the PDMS particles have moved to the sides of the droplet, the PDMS particles are difficult to see due to the dark ring around the droplet. This dark ring arises as a result of the different refractive indices of water and olive oil.<sup>32</sup> In the third experiment, a mixture of polystyrene particles and PDMS particles was encapsulated inside the droplets. Without the ultrasound, both particles species were positioned in the entire droplet [Fig. 4(e)], and when the ultrasound was applied at the fundamental resonance frequency, the polystyrene particles were focused to the center of the droplet, whereas the PDMS particles were moved towards the sides of the droplet [Fig. 4(f)]. This set of experiments demonstrates that particles encapsulated inside droplets can be moved to the pressure nodes or anti-nodes depending on the acoustic contrast of the particles.

To explore the technology for isolation of two particle species originally encapsulated in the same droplet, a trifurcation droplet splitter was implemented. Droplets containing a mixture of polystyrene particles and PDMS particles were generated, and at the trifurcation, each droplet was divided into three daughter droplets. Without the ultrasound, the polystyrene particles and the PDMS particles were visually found in all three daughter droplets [Fig. 5(a)], and when the ultrasound was applied at the fundamental resonance frequency, the polystyrene particles were focused in the center of the droplet and directed into the center daughter droplet, while the PDMS particles were directed into the side daughter droplets [Fig. 5(b)]. In the [supplementary material](#), a video of the droplet splitting and particle separation is available.

These results demonstrate that acoustophoresis is a suitable technology for binary particle separation in droplet microfluidic systems. During operation of the system, internal fluid motions and vortices were observed in the droplets both with and without the ultrasound applied,<sup>33,34</sup> and in order to focus the particles, the acoustic force needs to be stronger than the hydrodynamic force. Overcoming the hydrodynamic force is one of the main challenges in almost all applications where particles are manipulated inside

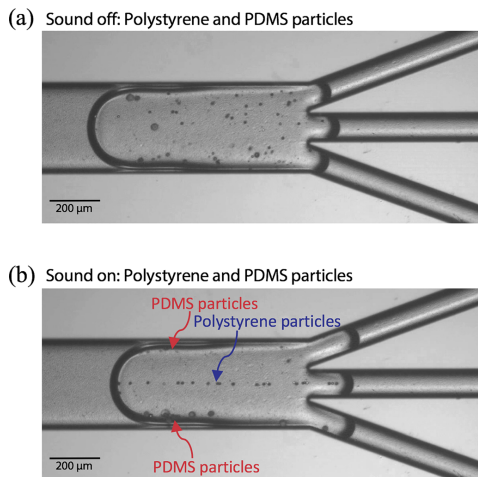


FIG. 5. A mixture of polystyrene particles and PDMS particles is encapsulated, and in the droplet splitter, each droplet is divided into three daughter droplets. Without the ultrasound applied, the two particle species are mixed in both the center and the side daughter droplets (a), while with the ultrasound applied, the polystyrene particles are directed into the center daughter droplet and the PDMS particles are directed into the side daughter droplets. The direction of flow is towards the right in the images.

droplets using external forces and may limit the throughput of the system. Compared with other particle manipulation methods, the presented method has the advantage of being label-free and generic as the only requirement is that the particles that are to be separated have different acoustic contrasts. Future work includes surface-functionalizing the particles to bind specific cells and biomolecules and combining the acoustic separation unit with other droplet unit-operators to be able to perform complex assays in droplets.

See [supplementary material](#) for a video of the movement of the PDMS particles in response to the onset of the ultrasound and a video showing droplet splitting and particle separation.

The authors would like to thank Mathias Ohlin, Klara Björnander Rahimi, Fredrik Ekström, Anders Holmberg, and Karolina Svensson (Uppsala University) for the microfabrication work. This work was funded by the Swedish Research Council, the Crafoord Foundation, the Royal Physiographic Society of Lund, and the Foundation Olle Engkvist Byggmästare.

<sup>1</sup>T. Schneider, J. Kreutz, and D. T. Chiu, *Anal. Chem.* **85**, 3476 (2013).

<sup>2</sup>I. S. Casadevall and A. DeMello, *Chem. Commun.* **47**, 1936 (2011).

<sup>3</sup>J. F. Edd, D. Di Carlo, K. J. Humphry, S. Köster, D. Irimia, D. A. Weitz, and M. Toner, *Lab Chip* **8**, 1262 (2008).

<sup>4</sup>A. M. Klein, L. Mazutis, I. Akartuna, N. Tallapragada, A. Veres, V. Li, L. Peshkin, D. A. Weitz, and M. W. Kirschner, *Cell* **161**, 1187 (2015).

<sup>5</sup>N. R. Beer, E. K. Wheeler, L. Lee-Houghton, N. Watkins, S. Nasarabadi, N. Hebert, P. Leung, D. W. Arnold, C. G. Bailey, and B. W. Colston, *Anal. Chem.* **80**, 1854 (2008).

<sup>6</sup>D. Pekin, Y. Skhiri, J.-C. Baret, D. Le Corre, L. Mazutis, C. B. Salem, F. Millot, A. El Harrak, J. B. Hutchison, J. W. Larson, D. R. Link, P. Laurent-Puig, A. D. Griffiths, and V. Taly, *Lab Chip* **11**, 2156 (2011).

<sup>7</sup>J. J. Agresti, E. Antipov, A. R. Abate, K. Ahn, A. C. Rowat, J.-C. Baret, M. Marquez, A. M. Klibanov, A. D. Griffiths, and D. A. Weitz, *Proc. Natl. Acad. Sci. U.S.A.* **107**, 4004 (2010).

<sup>8</sup>S. L. Sjöstrom, Y. Bai, M. Huang, Z. Liu, J. Nielsen, H. N. Joansson, and H. A. Svahn, *Lab Chip* **14**, 806 (2014).

<sup>9</sup>M. Tenje, A. Fornell, M. Ohlin, and J. Nilsson, *Anal. Chem.* (to be published).

<sup>10</sup>J. C. Baret, O. J. Miller, V. Taly, M. Ryckelynck, A. El-Harrak, L. Frenz, C. Rick, M. L. Samuels, J. B. Hutchison, J. J. Agresti, D. R. Link, D. A. Weitz, and A. D. Griffiths, *Lab Chip* **9**, 1850 (2009).

<sup>11</sup>T. Franke, A. R. Abate, D. Weitz, and A. Wixforth, *Lab Chip* **9**, 2625 (2009).

<sup>12</sup>A. Huebner, D. Bratton, G. Whyte, M. Yang, A. J. DeMello, C. Abell, and F. Hollfelder, *Lab Chip* **9**, 692 (2009).

<sup>13</sup>J. H. Jung, G. Destgeer, J. Park, H. Ahmed, K. Park, and H. J. Sung, *Anal. Chem.* **89**, 2211 (2017).

<sup>14</sup>A. Fornell, J. Nilsson, L. Jonsson, P. K. P. Rajeswari, H. N. Joansson, and M. Tenje, *Anal. Chem.* **87**, 10521 (2015).

<sup>15</sup>A. Fornell, M. Ohlin, F. Garofalo, J. Nilsson, and M. Tenje, *Biomicrofluidics* **11**, 31101 (2017).

<sup>16</sup>S. Han, H. S. Kim, and A. Han, *Bioelectron.* **97**, 41 (2017).

<sup>17</sup>E. Brouzes, M. Medkova, N. Savenelli, D. Marran, M. Twardowski, J. B. Hutchison, J. M. Rothberg, D. R. Link, N. Perrimon, and M. L. Samuels, *Proc. Natl. Acad. Sci. U.S.A.* **106**, 14195 (2009).

<sup>18</sup>R. Gao, Z. Cheng, A. deMello, and J. Choo, *Lab Chip* **16**, 1022 (2016).

<sup>19</sup>G. K. Kurup and A. S. Basu, *Biomicrofluidics* **6**, 22008 (2012).

<sup>20</sup>M. Hein, M. Moskopp, and R. Seemann, *Lab Chip* **15**, 2879 (2015).

<sup>21</sup>F. Petersson, A. Nilsson, C. Holm, H. Jonsson, and T. Laurell, *Lab Chip* **5**, 20 (2005).

<sup>22</sup>J. Shi, H. Huang, Z. Stratton, Y. Huang, and T. J. Huang, *Lab Chip* **9**, 3354 (2009).

<sup>23</sup>P. Augustsson, C. Magnusson, M. Nordin, H. Lilja, and T. Laurell, *Anal. Chem.* **84**, 7954 (2012).

<sup>24</sup>I. Leibacher, P. Reichert, and J. Dual, *Lab Chip* **15**, 2896 (2015).

<sup>25</sup>P. R. Rogers, J. R. Friend, and L. Y. Yeo, *Lab Chip* **10**, 2979 (2010).

<sup>26</sup>H. Bruus, *Lab Chip* **12**, 1014 (2012).

<sup>27</sup>C. Grenvall, P. Augustsson, J. R. Folkenberg, and T. Laurell, *Anal. Chem.* **81**, 6195 (2009).

<sup>28</sup>S. V. V. N. Kothapalli, M. Wiklund, B. Janerot-Sjöberg, G. Paradossi, and D. Grishenkov, *Ultrasonics* **70**, 275 (2016).

<sup>29</sup>K. W. Cushing, M. E. Piyasena, N. J. Carroll, G. C. Maestas, B. A. López, B. S. Edwards, S. W. Graves, and G. P. López, *Anal. Chem.* **85**, 2208 (2013).

<sup>30</sup>K. Cushing, E. Undvall, Y. Ceder, H. Lilja, and T. Laurell, *Anal. Chim. Acta* **1000**, 256 (2018).

<sup>31</sup>Y. H. Choi, K. H. Chung, H. B. Hong, and W. S. Lee, *Int. J. Polym. Mater. Polym. Biomater.* **66**, 1 (2017).

<sup>32</sup>O. Carrier, F. G. Ergin, H.-Z. Li, B. B. Watz, and D. Funfschilling, *J. Micromech. Microeng.* **25**, 84014 (2015).

<sup>33</sup>H. Kinoshita, S. Kaneda, T. Fujii, and M. Oshima, *Lab Chip* **7**, 338 (2007).

<sup>34</sup>M. Ohlin, A. Fornell, H. Bruus, and M. Tenje, *J. Micromech. Microeng.* **27**, 84002 (2017).